Maxizyme, a novel RNA motif with high potential as gene-inactivating agent

1998

Tomoko kuwabara

Maxizyme,
a novel RNA motif with high potential as gene-inactivating agent

Division of Applied Biochemistry
Doctoral Degree Program in Agricultural Sciences
University of Tsukuba

Tomoko Kuwabara

Contents

Abbreviations

A	adenine, adenosine, 2'-deoxyadenosine
ATP	adenosine triphosphate
BCR	breakpoint cluster region
bp	base pair(s)
C	cytosine, cytidine, 2'-deoxycitidine
CML	chronic myelogenous leukemia
DNA	deoxyribonucleic acid
DNase	deoxyribonuclease
Ea	activation energy
EDTA	ethylenediaminetetraacetic acid
G	guanine, guanosine
h	hour(s)
HDV	human hepatitis delta virus
HIV	human immunodeficiency virus
IL-3	interleukin-3
k_{cat}	catalytic constant (the turn number)
K_M	Michaelis constant
k_{obs}	observed rate constant
luc	luciferase
min	minute(s)
mRNA	messenger RNA
NMR	nuclear magnetic resonance
nts	nucleotides
PAGE	polyacrylamide gel electrophoresis

PCR	polymerase chain reaction
RNA	ribonucleic acid
RNase	ribonuclease
SDS	sodium dodecyl sulfate
T	thymine, 2'-deoxythymidine
TBE	tris-borate-EDTA
Tris	tris(hydroxymethyl) aminomethane
tRNA	transfer RNA
U	uracil, uridine
UV	ultraviolet

Chapter I
General introduction

The *trans*-acting hammerhead ribozyme consists of an antisense section (stem I and stem III) and a catalytic domain with a flanking stem II-loop section (Fig. 1). Over the past a few years, there have been several attempts to determine both the overall global structure and the detailed atomic structure of the hammerhead ribozyme. The X-ray crystal structures determined by McKay's group and Scott's and Klug's group are nearly identical in terms of tertiary folding and conformation although the components of the two types of crystals examined were quite different: one type was an RNA-DNA complex in a high concentration of Li_2SO_4 (Pley *et al.*, 1994) and the other type was an all-RNA complex with a 2'-methoxy-2'-deoxyribose at the cleavage site in a solution of lower ionic strength (Scott *et al.*, 1995) or, alternatively, a freeze-trapped intermediate of an unmodified all-RNA complex (Scott *et al.*, 1996). The freeze-trapped conformational intermediate was stabilized primarily by a hydrogen bond between the furanose oxygen of C_{17} and the 2'-OH of $U_{16.1}$. All ribozymes were γ-shaped in the crystals (Fig. 1), with stems I and II forming the arm of the γ and stem III forming the base, with stem I and stem II being adjacent to each other and stems II and III being stacked colinearly to form a pseudo-A-form helix.

In the X-ray structures the catalytic core is divided into two regions: domain I consisting of $C_3U_4G_5A_6$ and domain II consisting of nucleotides $G_{12}A_{13}A_{14}$ and $U_7G_8A_9$. The nucleotides of domain II form two reversed-Hoogsteen G-A base-pairs between G_8-A_{13} and A_9-G_{12}, and a non-Watson-Crick A_{14}-U_7 base-pair that consists of one hydrogen bond. This extended stem II stacks onto the non-Watson-Crick base-pair, $A_{15.1}$-$U_{16.1}$, resulting in formation of a pseudo-A-form helix by stems II and III (Pley *et al.*, 1994; Scott *et al.*, 1995, 1996; Scott and Klug, 1996). The adjacent non-Watson-Crick A-U base-pairs (A_{14}-U_7 and $A_{15.1}$-$U_{16.1}$) form the basis of a three-way junction. The four

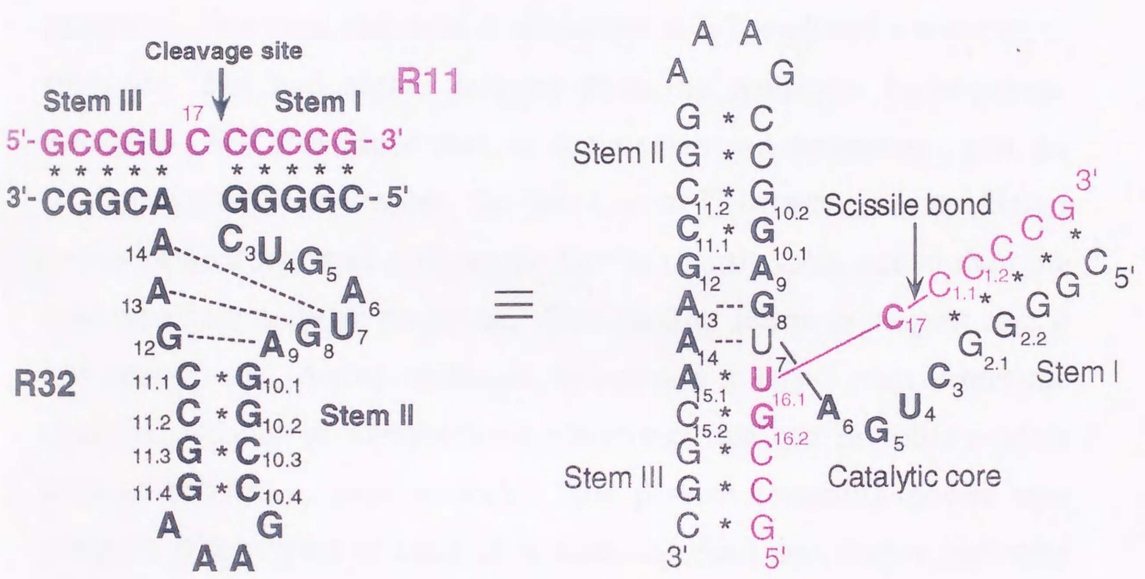

Figure 1 Secondary structures of the wild-type hammerhead ribozyme (R32). A schematic representation of the overall folding of the hammerhead ribozyme is also shown on the right.

nucleotides ($C_3U_4G_5A_6$) of domain I form a "uridine-turn" motif, allowing the phosphate backbone to turn and connect with stem I. Since the uridine-turn motif conforms to the general sequence requirement UNR (where N is any nucleotide and R represents a purine), an attempt at selection *in vitro* was made to determine whether other sequences might be possible in the hammerhead's catalytic core. Active sequences conformed broadly to the consensus core sequence except at A_9, and no sequences were associated with higher activity than that of the hammerhead with the consensus core, an indication that the consensus sequence derived from viruses and virusoids is probably the optimal sequence. However, chemical modification at U_7 produced a non-natural ribozyme that had higher activity than the wild-type hammerhead ribozyme. We also found that, in some cases and depending upon the target-recognition sequences, the insertion of G between A_9 and $G_{10.1}$ results in production of a ribozyme that is slightly more active than the wild-type hammerhead ribozyme. This finding seems to suggest that it was unnecessary, during evolution, to increase to any further extent the catalytic activity of hammerhead ribozymes for use in rolling-circle mechanisms since, most probably, the present trimming power was adequate with respect to rates of replication. Such speculation indicates that it might be possible to select *in vitro* or *in vivo*, or to engineer, hammerhead ribozymes that are better catalysts than wild-type forms.

It has been well established that ribozymes are metalloenzymes (Kazakov and Altman, 1991; Dahm *et al.*, 1993; Piccirilli *et al.*, 1993; Pyle, 1993; Steitz and Steitz, 1993; Uchimaru *et al.*, 1993; Yarus, 1993; Uebayashi *et al.*, 1994; Sawata *et al.*, 1995; Pontius *et al.*, 1997; Warashina *et al.*, 1997; Weinstein *et al.*, 1997; Zhou *et al.*, 1996, 1997, 1998). Scott *et al.* proposed various Mg^{2+}-binding sites, two of which are thought to be important for catalysis (Scott *et al.*, 1995, 1996). The

first site is thought to involve $Mg(H_2O)_5^{2+}$ bound to the *pro-S* oxygen of the 5'-phosphate of A9, with further hydrogen bonding associated with G8, G10.1, and G12 (alternatively, $Mg(H_2O)_5^{2+}$ might be bound to the *pro-R* oxygen), and this binding is thought to have a structural role (Scott *et al.*, 1995). The second, and perhaps a more interesting site, seems to be in the vicinity of the cleavage site. At this site a Mg^{2+} ion is thought to be bound directly to the *pro-R* oxygen of the scissile phosphate in the freeze-trapped conformational intermediate (Scott *et al.*, 1996). The hydrated Mg^{2+} ion might participate directly in catalysis by acting as a base to facilitate the deprotonation of the 2'-OH of C17, prior to nucleophilic attack at the scissile phosphate. However, crystal structures generally represent energy minima and do not provide direct and detailed structural information about transition states unless the structural data represent a deliberately designed analog of a transition state. Because the conformation revealed by all the available crystallographic structures would not allow in-line attack by the 2'-OH on the scissile phosphorus-oxygen bond that is absolutely required for activity, none of them represents the exact catalytic conformation. It is apparent that substantial twisting at the cleavage site would be required for in-line attack and a specific proposal for rearrangement at the cleavage site has been presented, based on the X-ray structures of hammerhead ribozymes. (Scott *et al.*, 1995, 1996)

Further analysis by Scott indicates the probable invalidity of the earlier postulate (Scott *et al.*, 1996) that the Mg^{2+} ion bound to the *pro*-R oxygen of the scissile phosphate in the ground state might move, together with the phosphate, into a conformation more suitable for in-line attack: Scott recently trapped an intermediate with an advanced conformational change, where the phosphate had moved considerably. However, the metal ion (this time a Co^{2+} ion) associated with N7 of A1.1 and did not

move with the *pro-R* oxygen. The exact number and location of catalytic metal ion(s) in the transition state remain to be determined.

In striking contrast to proteinaceous enzymes, which do not always require metal ions for their activity, all ribozymes have an absolute requirement for metal ions for their activity. Metal ions in ribozymes have two distinct functions: in one case they aid in the structural stabilization of the folded RNA and in the second case they act as the catalytic cofactor that allows the RNA to act as a metalloenzyme. In hammerhead ribozymes, metal ions such as Mg^{2+}, Mn^{2+}, Ca^{2+} and Co^{2+} can participate both in RNA folding and in catalysis. Similarly, Sr^{2+} and Ba^{2+} ions can perform both roles but to a much lesser extent. Other metal ions, such as Cd^{2+} and Zn^{2+}, can participate in catalysis only in the presence of RNA-folding agents such as polyamines and spermine, an observation that suggests that Cd^{2+} and Zn^{2+} ions can only play a catalytic role and the structure of the ribozyme is dependent on polyamines or spermine.

In attempts to define the sequence requirements for an active structure of a hammerhead ribozyme that help the ribozyme to select appropriate target sequences, extensive mutagenesis studies of the conserved region have been performed (Koizumi *et al.*, 1988; Ruffer *et al.*, 1990; Perriman *et al.*, 1992; Shimayama *et al.*, 1995; Zoumadakis and Tabler, 1995). Several such studies were carried out to examine the importance of the conserved trinucleotide GUC at the cleavage site. Early results revealed that G at the third position in the triplet, which might extend stem I by forming a G_{17}:C_3 pair, inhibited the cleavage reaction in all but one case and, moreover, that U at the central position was required for efficient cleavage (Koizumi *et al.*, 1988; Ruffer *et al.*, 1990; Perriman *et al.*, 1992). The accumulated data from mutagenesis studies led to the generally accepted NUX rule (where N can be A, U, G

or C; X can be A, U or C), which states that any oligonucleotide with a NUX triplex can be cleaved by hammerhead ribozymes. Our detailed kinetic analysis (Shimayama *et al.*, 1995), in which we measured both k_{cat} and K_m, indicated that GUC was cleaved most efficiently in a manner that depended both on k_{cat} and k_{cat}/K_m, with CUC and UUC coming next. Therefore, when a target site in a *trans*-acting system (an intermolecular reaction) is chosen, GUC or CUC may be preferred. However, in *cis*-acting systems (intramolecular reactions), in which K_m values are irrelevant, other triplets, such as AUC, GUA, and AUA, may be chosen since these triplets are associated with high values of k_{cat}. In fact, the minus strand of the virusoid of Lucerne transient streak virus, (-)vLTSV, and the plus strand of the satellite RNA of barley yellow dwarf virus, (+)sBYDV, use the GUA triplet and the AUA triplet, respectively, for hammerhead-catalyzed cleavage during their replication (Shimayama *et al.*, 1995).

The minimum reaction scheme, consisting at least three steps. First, the substrate binds to the ribozyme to form a Michaelis-Menten complex via formation of base pairs at stems I and III (k_{assoc}). Then, a specific phosphodiester bond (on the 3'-side of the NUX triplet) in the bound substrate is cleaved by the action of metal ions (k_{cleav}) to produce a 2',3'-cyclic phosphate and a 5'-hydroxyl group. Finally, the cleavage fragments dissociate from the ribozyme and the liberated ribozyme is now available for a new series of catalytic events (k_{diss}).

The dependence on temperature of the rate-limiting step was detected by analysis of an Arrhenius plot (Takagi and Taira, 1995; Warashina *et al.*, 1997). Distinct changes in the slope of the plot provided evidence for three different rate-limiting steps in the hydrolysis of an 11-mer substrate (S11, Fig. 1) by the 32-mer ribozyme (R32, Fig. 1). At mid-range temperatures of 25-50°C, the chemical cleavage step

(k_{cleav}) is the rate-limiting step, indicating that the cleaved fragments dissociate from the ribozyme at a higher rate than the rate of the chemical reaction ($k_{cleav} < k_{diss}$). At temperatures below 25°C, the cleaved fragments adhere to the ribozyme more tightly and the product-dissociation step becomes the rate-limiting step ($k_{diss} < k_{cleav}$). Above 50°C, the rate of the reaction decreases because, at such high temperatures, the formation of the Michaelis-Menten complex (formation of a duplex) is hampered by thermal melting (the melting temperature of stem II of R32 is above 80°C and, therefore, the stem II and loop region is unaffected between about 50 and 60°C).

The efficient binding of a hammerhead ribozyme to its cleavage site in an intracellular target RNA is an obvious requirement for the eventual use of the ribozyme as a therapeutic agent. The binding is influenced by the length of the ribozyme antisense arms (stems I and III). Kinetic models of the action of hammerhead ribozymes and analyses of thermodynamic parameters predict that ribozymes with short antisense arms have a high turnover rate when compared to their counterparts with long arms. However, in some cases, hammerhead ribozyme with long antisense arms have been found to be more active in the cell than short-arm derivatives. In the cellular environment, the rate-limiting step is not always the chemical cleavage step and, therefore, a ribozyme's activity *in vitro* does not necessarily reflect its activity *in vivo*. The stability of ribozymes *in vivo* appears to be more important in the intracellular efficacy of ribozymes. It is, however, also important to use ribozymes with short arms in functional analysis of kinetics *in vitro*, to ensure measurement of the chemical step.

Helix II is the only helix in the hammerhead ribozyme that is not directly involved in binding of the substrate. In a systematic study, in which the length and the base composition of helix II were varied, the

minimal length of the helix II was found to be two base pairs, with a requirement for a $G_{10.1}$-$C_{11.1}$ base pair for maximal activity (Tuschl and Eckstein, 1993). So called minizymes are smaller versions of a hammerhead ribozyme in which helix II and loop II are replaced by a short linker that joins A_9 and G_{12} (Fig. 2). The linker can consist of a few nucleotides that cannot form Watson-Crick base pairs among themselves (McCall *et al.*, 1992). Several groups have replaced the nucleotide-loop of helix II with polyethylene glycol (Fu and McLaughlin, 1992; Thomson *et al.*, 1993; Hendry *et al.*, 1994) or abasic nucleotide (Sugiyama *et al.*, 1996), without complete loss of activity when at least two base pairs remains in helix II. However, the activities of most minizymes are very low (Fu and McLaughlin, 1992; McCall *et al.*, 1992; Thomson *et al.*, 1993; Tuschl and Eckstein, 1993; Long and Uhlenbeck, 1994; Hendry *et al.*, 1994, 1995; Sugiyama *et al.*, 1996). I found that minizymes with short oligonucleotide linkers instead of the stem-loop II region can form homo- or heterodimers that are very active (Amontov and Taira, 1996; Amontov *et al.*, 1996; Kuwabara *et al.*, 1996). These minizymes form dimeric structures with two catalytic centers, two binding sites and a single, common stem II. The activity of one homodimeric minizyme was found to be similar to that of the full-sized ribozyme (Amontov and Taira, 1996). Such dimeric hammerhead structures have a number of additional advantages. In particular, they are very compact divalent structures that (in the case of heterodimers) can be targeted individually to two different cleavage sites and, moreover, they can be designed in such a way that it is only in the presence of a specific sequence that the heterodimeric minizyme can form an active catalytic core (Kuwabara *et al.*, 1996, 1998b). Since minizymes are able to cleave their RNA targets *in vitro* and *in vivo* (Kuwabara *et al.*, 1998a, 1998b, 1998c), it is clear that the stem/loop II is not essential for cleavage as long

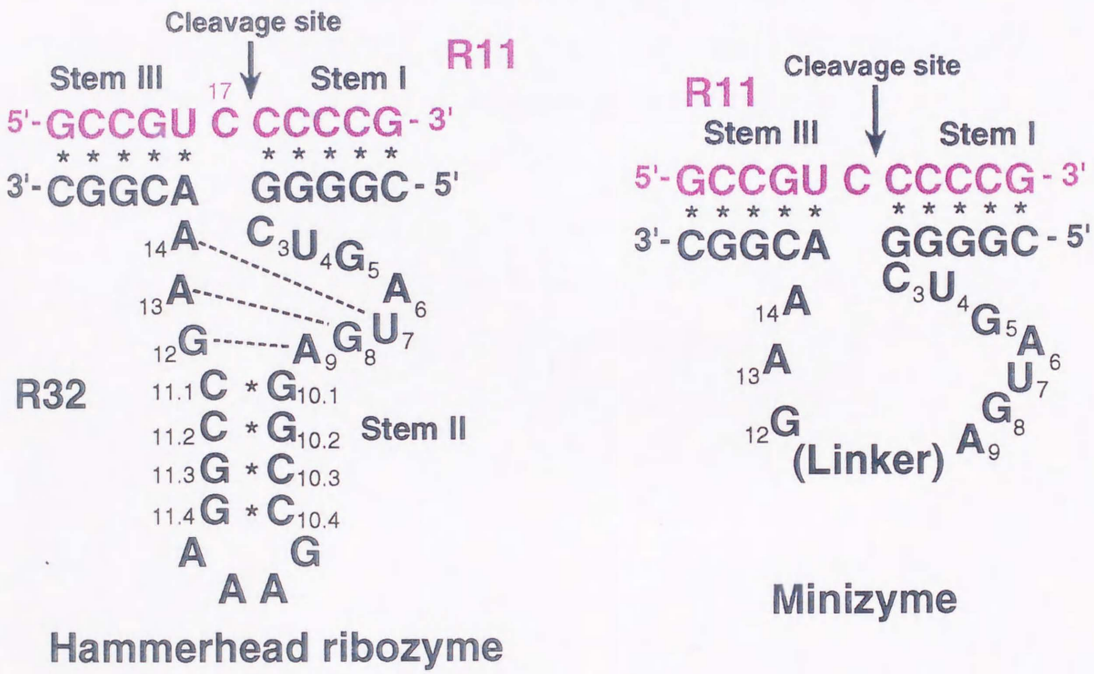

Figure 2 Secondary structures of the wild-type hammerhead ribozyme and the minizyme. Minizymes are smaller versions of a hammerhead ribozyme in which stem II and loop II are replaced by a short linker that joins A9 and G12.

as the $G_{10.1}$-$C_{11.1}$ base pair is maintained in the dimeric structure, most probably to allow capture of the structurally important Mg^{2+} ion.

Chapter II
Characterization of several kinds of dimeric minizyme: simultaneous cleavage at two sites in HIV-1 tat mRNA by dimeric minizymes *in vitro*

Introduction

The hammerhead ribozyme is one of the smallest RNA enzymes (Forster and Symons, 1987; Haseloff and Gerlach, 1988; Symons, 1989). Because of its small size and potential utility as an antiviral agent, it has been extensively investigated in terms of the mechanism of its action and possible applications *in vivo* (Kazakov and Altman, 1991; Dahm *et al.*, 1993; Piccirilli *et al.*, 1993; Pyle, 1993; Steitz and Steitz, 1993; Uchimaru *et al.*, 1993; Yarus, 1993; Uebayashi *et al.*, 1994; Sawata *et al.*, 1995; Pontius *et al.*, 1997; Warashina *et al.*, 1997; Weinstein *et al.*, 1997; Zhou *et al.*, 1996, 1997, Zhou and Taira, 1998). It was first recognized as the sequence motif responsible for self-cleavage (*cis* action) in the satellite RNAs of certain viruses (Symons, 1989). The putative consensus sequence required for activity has three duplex stems and a conserved "core" of two non-helical segments, plus an unpaired nucleotide at the cleavage site. The *trans*-acting hammerhead ribozyme, which was developed by Haseloff and Gerlach (Haseloff and Gerlach, 1988), consists of an antisense section (stem I and stem III) and a catalytic domain with a flanking stem/loop II section (Fig. 1). In attempts to identify functional groups and to elucidate the role of the stem II region, various modifications and deletions have been made in this region (Fu and McLaughlin, 1992; McCall *et al.*, 1992; Thomson *et al.*, 1993; Tuschl and Eckstein, 1993; Long and Uhlenbeck, 1994; Hendry *et al.*, 1994, 1995). For the application of such enzymes as therapeutic agents for the treatment of infectious diseases, minimized hammerhead ribozymes (minizymes; Fig. 2) seem to be particularly attractive (Hendry *et al.*, 1995). However, the activities of minizymes are two to three orders of magnitude lower than those of the parental hammerhead ribozymes, a result that led to the suggestion that minizymes might not be suitable as

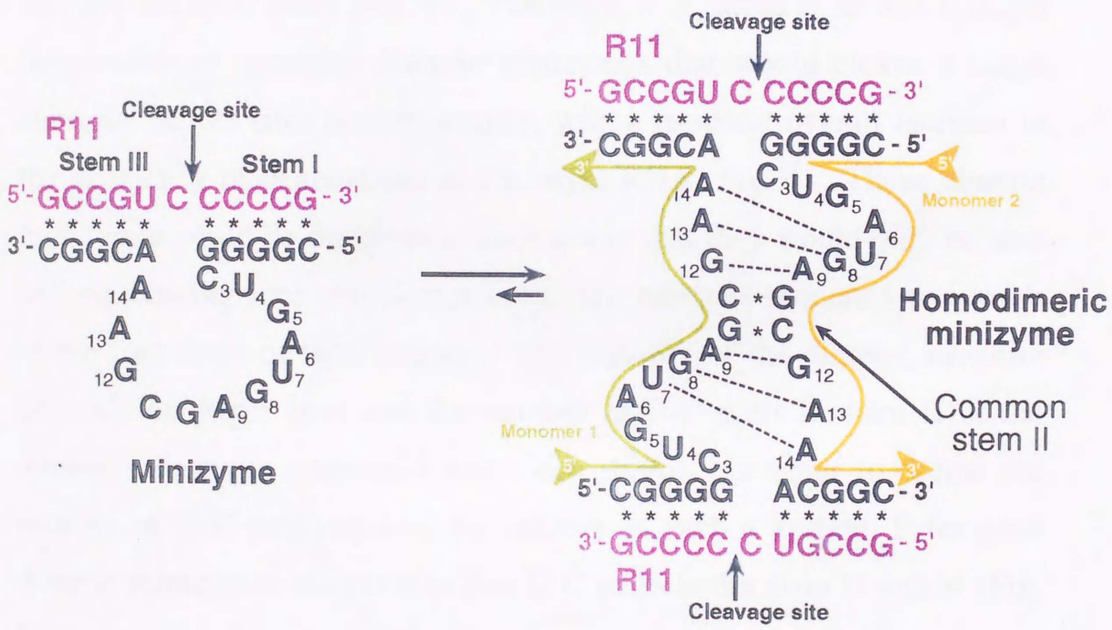

Figure 3 Secondary structure of the minizyme that was capable of forming a homodimer (Mz22).

gene-inactivating reagents (Long and Uhlenbeck, 1994). Thus, conventional hammerhead ribozymes with a deleted stem II (minizymes; Fig. 2) have been considered to be crippled structures and have attracted minimal interest because of their extremely low activity, as compared to that of the full-sized ribozyme.

We reported recently the results of kinetic analyses that indicated that some minizymes have cleavage activity nearly equal to that of the wild-type hammerhead ribozyme, and we presented evidence that minizymes with high-level activity form dimeric structures (Amontov and Taira, 1996). Such dimeric minizymes have two different binding sites and two catalytic cores (Fig. 3). Therefore, it occurred to us that it might be possible to construct dimeric minizymes that would cleave a target substrate at two sites simultaneously, with a resultant overall increase in the efficiency of degradation of the target RNA (Fig. 4). These dimeric minizymes could be designed in such a way that they would only be able to form binding sites complementary to the substrate sequence as a result of the formation of heterodimers. The stability of the dimeric structure depends on Mg^{2+} ions and the number of G-C pairs in stem II of the dimeric minizyme (Amontov and Taira, 1996). In order to define the number of G-C pair required for activity in such a system, I designed dimeric minizymes with two to five G-C pairs in the stem II region (Fig. 5).

I selected HIV-1 tat mRNA as the target substrate of the dimeric minizymes. Hammerhead ribozymes can cleave any RNA with a high degree of sequence specificity via recognition of the Watson-Crick type at stem I and stem III. The target site must contain the NUX triplet (N = G, A, C, or U; X = A, C, or U), but the efficiency of cleavage depends on the combination of N and X (Koizumi *et al.*, 1988; Ruffer *et al.*, 1990; Perriman *et al.*, 1992; Shimayama *et al.*, 1995). In this study,

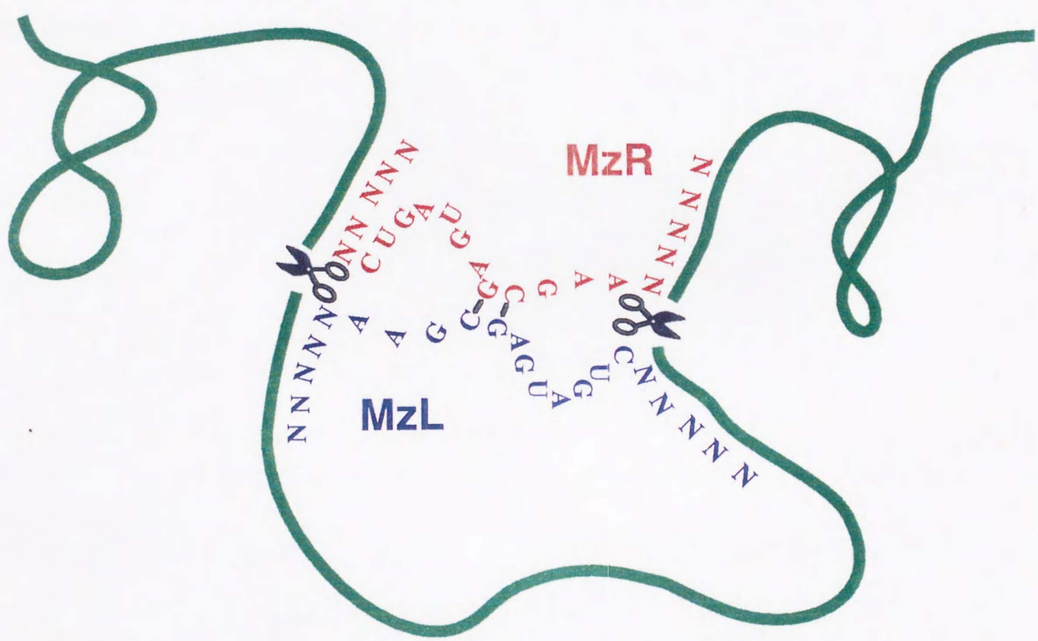

Figure 4 Schematic representation of the heterodimeric minizyme which can cleave an mRNA at two sites simultaneously.

dimeric minizymes were designed to cleave HIV-1 tat mRNA at two GUC triplets (GUC triplet-1 and GUC triplet-2, located 51 nt and 189 nt, respectively, from the 5' end of the substrate; Fig. 6) with an internucleotide distance of 138 nts between them. A computer-generated (MulFold) prediction of the secondary structure of HIV-1 tat mRNA is shown in Figure 6.

In this chapter I describe the physical properties of each heterodimeric minizyme and I demonstrate that all heterodimeric minizymes tested were capable of cleaving the HIV-1 tat mRNA at both GUC triplets simultaneously. Moreover, I show that the activity of the minizymes increased with increases in the length of the linker sequence of the dimer.

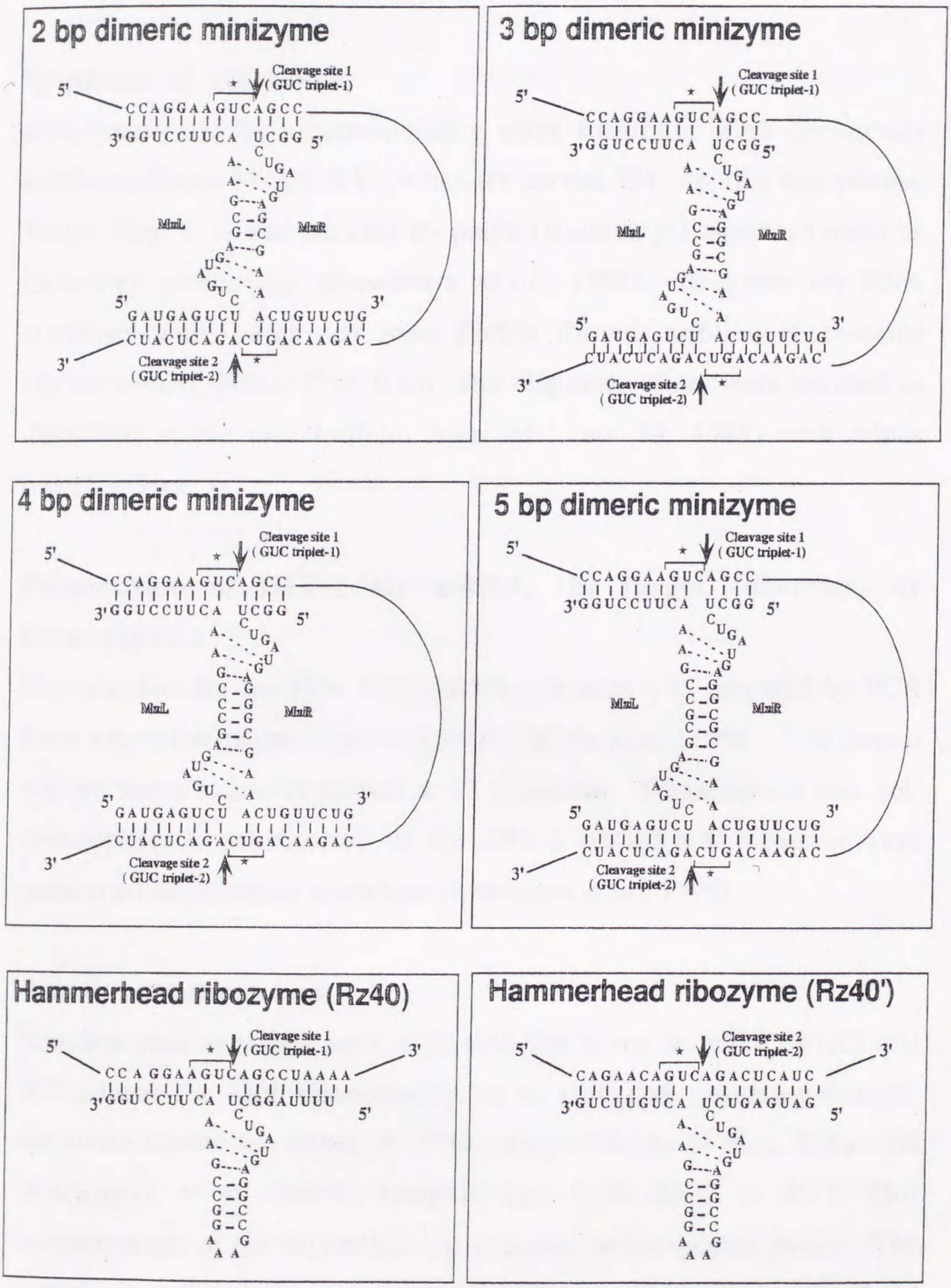

Figure 5 The secondary structures of the various dimeric minizymes used in this study. As controls, I used the parental hammerhead ribozyme (Rz40), targeted to GUC triplet-1, and Rz40', targeted to a 19-meric substrate (S19) that contained GUC triplet-2 site.

Materials and methods

Synthesis of ribozymes

Ribozymes and their corresponding short substrates were chemically synthesized on a DNA/RNA synthesizer (model 394; Applied Biosystems, Foster City, CA) and purified by polyacrylamide gel electrophoresis as described previously (Kuwabara *et al.*, 1996). Reagents for RNA synthesis were purchased from Perkin Elmer, Applied Biosystems Division (ABI; Foster City, CA). The oligonucleotides were purified as described in the user bulletin from ABI (no. 53; 1989) with minor modifications.

Preparation of HIV-1 tat mRNA, the target substrate, by transcription

The template for the HIV-1 tat mRNA substrate was prepared by PCR from a template plasmid, pcD-SRα/tat (Takebe *et al.*, 1988). The primer for the sense strand contained a T7 promoter. Transcription and gel-electrophoretic purification of the HIV-1 tat mRNA substrate were performed as described elsewhere (Kuwabara *et al.*, 1996).

Kinetic measurements

Reaction rates were measured, in 25 mM $MgCl_2$ and 50 mM Tris-HCl (pH 8.0; adjusted at each temperature), under ribozyme-saturating (single-turnover) conditions either at 37°C (measurements of k_{cat}, k_{obs}, and $K_{d(app)}$) or at various temperatures from 20°C to 60°C [for measurements of the dependence on temperature (Arrhenius plots)]. The reactions were usually initiated by the addition of $MgCl_2$ to a buffered solution that contained the minizymes and the substrate, and mixtures were then incubated at the chosen temperature. The 5'-terminus of the

short substrate (S19), which included GUC triplet-2 and has sequence 5'-CAGAACA-(GUC)-AGACUCAUC-3' (the binding sites for the dimeric minizymes, 18 nucleotides in all, are underlined and the GUC triplet is shown in parenthesis), was labeled with [γ-^{32}P]-ATP by T4 polynucleotide kinase (Takara Shuzo, Kyoto). The HIV-1 tat mRNA was labeled internally with [α-^{32}P]-CTP during transcription *in vitro* by T7 RNA polymerase (Takara Shuzo). In all cases, kinetic measurements were made under conditions where all the available substrate was expected to form a Michaelis-Menten complex, at high concentrations of minizymes (from 50 nM to 10 μM).

Reactions were stopped by removal of aliquots from the reaction mixture at appropriate intervals and mixing them with an equivalent volume of a solution that contained 100 mM EDTA, 9 M urea, 0.1% xylene cyanol, and 0.1% bromophenol blue. The substrate and the products of the reaction were separated by electrophoresis on a 5% to 20% polyacrylamide/7 M urea denaturing gel and were detected by autoradiography. The extent of cleavage was determined by quantitation of radioactivity in the bands of substrate and products with a Bio-Image Analyzer (BAS2000; Fuji Film, Tokyo).

Measurements of melting temperatures (Tm) of the dimeric minizymes

In order to determine the Tm of the duplex regions (G-C pairs) with two, three, four, and five base pairs, respectively, in stem II of the dimeric minizymes, I monitored the thermal denaturation of the ribozymes with a UV spectrophotometer (model 2100S; Shimadzu, Kyoto). Solutions of the dimeric minizymes (2 μM) were prepared in 50 mM Tris-HCl buffer (pH 8.0) that contained 25 mM $MgCl_2$. After degassing, these samples, without Mg^{2+} ions, were preheated at 80°C for 3 minutes and then slowly

cooled to 5°C over the course of 20 minutes, and then a concentrated solution of Mg^{2+} ions was added to each sample to give a final concentration of $MgCl_2$ of 25 mM. The absorption of the samples at 260 nm was monitored continuously at 5°C for 10 min and then the temperature was raised from 5°C to 80°C at a rate of 1°C/min. The Tm was determined by plotting the derivative of the thermal denaturation curve.

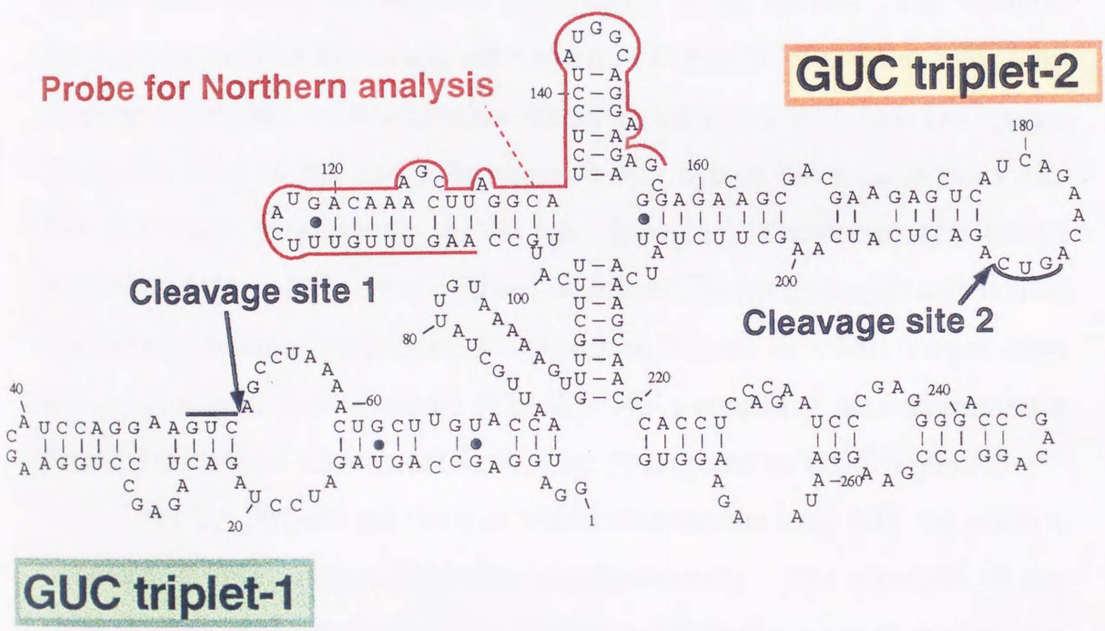

Figure 6 The secondary structure of HIV-1 tat mRNA, as predicted by a computer program. Cleavage site 1 (GUC triplet-1) and cleavage site 2 (GUC triplet-2) are indicated by arrows.

Results

Simultaneous cleavage of HIV-1 tat mRNA at two independent sites by dimeric minizymes

We demonstrated previously that minizymes with high-level activity form dimeric structures (Amontov and Taira, 1996). The stability of dimeric minizymes depends on the concentration of Mg^{2+} ions, whether or not the minizymes are bound to their substrate, and the number of G-C pairs in the common stem II region. Since the dimeric minizymes were expected to cleave substrates at two independent sites, I examined several kinds of dimeric minizyme, which differed from one another in the length of stem II, for their ability to serve as gene-inactivating agents. The dimeric minizymes used in this study are shown in Figure 5. I use the term 2 bp dimeric minizyme, to describe the dimeric minizyme with two G-C pairs. Thus, the 3 bp, 4 bp, and 5 bp dimeric minizymes have three, four and five G-C pairs, respectively, in the stem II region. The substrate selected in this study was HIV-1 tat mRNA, which is 272 bp in length and whose predicted secondary structure is shown in Figure 6. Two target sites were selected in this substrate (Fig. 6). As a control, I also examined a parental wild-type ribozyme (Rz40, Fig. 5) targeted to GUC triplet-1.

All the dimeric minizymes tested cleaved the long HIV tat mRNA substrate at two independent sites simultaneously. The strength of the activity depended on the number of G-C pairs in the stem II region: the activity increased with increasing numbers of G-C pairs. For simultaneous cleavage at two sites in the substrate by the dimeric minizymes, it seems that it was important that the two catalytic cores were stabilized by a strong dimeric structure. Such a hypothesis explains why the 5 bp dimeric minizyme had the highest activity.

Our previous kinetic analysis demonstrated that, when a short substrate (11-mer) was used, a dimeric minizyme with two G-C base pairs retained 65% of the activity of the parental hammerhead ribozyme (Amontov and Taira, 1996). When the target site is embedded in a long RNA substrate, a very stable common stem II is required (depending on the sequence of the target site). The cleavage activity of the 5 bp dimeric minizyme was even higher than that of the full-sized hammerhead ribozyme because the latter full-sized ribozyme was able to cleave at the GUC triplet-1 only.

Kinetic parameters for the cleavage of a short 19-meric substrate by dimeric minizymes

In order to characterize in further detail the properties of dimeric minizymes, I determined the kinetic parameters of cleavage using a short 19-meric substrate (S19) that contained GUC triplet-2. The sequence of this substrate is shown in Figure 5. I chose a substrate that contained GUC triplet-2 and not GUC triplet-1 because from the computer prediction, I expected the former sequence to be less likely to form inactive dimeric minizymes. In order to ensure that I measured only the rate of the pure chemical cleavage step (k_{cleav}), all reactions in this study were carried out under single-turnover conditions.

The rate constants of the dimeric minizymes, which were determined with the short S19 substrate, are shown in Table 1. As can be seen from Table 1, the 5 bp dimeric minizyme had the highest cleavage activity, with a k_{cat} of 0.24 min^{-1}, which was forty times greater than that of the 2 bp dimeric minizyme. The cleavage activity of dimeric minizymes increased with increases in the number of G-C pairs in the stem II region of the dimeric minizyme, in agreement with the observations made with the much longer HIV-1 tat mRNA. Thus, it is

Table 1 Kinetic parameters of the dimeric minizymes

Minizymes	k_{cat} (min^{-1})	$K_{d(app)}$ (μM)
2 bp dimeric minizyme	**0.006**	**1.0**
3 bp dimeric minizyme	**0.014**	**0.55**
4 bp dimeric minizyme	**0.042**	**0.067**
5 bp dimeric minizyme	**0.24**	**0.22**

*All reaction rates were measured, in 25 mM $MgCl_2$ and 50 mM Tris-HCl (pH 8.0), under ribozyme-saturating (single-turnover) conditions at 37°C. In all cases, kinetic measurements were made under conditions where all the available substrate was expected to form a Michaelis-Menten complex, with high concentrations of ribozyme (from 50 nM to 10 μM).

clear that, even for a short substrate, a stable common stem II is preferable.

In order to investigate the stability of the dimeric minizymes used in this study, I determined $K_{d(app)}$ for each under single-turnover conditions from Lineweaver-Burk plots. The $K_{d(app)}$ of the dimeric minizymes decreased with increasing numbers of G-C pairs in the stem II region of the dimeric minizyme. The previously determined $K_{d(app)}$ of the homodimeric minizyme with two G-C pairs was 5.1 μM and that of a homodimeric minizyme with four G-C pairs was 0.17 μM (Amontov and Taira, 1996). As compared with these values, in general, the values of $K_{d(app)}$ of the present dimeric minizymes (heterodimeric minizymes) tended to be lower. In accord with the previous observation, in general, the longer was the common stem II, the lower was the $K_{d(app)}$ value. However, for some unknown reason, the $K_{d(app)}$ of the 4 bp dimeric minizyme was unexpectedly low. The value of $K_{d(app)}$ for the 4 bp dimeric minizyme does not reflect the melting temperature for the dissociation of the dimeric structure, as described in the next section.

Melting curves for dimeric minizymes determined in the absence of substrates

In order to examine the effects of the G-C pairs in the stem II region on the stability of the dimeric minizymes, I investigated the melting properties of each dimeric minizyme in the absence of substrates. The reaction conditions for the generation of melting curves were the same as those in the kinetic experiments. In particular, the reaction mixtures included 25 mM $MgCl_2$. The concentrations of minizymes were 2 μM (higher than the respective values of $K_{d(app)}$). Moreover, in order to distinguish intermolecular melting from intramolecular melting, the dependence of Tm on the concentration of each minizyme was examined.

Table 2 Thermodynamic parameters

	2 bp dimeric minizyme	3 bp dimeric minizyme	4 bp dimeric minizyme	5 bp dimeric minizyme	Rz40'
Ea (kcal/mol)	29.0	27.2	24.0	20.0	21.1
$\Delta G^{\neq}$ (kcal/mol) at 35°C	21.2	21.0	20.7	20.1	20.5
$\Delta H^{\neq}$ (kcal/mol) at 35°C	28.4	26.6	23.4	19.4	20.5
$\Delta S^{\neq}$ (kcal/mol) at 35°C	23.4	18.2	8.8	-2.3	-0.2
Tm (°C) at 0.4 μM	51.0	55.0	59.8	61.3	---
Tm (°C) at 2 μM	55.0	57.5	62.0	64.8	---

Thus, thermal denaturation profiles were also recorded at the five-fold lower concentration of minizymes of 0.4 μM.

For the 2 bp dimeric minizyme, the Tm of stem II region was identified as 55°C at 2 μM minizymes, and it shifted to 51.0°C when a five-fold lower concentration (0.4 μM) of minizymes was used (Table 2). I identified the Tm of the G-C pairs in the 3 bp dimeric minizyme as 57.5°C, and it shifted to 55°C upon dilution. In this case, other melting temperatures were concentration-independent. For the 4 bp dimeric minizyme, the Tm of G-C pairs was 62.0°C at 2 μM, and the Tm shifted to 59.8°C at a five-fold lower concentration. The Tm for the 5 bp dimeric minizyme was determined to be 64.8°C. At a lower concentration, it shifted to 61.3°C. These data demonstrate that the Tm of dimeric minizymes that reflects the stability of the dimeric structure increased with increases in the length of the stem II regions: when the concentration of the minizymes was 2 μM, the Tm of the stem II regions of 2 bp, 3 bp, 4 bp, and 5 bp dimers were, respectively, 55.0°C, 57.5°C, 62.5°C, and 64.8°C (Table 2).

Arrhenius plots

Since the melting temperatures reported in the previous section represented the dissociation of dimers in the absence of any substrate, I next examined the thermal stability of each dimeric minizyme in the active complex with its substrate by examining the dependence of the cleavage activity on temperature. The substrate used in this analysis was same as that used for kinetic measurements (S19).

The activation energy for a reaction can be determined by measuring the rate constant of the reaction (k) at different temperatures and plotting $\ln k$ versus $1/T$ (to yield a so-called Arrhenius plot, *e.g.*, Fig. 7). The Arrhenius plot itself may be non-linear if different steps become

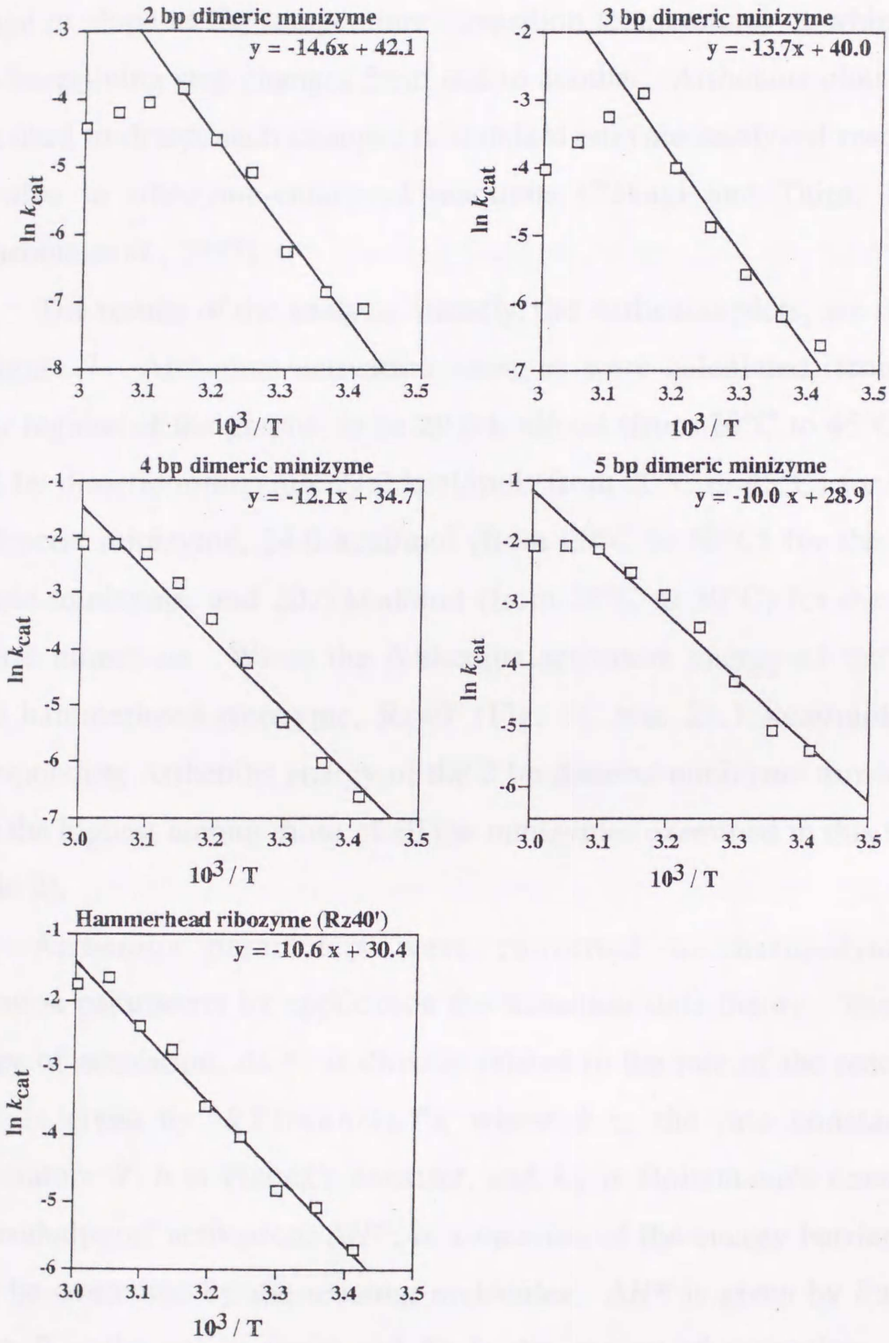

Figure 7 Arrhenius plots of data obtained from reactions with dimeric minizymes and Rz40' under single-turnover conditions. Reactions were carried out in 50 mM Tris-HCl (pH 8.0) and 25 mM $MgCl_2$. Concentrations: 5'-^{32}P-labeled substrate (S19), 50 nM; 2 bp dimeric minizyme, 5 μM; 3 bp dimeric minizyme, 3 μM; 4 bp and 5 bp dimeric minizyme, 2 μM; Rz40', 300 nM.

the rate-determining step at different temperatures (Takagi and Taira, 1995; Warashina *et al.*, 1997). In some cases, the plot may show a sharp change in slope at the temperature (transition temperature) at which the rate-determining step changes from one to another. Arrhenius plots have been used to detect such changes in standard enzyme-catalyzed reactions and also in ribozyme-catalyzed reactions (Takagi and Taira, 1995; Warashina *et al.*, 1997).

The results of the analysis, namely, the Arrhenius plots, are shown in Figure 7. Arrhenius activation energies were calculated, from the linear regions of the graphs, to be 29.0 kcal/mol (from 20°C to 45°C) for the 2 bp dimeric minizyme, 27.2 kcal/mol (from 20°C to 45°C) for the 3 bp dimeric minizyme, 24.0 kcal/mol (from 20°C to 50°C) for the 4 bp dimeric minizyme, and 20.0 kcal/mol (from 20°C to 50°C) for the 5 bp dimeric minizyme. While the Arrhenius activation energy of the full-sized hammerhead ribozyme, Rz40' (Fig. 5), was 21.1 kcal/mol, the corresponding Arrhenius energy of the 2 bp dimeric minizyme turned out to be the highest among those of all the minizymes examined in this study (Table 2).

Arrhenius parameters were converted to thermodynamic activation parameters by application the transition state theory. The free energy of activation, $\Delta G^{\neq}$, is directly related to the rate of the reaction. $\Delta G^{\neq}$ is given by $-RT\ln(kh/k_{B}T)$, where k is the rate constant at temperature T, h is Planck's constant, and k_{B} is Boltzmann's constant. The enthalpy of activation, $\Delta H^{\neq}$, is a measure of the energy barrier that must be overcome by the reacting molecules. $\Delta H^{\neq}$ is given by $Ea-RT$, where R is the gas constant and Ea is the energy of activation. The entropy of activation, $\Delta S^{\neq}$, is a measure of the fraction of reactants that have sufficient activation enthalpy and can actually react; $\Delta S^{\neq}$ includes,

for example, concentration and solvent effects, steric requirements and orientational requirements. $\Delta S^{\neq}$ is equivalent to $(\Delta H^{\neq} - \Delta G^{\neq})/T$.

The calculated energy parameters for the minizyme-catalyzed single-turnover reactions at 35°C are listed in Table 2. Naturally, $\Delta G^{\neq}$ (k_{cat}) is a function of $\Delta H^{\neq}$ and $T\Delta S^{\neq}$. It is of interest that, while $\Delta S^{\neq}$ is negative for the previously examined ribozyme (Takagi and Taira, 1995) and also for the relatively active ribozymes, such as Rz40' and 5 bp dimeric minizyme, examined in this study (Table 2), indicating a more precise conformation in the transition state than in the Michaelis-Menten complex, $\Delta S^{\neq}$ is positive for the less active dimeric minizymes, such as the 2 bp, 3 bp, and 4 bp minizymes (Table 2). This result indicates that the activated Michaelis-Menten complexes of the less active dimeric minizymes require more precise orientation than that of their respective transition-state structures. It is also to be noted that, while the value of $\Delta S^{\neq}$ differs dramatically among the minizymes, the discrepancy is compensated for by $\Delta H^{\neq}$, such that $\Delta G^{\neq}$ remains almost the same for all the ribozymes examined in this study.

In case of the dimeric minizymes with a short common stem II, as can be seen in Figure 7, the rate of the reaction decreased at high temperatures (above 45 to 50°C). This decrease occurred because the formation of active dimeric structures at such high temperatures was hampered by thermal melting. (Therefore, the rates of reactions above 45 to 50°C do not reflect k_{cat}.) This conclusion is in agreement with the deduction from the derivative curves of Tm that the disruption of dimeric structures, which depended on the stability of G-C pairs in the stem II region, began when the temperature was raised above 40°C. Therefore, in general, the shorter was the common stem II, the lower was the transition temperature for the loss of activity (Fig. 7).

Discussion

In this chapter, I examined a new form of shortened hammerhead ribozymes, namely, dimeric minizymes, in terms of their activities as gene-inactivating agents. Although the previously studied homodimeric minizyme, with two G-C pairs in the common stem II (Fig. 3), retained 65% of the activity of the parental hammerhead ribozyme (Fig. 2), the present analysis demonstrated that the longer is the common stem II, the higher is the cleavage activity of the dimeric minizyme, at least when the target site is part of HIV-1 tat mRNA. The activity was correlated with the stability of the dimeric minizymes, as determined from thermal melting curves, as well as from Arrhenius plots. Since these dimeric ribozymes successfully cleaved the long target RNA at two independent sites, it appears that the dimeric minizyme is a new variant of the conventional hammerhead ribozyme that has considerable potential utility as a gene-inactivating agent.

Chapter III

Formation *in vitro* and in cells of a catalytically active dimer by $tRNA^{Val}$-driven short ribozymes

Introduction

Hammerhead ribozymes catalyze the sequence-specific cleavage of RNA (Symons, 1989). Ribozymes, including hammerheads, are recognized as metalloenzymes (Kazakov and Altman, 1992; Dahm *et al.*, 1993; Piccirilli *et al.*, 1993; Steitz and Steitz, 1993; Eckstein and Lilley, 1996) and their mechanism of action is being clarified (Sawata *et al.*, 1995; Pontius *et al.*, 1997; Weinstein *et al.*, 1997; Zhou *et al.*, 1997; Lott *et al.*, 1998; Zhou and Taira, 1998). Recently, crystallographic studies by two groups have provided three-dimensional structures of hammerhead ribozymes in different configurations (Pley, 1994; Scott *et al.*, 1995, 1996), and the overall folding of the two reported structures is nearly identical. In the X-ray structures, the catalytic core is divided into two regions: domain I, consisting of nucleotides (nt) $C_3U_4G_5A_6$; and domain II, consisting of nt $G_{12}A_{13}A_{14}$ and $U_7G_8A_9$. A pseudo-A-form helix is formed by stems II and III (Fig. 1). Since the stem/loop II region appeared initially not to be directly involved in catalysis, attempts were made to delete extra sequences from this region (McCall *et al.*, 1992). For development of chemically synthesized ribozymes as potential therapeutic agents, it would certainly be advantageous to remove any surplus nucleotides that are not essential for catalytic activity. Such removal would obviously reduce the cost of synthesis, increase the overall yield of the desired polymer, and simplify purification. These considerations led to the production of minizymes, namely, conventional hammerhead ribozymes with a deleted stem/loop II region (McCall *et al.*, 1992; Tuschl and Eckstein, 1993; Fu *et al.*, 1994; Long and Uhlenbeck, 1994). However, the activities of the minizymes were two to three orders of magnitude lower than those of the parental hammerhead ribozymes, a result that led to the suggestion that

minizymes might not be suitable as gene-inactivating agents (Long and Uhlenbeck, 1994).

We found previously that some minizymes had high cleavage activities that were nearly identical to that of the wild-type parental hammerhead ribozyme (R32, Amontov and Taira, 1996). Moreover, the active species appeared to form dimeric structures with a common stem II (Fig. 3). I demonstrated that heterodimeric minizymes might be potentially useful as gene-inactivating agents since a heterodimer, because of its two independent catalytic cores, can cleave a single substrate at two independent sites simultaneously (Kuwabara *et al.*, 1996). For the application of such minizymes to gene therapy for the treatment of infectious diseases, it is also important to express them constitutively *in vivo* under the control of a strong promoter. As a first step toward this goal, I explored the possibility of using the promoter of a human gene for $tRNA^{Val}$, which is recognized by RNA polymerase III (Geiduschek and Tocchini-Valentini, 1988; Perriman and de Feyter, 1997). I examined whether $tRNA^{Val}$-embedded minizymes might be able to form catalytically competent dimeric structures. Since elucidation of the higher-order structure of dimeric minizymes is also of great interest to us, I performed NMR studies to examine the putative dimerization. Initially, I anticipated that the $tRNA^{Val}$ portion of the $tRNA^{Val}$-embedded minizymes might potentially cause steric hindrance that might inhibit dimerization. However, I confirmed, by gel-shift analysis and by kinetics, that the $tRNA^{Val}$-embedded minizyme could form an active dimer. Moreover, molecular modeling studies suggested a novel dimeric structure for the tRNA-embedded minizyme.

Most importantly, the $tRNA^{Val}$-embedded minizyme was found to be more active than the parental hammerhead ribozyme not only *in vitro*

but also in cultured cells. Therefore, $tRNA^{Val}$-embedded minizymes should be considered as potential candidates for gene-inactivating agents.

Materials and methods

Synthesis of ribozymes

Minizymes and their substrates were synthesized chemically on a DNA/RNA synthesizer [model 394; Perkin Elmer, Applied Biosystems (ABI), Foster City, CA]. Reagents for RNA synthesis were purchased from Glen Research (Virginia). Oligonucleotides were purified as described in the user bulletin from ABI (no. 53; 1989) with minor modifications. Further purification was performed by polyacrylamide gel electrophoresis, as described previously (Kuwabara *et al.*, 1996).

Construction of a plasmid for expression of tRNA-embedded ribozymes (tRNA^{Val}-Mz/pUC-dt and tRNA^{Val}-R32/pUC-dt)

Chemically synthesized oligonucleotides encoding a homodimeric minizyme (Fig. 8, bottom left) or a hammerhead ribozyme (R32) and pol III termination sequence (Geiduschek and Tocchini-Valentini, 1988) were converted to double-stranded sequences by PCR. After digestion with *Csp* 45 I and *Sal* I, the appropriate fragment was cloned downstream of the tRNA^{Val} promoter of tRNA^{Val}/pUC-dt (which contained the chemically synthesized promoter for a human gene for tRNA^{Val} between the *Eco*RI and *Sal* I sites of pUC19). The sequences of the constructs were confirmed by direct sequencing. Corresponding inactive ribozyme-coding plasmids were similarly constructed.

Preparation of tRNA^{Val}-embedded minizymes and the tRNA^{Val}-embedded hammerhead ribozyme by transcription

tRNA^{Val}-Mz/pUC-dt and tRNA^{Val}-R32/pUC-dt were used as DNA templates for PCR to construct the DNA templates for transcription. Primers were synthesized for each template, and the sense strand

contained the T7 promoter. Downstream of the promoter sequence, I inserted three G residues for more efficient transcription. Products of PCR were gel-purified. T7 transcription *in vitro* and purification were performed as described elsewhere (Kuwabara *et al.*, 1996).

Assay of the effect of the concentration of the pseudosubstrate on the cleavage activity of the heterodimeric minizyme

I examined the dependency on the concentration of the pseudosubstrate (PsS, Amontov and Taira, 1996) of the cleavage activity of the heterodimeric minizyme in 25 mM $MgCl_2$ and 50 mM Tris-HCl (pH 8.0), under substrate-saturating (multiple-turnover) conditions at 37°C. S11 was labeled with [γ-^{32}P]-ATP by T4 polynucleotide kinase (Takara Shuzo, Kyoto, Japan). The heterodimeric minizyme (MzL and MzR) was incubated at 1 μM with 3 μM S11, which contained a trace of 5'-^{32}P-labeled S11, at various concentrations of PsS (0 M, 200 nM, 500 nM, 750 nM and 1 μM). Reactions were usually initiated by the addition of $MgCl_2$ to a buffered solution that contained heterodimeric minizyme together with the substrate, and each resultant mixture was then incubated at 37°C. The cleavage activity increased linearly with increases in the concentration of the pseudosubstrate (data not shown), a clear demonstration that formation of the dimer was essential for efficient cleavage of the substrate and, moreover, that the dimeric structure could be stabilized in the presence of the (pseudo)substrate.

Kinetic measurements

Kinetic measurements of reactions catalyzed by $tRNA^{Val}$-Mz and $tRNA^{Val}$-R32 were performed with 2 nM 5'-^{32}P-labeled S11. Reaction rates were measured, in 25 mM $MgCl_2$ and 50 mM Tris-HCl (pH 8.0), under single-turnover conditions with high concentrations of $tRNA^{Val}$-

Mz and $tRNA^{Val}$-R32 (from 50 nM to 3 μM) at 37°C. The extent of cleavage was determined by quantitation of radioactivity in the bands of substrate and product with a Bio-Image Analyzer (BAS2000; Fuji Film, Tokyo).

NMR spectroscopy

NMR experiments were performed with an ALPHA-500 spectrometer (JEOL, 500 MHz for ^1H) and an AMX-600 (Bruker, 600 MHz for ^1H). The ^1H chemical shifts were determined relative to the internal standard, 2-methyl-2-propanol (1.23 ppm). All one-dimensional NMR spectra were collected in H_2O-D_2O (4:1, v/v) that contained 0.1 M NaCl and 10 mM phosphate buffer (pH 7.0) using a 1-1 solvent suppression sequence (Leontis *et al.*, 1995). The sample concentrations of R32 and the minizyme were 64 OD/mL and 30 OD/mL, respectively. Before NMR measurements, the samples were preheated to 90°C and slowly cooled to 5°C over 30 min.

Molecular modeling of tRNA embedded dimeric minizyme

Molecular model of the tRNA embedded dimeric minizyme was constructed from the coordinates of the crystal structure of the hammerhead ribozyme [NDB entries UHX026 (Pley *et al.*, 1994)] and yeast $tRNA^{Phe}$ [6TNA (Sussman *et al.*, 1978)]. Model of the dimeric minizyme was built as follows: the coordinate was transferred to PC-based software HyperChem (Hypercube, Inc.), and truncated at the $G_{10.1}$:$C_{11.1}$ pair in stem II. Then two copies of the truncated ribozyme were connected at the $G_{10.1}$:$C_{11.1}$ pair to give the geometry of an A-type helix. Next, I prepared the tRNA moiety by joining a canonical A-form RNA duplex at the G-U wobble pair of the acceptor stem, which resulted in a structure with 17 base pairs in an extended acceptor stem.

The overall model was made by connecting two extended acceptor stems of tRNA moieties with each stem I in the dimeric minizyme.

Gel-shift assay of the $tRNA^{Val}$-embedded enzymes

Two nM each of 5'-^{32}P-labeled $tRNA^{Val}$ RNA, $tRNA^{Val}$-R32 and $tRNA^{Val}$-Mz were incubated with 0, 200 nM, 1 μM, 10 μM and 30 μM of non-labeled respective RNA in 25 mM $MgCl_2$ and 50 mM Tris-HCl (pH 8.0) at 37°C for 20 minutes. The trace amount of $tRNA^{Val}$-Mz (2 nM) was also incubated with non-labeled $tRNA^{Val}$ RNA and loaded on the same non-denaturing gel. The reaction products were separated on a non-denaturing gel and the amounts of complexes were analyzed with a Bio-Image Analyzer (BAS2000).

Culture and transfection of cells

HeLa cells were cultured in Dulbecco's modified Eagle's medium (DMEM; Gibco BRL, Gaithersburg, MD) supplemented with 10% (v/v) fetal bovine serum (FBS; Gibco BRL). Transfection was carried out by using Lipofectin reagent (Gibco BRL) according to the manufacture's protocol.

Northern blotting analysis

Plasmid vectors $tRNA^{Val}$-Mz/pUC-dt, $tRNA^{Val}$-R32/pUC-dt and $tRNA^{Val}$/pUC-dt were used to transfect HeLa cells in combination with Lipofectin Reagents (Gibco-BRL, MD, USA). After culturing for 36 hours at 37°C, total RNA was isolated with ISOGEN™ (Nippon Gene Co., Toyama). Fifteen μg of total RNA per sample were denatured in glyoxal and dimethyl sulfoxide, subjected to electrophoresis in 2.4% NuSieve™ (3:1) agarose gel (FMC Inc., ME, Rockland), and transferred to a Hybond-N™ nylon membrane (Amersham Co., Buckinghamshire,

UK). The membrane was probed with synthetic oligonucleotides (5'-TTG CCT TTT CGC TCA GCC CCG TTT GTT GG-3', complementary to the sequence of minizyme; and 5'-GCC GTT TCG GCC TTT CGG CCT CAT CAG CCC CG-3', complementary to the sequence of R32) that had been labeled with ^{32}P by T4 polynucleotide kinase (Takara Shuzo Co., Kyoto). Prehybridization and hybridization were performed with the same solution (5x SSPE, 50% formamide, 5x Denhart's solution, 0.5% SDS, 150 mg/mL calf thymus DNA). Final washing was performed in 2x SSPE, 1% SDS at 50°C for 30 min.

Cleavage activities of RNAs extracted from HeLa cells

Thirty μg of total RNAs extracted from HeLa cells that had been transfected with $tRNA^{Val}$-Mz/pUC-dt or $tRNA^{Val}$-R32/pUC-dt were incubated with 2 nM ^{32}P-labeled S11 in a solution that contained 50 mM Tris-HCl (pH 8.0) and 25 mM $MgCl_2$ at 37°C. Cleavage products were analyzed as described above.

Luciferase assay

The target gene-expressing plasmid, which encoded the chimeric S11 sequence-luciferase gene (pGV-C2/S11), was constructed by inserting the following S11-containing sequence, caa aaa gct tgc cgt ccc ccg cag ctg gaa ttc aga tat cct gca gcc gtc ccc cga aag ctt ggc a, to pGV-C2 plasmid (PicaGene, Toyo-inki, Tokyo, Japan). Luciferase activity was measured with a PicaGene kit (Toyo-inki, Tokyo, Japan) as described elsewhere (Koseki *et al.*, 1997). In order to normalize the efficiency of transfection by reference to β-galactosidase activity, cells were co-transfected with pSV-β-Galactosidase Control Vector (Promega, Madison, WI) and then the chemiluminescent signal due to β-galactosidase was determined with a

luminescent β-galactosidase genetic reporter system (Clontech, Palo Alto, CA) as described previously (Koseki *et al.*, 1997).

Results

Detection of minizyme dimers by high-resolution NMR spectroscopy

We reported previously that some minizymes have cleavage activity that is nearly equal to that of the wild-type hammerhead ribozyme (Amontov and Taira, 1996). In the active minizymes, the linker sequences that replaced the stem/loop II region were palindromic so that two minizymes were capable of forming a dimeric structure with a common stem II. Since the result of kinetic analysis supported the proposed dimerization of minizymes, I decided to seek more direct evidence for the existence of a homodimeric minizyme by NMR spectroscopy. In solution in the absence of its substrate, the parental hammerhead ribozyme (R32, Fig. 8) consisted of not only the expected GAAA loop II, stem II, and the non-Watson-Crick three-base-paired duplex (consisting of U_7:A_{14}, G_8:A_{13}, and A_9:G_{12}) but also of an originally unexpected four-base-paired duplex (consisting of $G_{2.1}$:$C_{15.5}$, C_3:$G_{15.4}$, U_4:$G_{15.3}$, and G_5:$C_{15.2}$) that included a wobble G:U base pair (Fig. 8, Orita *et al.*, 1996). In this configuration, the recognition arms of R32 were unavailable (the substrate-recognition regions formed intramolecular base pairs).

NMR spectra for the minizyme in the absence of its substrate were recorded under conditions identical to those used for the parental ribozyme (Orita *et al.*, 1996). As indicated by dotted lines in the spectrum, recorded at 5°C (bottom right, Fig. 8), all the resonances of imino protons corresponding to those that were expected to be in a similar environment to those in R32 were recognized. The only imino proton in the minizyme that was expected to be in a different environment from that in R32 was the imino proton of $G_{10.1}$ because it should be sandwiched between A_9 and $C_{11.1}$ in the minizyme while it is sandwiched

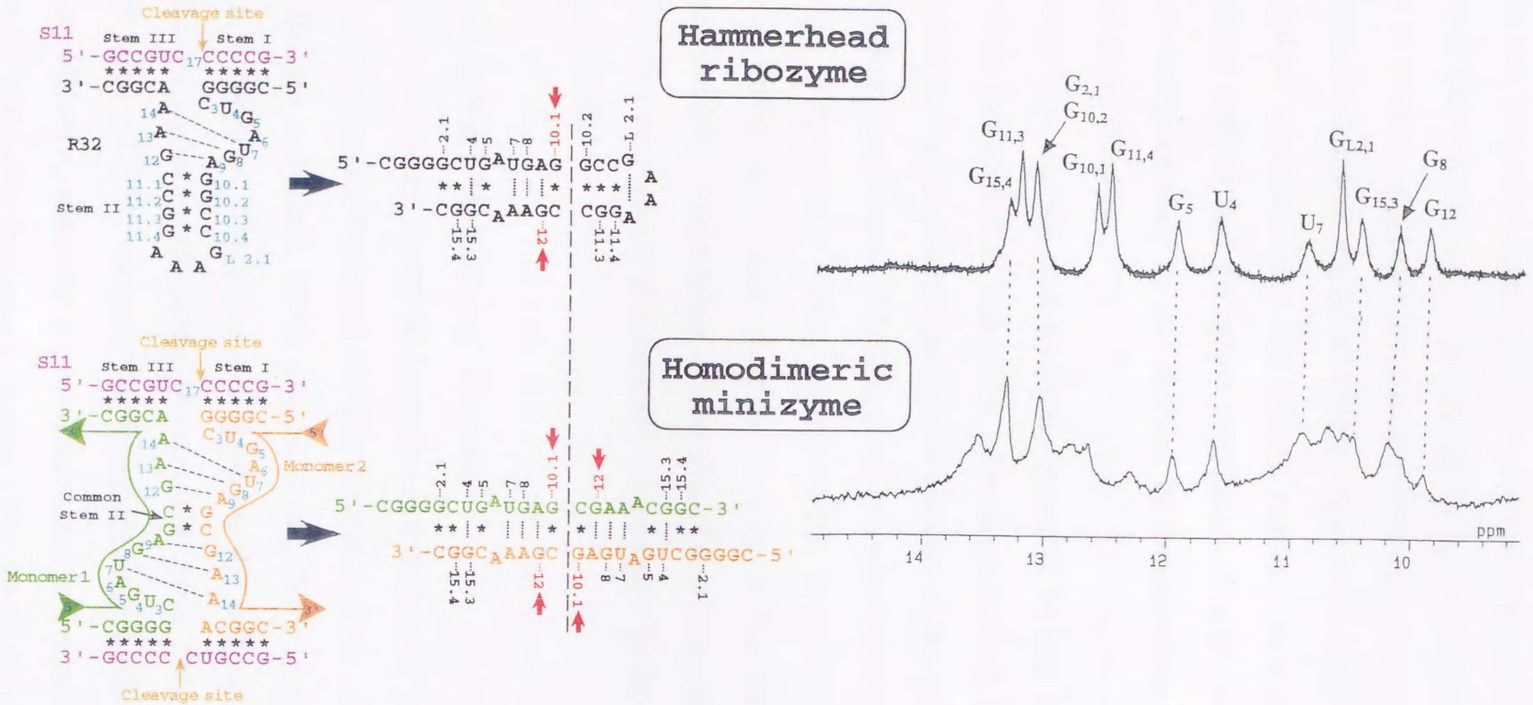

Figure 8 Secondary structures and NMR spectra of a hammerhead ribozyme (R32) and a minizyme. NMR spectra were recorded in the absence of the substrate (S11). Apparent secondary structures of R32 and the homodimeric minizyme are shown in the center, and the imino proton NMR spectra of R32 and a homodimeric minizyme [in 0.1 M NaCl, 10 mM sodium phosphate buffer (pH 7.0) at 5°C] are shown on the right.

between A9 and G10.2 in R32. The presence of the G12 signal strongly supports the proposed homodimeric structure of the minizyme in the absence of substrate since, if the minizyme had existed in a monomeric form, it is unlikely that the resonance of the G12 imino proton would occur with an identical chemical shift to that of the G12 imino proton in R32. Taken together with the kinetic results (data not shown), the observations suggest that the major population of minizymes should be in a dimeric form not only in the absence of the substrate but also in the presence of the substrate.

Since the signals due to imino protons of the minizyme were broader than those of R32 and since other signals were also detected, it appears that the homodimeric minizyme existed in the presence of other contaminating conformers. NMR spectra of imino protons changed with changes in temperature. The duplex of the homodimeric minizyme melted at a lower temperature than the melting of R32 (data not shown). The lower melting temperature of the dimeric minizyme was expected because of its intermolecular base-pairs, in contrast to the intramolecular base-pairs in R32.

Design of $tRNA^{Val}$ delivery vectors

Ribozymes have been shown to be potent inhibitors of gene expression and viral function (Sarver *et al.*, 1990; Altman, 1993; Marschall *et al.*, 1994; Sullenger and Cech, 1994; Leavitt *et al.*, 1996; Good *et al.*, 1997). There are, at present, two basic strategies for the delivery of ribozymes into cells: endogenous delivery, whereby a gene for a ribozyme is delivered into cells by means, for example, of a viral vector; and exogenous delivery, whereby a pre-synthesized ribozyme is applied to cells with or without a polymeric carrier. The small size of minizymes makes them amenable to chemical synthesis and modification for

exogenous delivery. One of the advantages of endogenously delivered ribozymes is that ribozymes that have no detrimental effects can be produced constitutively and continuously. Therefore, I have explored the possibility of the endogenous expression of minizymes.

Success in the use of ribozymes *in vivo* to knock out a specific gene depends not only on the selection of the target site but also on the design of the expression vector; the latter determines the level of expression, as well as the half-life of the expressed ribozyme (Eckstein and Lilly, 1996). The delivery and expression of ribozymes in eukaryotic cells have been achieved, for the most part, by use of RNA polymerase II-based (pol II-based) promoters. Although there is a large body of literature that suggests that pol II-based ribozyme constructs might be successful in reducing the activity of a target gene (Sun *et al.*, 1996), some studies have provided evidence for alternative modes of delivery, namely, RNA polymerase III-based (pol III-based) delivery systems (Perriman and de Feyter, 1997). While pol II promoters might allow tissue-specific or regulatable expression, pol III transcripts might be expressed at significantly higher levels. High-level expression under control of the pol III promoter would be advantageous for minizymes and enhance the likelihood of their dimerization. Therefore, I chose the promoter of a human gene for $tRNA^{Val}$, which has been used successfully in the suppression of target genes by ribozymes (Yamada *et al.*, 1994; Baier *et al.*, 1994; Yu *et al.*, 1995; Kawasaki *et al.*, 1996, 1998; Bertrand *et al.*, 1997).

The design of $tRNA^{Val}$-embedded ribozymes was based on the previous success in attaching a ribozyme sequence to the 3' side of the $tRNA^{Val}$ portion to yield a very active ribozyme that cleaved either p300 mRNA or CBP mRNA in cultured cells (Kawasaki *et al.*, 1996, 1998). The minizyme (Fig. 8, bottom left) was similarly embedded in the 3'

portion of the $tRNA^{Val}$ sequence ($tRNA^{Val}$-Mz). The parental hammerhead ribozyme (R32), which targets the same substrate (S11), was also embedded in the 3' portion of the $tRNA^{Val}$ sequence ($tRNA^{Val}$-R32). In both cases, extra sequences were inserted, so that (i) the transcript would not be processed by RNase P and (ii) the substrate-recognition arms would be more accessible upon disruption of the intramolecular stem.

Cleavage activities of $tRNA^{Val}$-embedded ribozymes *in vitro*

In the case of the $tRNA^{Val}$-embedded minizyme ($tRNA^{Val}$-Mz), I were initially worried about the possibility that the $tRNA^{Val}$ portion might cause severe steric hindrance that might inhibit dimerization, with resultant production of monomeric minizymes with extremely low activity. To our surprise, $tRNA^{Val}$-Mz had significant cleavage activity and the k_{cat} value of $tRNA^{Val}$-Mz was 7-fold higher than that of $tRNA^{Val}$-R32: The k_{cat} values for $tRNA^{Val}$-Mz and $tRNA^{Val}$-R32 were 0.3 min^{-1} and 0.04 min^{-1}, respectively. According to the computer prediction of the most stable secondary structure, both $tRNA^{Val}$-Mz and $tRNA^{Val}$-R32 appeared to have the same accessibility for binding of the substrate. Thus, I can conclude that the steric hindrance was minimal and the $tRNA^{Val}$-embedded minizymes could successfully form dimeric structures with strong catalytic activity.

In general, a naked ribozyme without extra sequences is more active than a ribozyme embedded within a long transcript (Heidenreich and Eckstein, 1992) and, therefore, we previously designed a trimming vector to avoid surplus sequences (Ohkawa *et al.*, 1993). In accord with this notion, the activity of R32 (Sawata *et al.*, 1995) fell by two orders of magnitude upon transcription as a hybrid with the $tRNA^{Val}$ portion. Although the $tRNA^{Val}$ portion also lowered the activity of the present

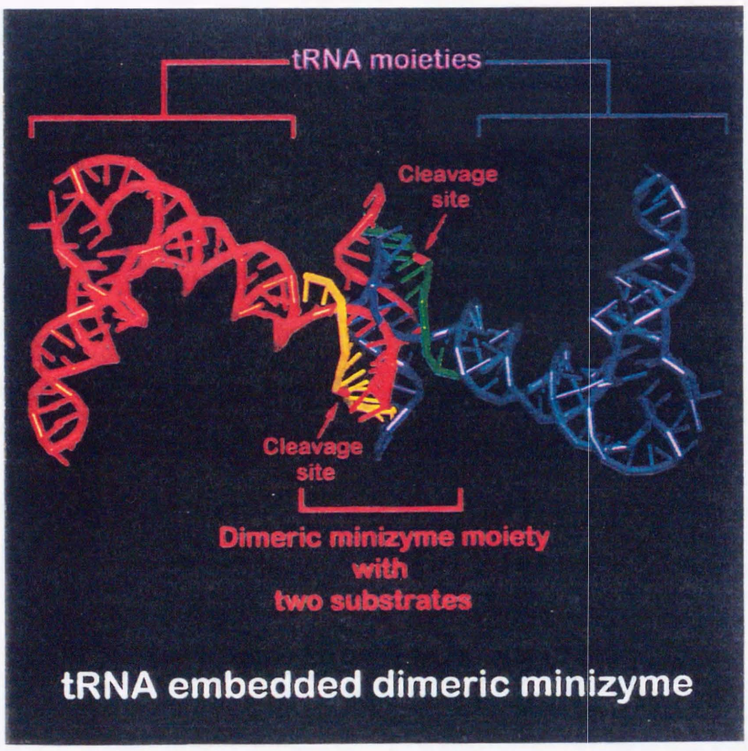

Figure 9 A model of the tRNA-embedded dimeric minizyme. In this model of the tRNA-embedded dimeric minizyme, the internal loop or linker is ignored and is assumed to be an A-form duplex. Each tRNA portion is shown in red or blue. The substrates (two molecules) are shown in yellow and green.

minizyme, the decrease was only about ten-fold. As a result, since both naked R32 and the corresponding naked minizyme had similar cleavage activity (Amontov and Taira, 1996), with a k_{cat} value of 2 to 4 min^{-1}, $tRNA^{Val}$-Mz turned out to be about 10-fold more active, upon being embedded into the $tRNA^{Val}$, than $tRNA^{Val}$-R32. The negative effect of the $tRNA^{Val}$ portion turned out to be smaller in the case of the minizyme than in the case of the parental hammerhead ribozyme.

Formation of dimeric structures by $tRNA^{Val}$-embedded minizymes

The $tRNA^{Val}$-embedded minizymes might be in an equilibrium between the monomeric and dimeric forms. Since the structural disturbance caused by the $tRNA^{Val}$ portion appeared less significant in $tRNA^{Val}$-Mz than in the parental $tRNA^{Val}$-R32, despite the fact that the former could function properly only as a dimer, I performed modeling studies, using the coordinates of the crystal structure of a hammerhead ribozyme (Pley *et al.*, 1994) and those of yeast $tRNA^{Phe}$ (Sussman *et al.*, 1978), to confirm that the formation of a homodimeric $tRNA^{Val}$-Mz would be feasible. In this modeling, two identical substrates, indicated in yellow and green were used (Fig. 9). Clearly, the resultant model structure appears feasible and steric hindrance by the two tRNA moieties is not a problem.

Next, I obtained more direct evidence, by gel-shift analysis in the absence of the substrate, for the formation of dimers by $tRNA^{Val}$-embedded minizymes (Fig. 10). As controls, $tRNA^{Val}$ transcripts, which contained a nonsense sequence between the $tRNA^{Val}$ portion and the terminator sequence, and $tRNA^{Val}$-R32 transcripts were also analyzed in parallel. Two nM each of 5'-^{32}P-labeled $tRNA^{Val}$ RNA, $tRNA^{Val}$-R32 and $tRNA^{Val}$-Mz were incubated with increasing concentrations of non-

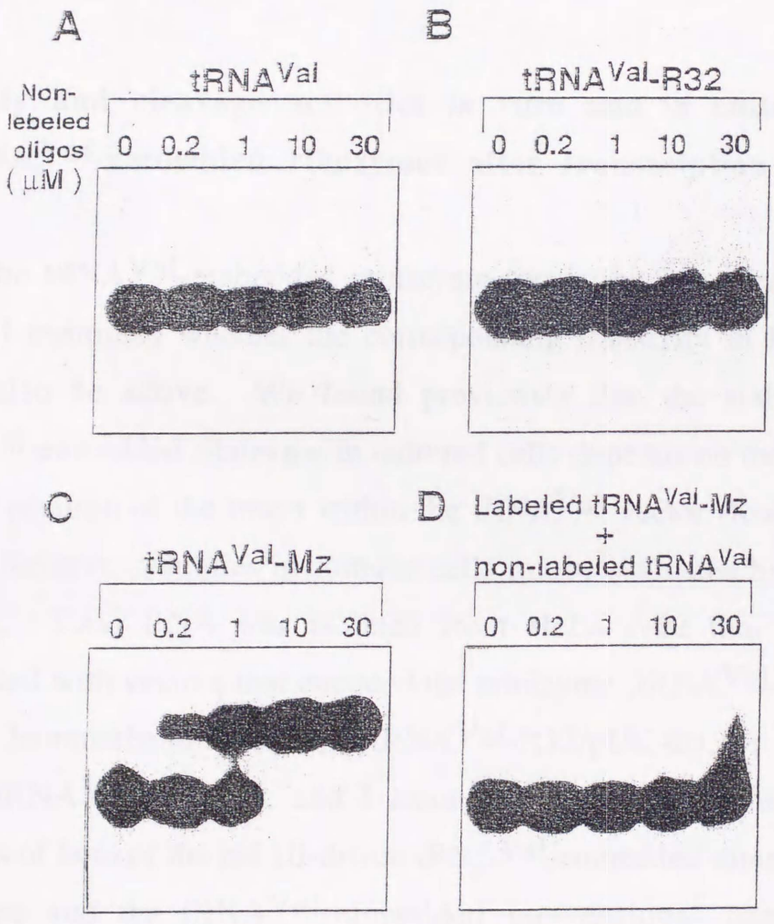

Figure 10 Detection of a dimeric form of $tRNA^{Val}$-Mz. Gel shift analysis reveals that the dimerization occurs only in the case of the $tRNA^{Val}$-Mz. Two nM of 5'-^{32}P-labeled $tRNA^{Val}$-enzyme was incubated with increasing amount of its non-labeled respective RNA in 25 mM $MgCl_2$ and 50 mM Tris-HCl (pH 8.0) at 37°C for 20 minutes. The $tRNA^{Val}$-Mz was also incubated with non-labeled $tRNA^{Val}$ RNA. The reaction products were separated on a non-denaturing gel.

labeled respective RNA. The trace amount of $tRNA^{Val}$-Mz (2 nM) was also incubated with non-labeled $tRNA^{Val}$ RNA and loaded on the same non-denaturing gel. Shifted bands (dimers) were observed only in the case of the $tRNA^{Val}$-Mz (Fig. 10). The dimeric form increased with increasing the concentration of the non-labeled $tRNA^{Val}$-Mz, supporting the intermolecular dimerization process. In contrast, the $tRNA^{Val}$-R32 and the $tRNA^{Val}$ transcripts remained in the monomeric form even at the concentrations of 30 μM.

Stability and cleavage activities *in vitro* and in cultured cells of $tRNA^{Val}$-embedded ribozymes after transcription in HeLa cells

Since the $tRNA^{Val}$-embedded minizyme transcribed *in vitro* was very active, I examined whether the corresponding transcript in HeLa cells might also be active. We found previously that the stability of a $tRNA^{Val}$-embedded ribozyme in cultured cells depends on the sequence and the position of the insert within the $tRNA^{Val}$ vector (Koseki *et al.*, 1999). Relative stabilities in cultured cells can be estimated by Northern blotting. Total RNA was isolated from HeLa cells that had been transfected with vectors that encoded the minizyme ($tRNA^{Val}$-Mz/pUC-dt), the hammerhead ribozyme ($tRNA^{Val}$-R32/pUC-dt), or $tRNA^{Val}$ itself ($tRNA^{Val}$/pUC-dt), and I examined levels of expression and activities of both of the pol III-driven $tRNA^{Val}$-embedded dimer-forming minizyme and the $tRNA^{Val}$-embedded conventional hammerhead ribozyme. Both $tRNA^{Val}$-Mz and $tRNA^{Val}$-R32 were expressed to a significant level in HeLa cells (Fig. 11A). Moreover, both transcripts were obviously stable in mammalian cells.

In order to confirm that the RNAs expressed in cultured cells had catalytic activity, I investigated cleavage of S11 by total RNA extracted

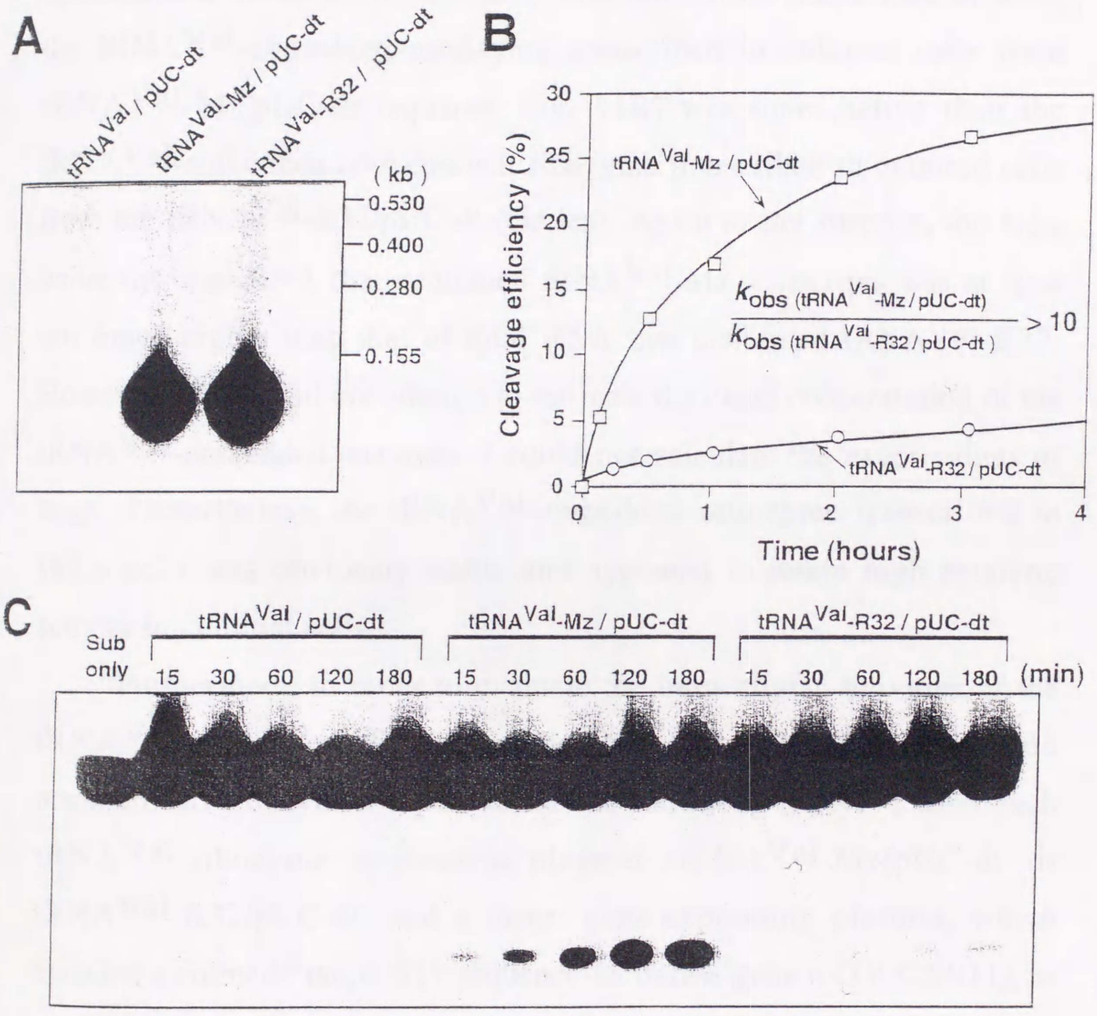

Figure 11 Expression and catalytic activities of the minizyme and a hammerhead ribozyme that were transcribed by pol III in cultured cells. (A) Northern blotting analysis on the expression of the pol III-driven minizyme and hammerhead ribozyme. The expression vectors tRNA^{Val}-Mz/pUC-dt, tRNA^{Val}-R32/pUC-dt and tRNA^{Val}/pUC-dt were used separately to transfect HeLa cells. Total RNA was extracted and transcripts were detected with probes that were complementary either to the minizyme or to R32. Time courses of the cleavage reactions (B) and cleavage activity of the extracted total RNAs (C) are also shown.

from HeLa cells that had been transfected with the various vectors (Figs. 11B and C). Although the equivalent amount of total RNA appeared to contain slightly more of the tRNA^{Val}-R32 transcript than the tRNA^{Val}-Mz transcript (Fig. 11A), I did not correct for this difference. In agreement with the results obtained with minizymes transcribed *in vitro*, the tRNA^{Val}-embedded minizyme transcribed in cultured cells from tRNA^{Val}-Mz/pUC-dt (squares, Fig. 11B) was more active than the tRNA^{Val}-embedded conventional ribozyme transcribed in cultured cells from the tRNA^{Val}-R32/pUC-dt (circles): Again to my surprise, the k_{obs} value for total RNA that contained tRNA^{Val}-Mz transcripts was at least ten times higher than that of total RNA that contained tRNA^{Val}-R32. However, since I did not attempt to estimate the exact concentration of the tRNA^{Val}-embedded enzymes, I could not calculate the exact values of k_{cat}. Nevertheless, the tRNA^{Val}-embedded minizyme transcribed in HeLa cells was obviously stable and appeared to retain high catalytic activity in cultured cells.

Furthermore, in order to evaluate the intracellular activities of the tRNA^{Val}-embedded dimeric minizymes and tRNA^{Val}-embedded hammerhead ribozymes, I performed the following assay. I used each tRNA^{Val}-ribozyme expression plasmid (tRNA^{Val}-Mz/pUC-dt or tRNA^{Val}-R32/pUC-dt) and a target gene-expressing plasmid, which encoded a chimeric target S11 sequence-luciferase gene (pGV-C2/S11), to co-transfect HeLa cells. After transient expression of both genes, in each cell lysate, I estimated the intracellular activity of each tRNA^{Val}-ribozyme by measuring the luciferase activity. The luciferase activity recorded when I used the target gene-expressing plasmid (pGV-C2/S11) was taken as 100% (Fig. 12). As other controls, tRNA^{Val}/pUC-dt, with only minimal tRNA^{Val} promoter and terminator sequences, and inactive minizyme- and inactive ribozyme-expression plasmids were also used.

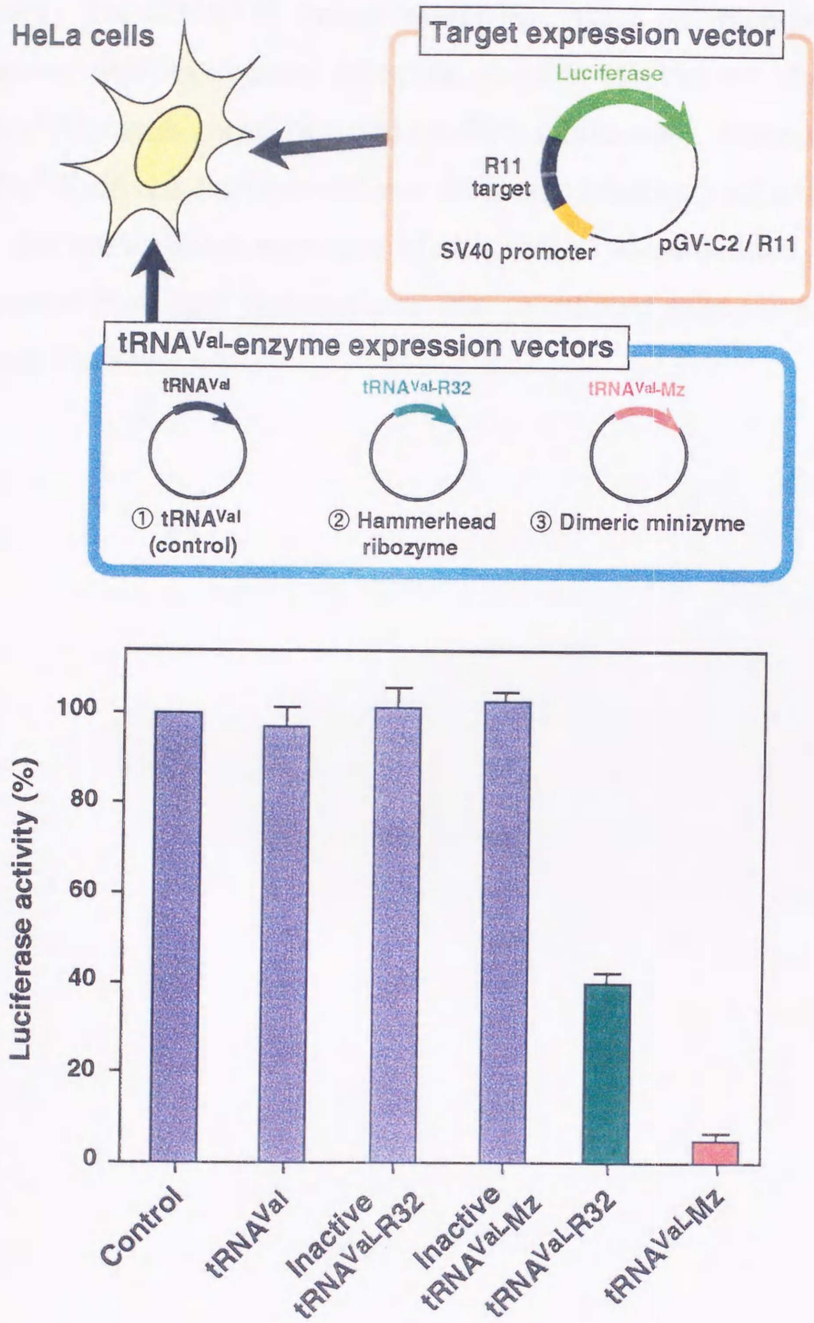

Figure 12 Activities of the $tRNA^{Val}$-embedded dimeric minizyme and hammerhead ribozyme in HeLa cells. Enzyme and target expression plasmids were used at 1:1 molar ratio to co-transfect HeLa cells. Luciferase activity was normalized based on the efficiency of transfection by reference to co-transfected β-galactosidase gene. The results are given as percentages relative to the control value of 100% (pGV-C2/S11). Potential errors in these values were found to be about 10% from results of triplicate experiments.

Inactive enzymes had a single G5→A5 substitution in the catalytic domain. The $tRNA^{Val}$-dimeric minizyme, which had high-level activity *in vitro*, was extremely effective (>95% inhibition), followed by $tRNA^{Val}$-hammerhead ribozyme (>55% inhibition). Since the inactive $tRNA^{Val}$-driven enzymes did not show any inhibitory effects, it is clear that the intracellular activities of the $tRNA^{Val}$-embedded ribozymes originated from their cleavage activities in cultured cells and not from the antisense effects.

Discussion

In the past, it was once believed that minizymes were significantly less active than the corresponding full-sized ribozymes. By contrast, the activities of the dimeric minizymes were demonstrated to be equal to those of the parental hammerhead ribozymes despite their smaller size (Amontov and Taira, *et al.*, 1996; Kuwabara *et al.*, 1996). Moreover, for the cleavage of a long substrate, namely, tat mRNA transcribed from HIV-1, synthetic minizymes were found to be more effective than "standard" ribozymes (Hendry *et al.*, 1995). The present study demonstrates that minizymes can be expressed by the use of tRNA vectors and the resultant $tRNA^{Val}$-embedded minizymes can form dimeric structures with high-level activities. Thus, not only chemically synthesized minizymes (McCall *et al.*, 1996; Hendry *et al.*, 1995) but also $tRNA^{Val}$-driven minizymes, including heterodimeric minizymes capable of cleaving a substrate at two independent sites simultaneously as described in chapter I, should be considered as potential gene-inactivating agents for use *in vivo*.

Chapter IV
Novel tRNA^{Val}-heterodimeric minizymes with high potential as gene-inactivating agents: Simultaneous cleavage at two sites in HIV-1 tat mRNA in cultured cells

Introduction

Hammerhead ribozymes catalyze the sequence-specific cleavage of RNA (Symons, 1989). Ribozymes, including hammerheads (Fig. 1), are metalloenzymes and their mechanism of action is being clarified (Zhou and Taira, 1998 and references therein). For the development of chemically synthesized ribozymes as potential therapeutic agents, attempts were made to remove any surplus nucleotides that are not essential for catalytic activity, leading to the production of initial minizymes, namely, conventional hammerhead ribozymes with a deleted stem/loop II region (McCall *et al.*, 1992; Thomson *et al.*, 1993; Tuschil and Eckstein, 1993; Fu *et al.*, 1994; Long and Uhlenbeck, 1994). However, the activities of the initial minizymes were two to three orders of magnitude lower than those of the parental hammerhead ribozymes and it seemed that minizymes might not be suitable as gene-inactivating agents (Long and Uhlenbeck, 1994).

In previous studies (Amontov and Taira, 1996), I found that some minizymes (Fig. 3) have high cleavage activity that is similar to that of the wild-type parental hammerhead ribozyme (Fig. 1). I demonstrated that these active minizymes formed dimeric structures with a common stem II, as shown in Figure 3. I then designed heterodimeric minizymes that can only form binding sites complementary to the substrate sequence when the individual minizymes form heterodimers. I later demonstrated *in vitro* that such heterodimeric minizymes, because of their two independent catalytic cores, could cleave HIV-1 tat mRNA (Fig. 6) at two independent sites simultaneously (Kuwabara *et al.*, 1996). I also found that increases in the length of the common stem II were associated with increases in the activity of heterodimeric minizymes *in vitro*. This is probably because minizymes with larger numbers of base pairs in the

common stem II formed a larger proportion of active heterodimers (Fig. 13) whereas, in the case of 2 bp heterodimeric minizymes (Fig. 13), the dimers were expected to generate a mixture of (2L•2L)-homodimers (consisting of two identical forms of minizyme left with 2 base pairs in the common stem II), (2R•2R)-homodimers (consisting of two identical forms of minizyme right), and the desired (2L•2R)-heterodimers (consisting of minizyme left and minizyme right). It is partly because of this mixed population of dimers that the activity of 2 bp minizymes was so low *in vitro* as compared with that of 5 bp minizymes. However, other studies demonstrated that the strand displacement activity of the cationic detergent CTAB (cetyltrimethylammonium bromide) enhanced the conversion of inactive misfolded minizymes, to active appropriately folded forms (Nakayama *et al.*, submitted for publication). As a result, even minizymes with a short common stem II such as 2 bp dimeric minizymes, which tend to form inactive structures *in vitro,* were found to have significant activity in the presence of CTAB, suggesting that they might be useful *in vivo*, in view of the fact that various facilitators of strand displacement reactions are known to exist *in vivo*.

In this study, I embedded two different minizymes (with 2 bp or 5 bp common stem II) and also a standard hammerhead ribozyme, separately, in the 3'-modified region of a human gene for $tRNA^{Val}$ so that each could be transcribed by RNA polymerase III (Tobian *et al.*, 1985; Geiduschek and Tocchini-Valentini, 1988; Cotten and Birnstiel, 1989; Yuyama *et al.*, 1992; Shore *et al.*, 1993; Baier *et al.*, 1994; Kandolf *et al.*, 1994; Perriman *et al.*, 1995; Thomson *et al.*, 1995; Kawasaki *et al.*, 1996; Li *et al.*, 1996; Bertrand *et al.*, 1997; Gebhard *et al.*, 1997; Perriman and de Feyter, 1997) because, for the application of these dimeric minizymes to gene therapy for the treatment of infectious

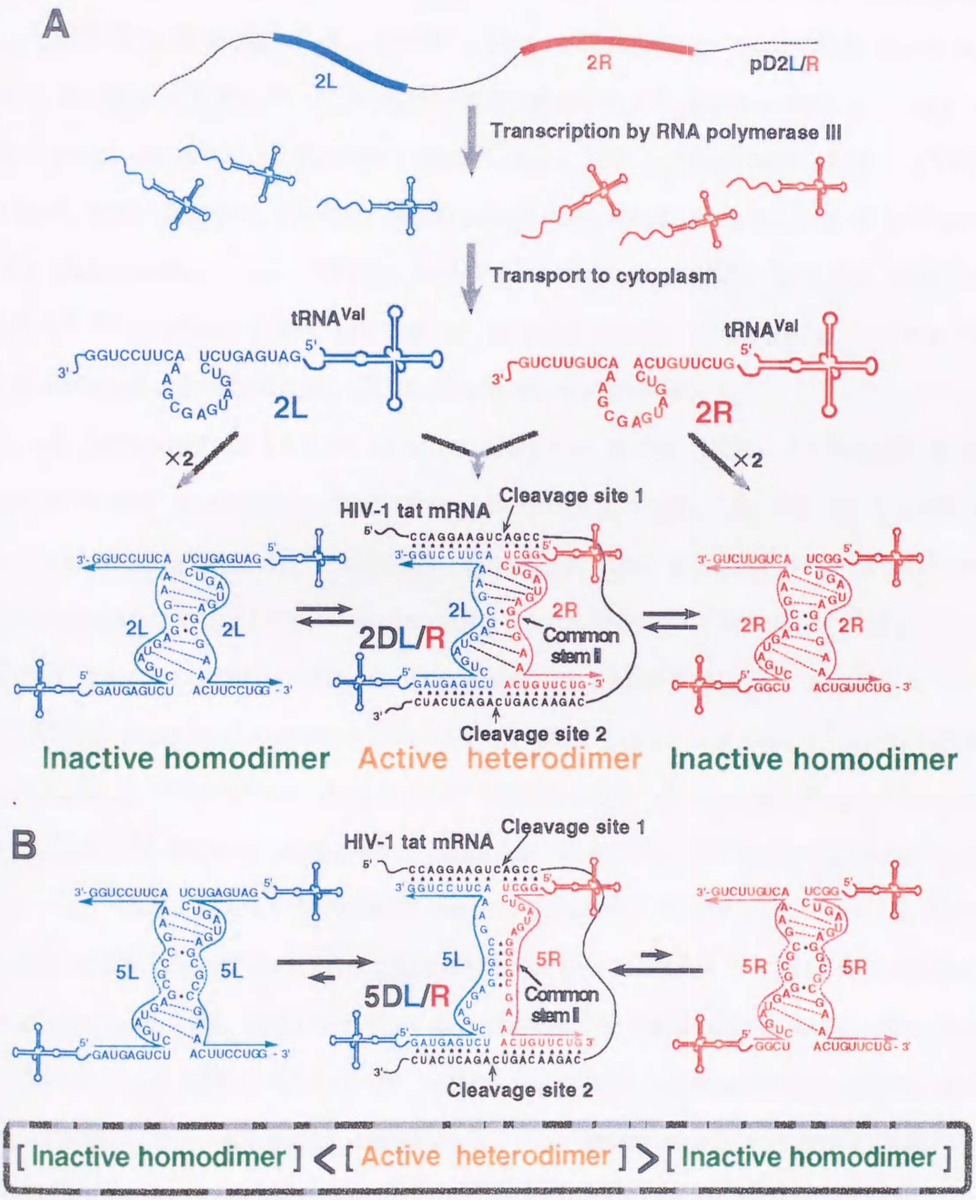

Figure 13 The active heterodimeric and inactive homodimeric forms of (A) the 2 bp or (B) the 5 bp dimeric minizymes under the control of a human $tRNA^{Val}$-promoter. (A) A large fraction of the population of dimers is expected to be in the inactive homodimeric forms. (B) The formation of active forms is favored because perfect base pairing occurs only in the case of active complexes.

diseases, such as AIDS, it is important that the minizymes be expressed constitutively and under the control of a strong promoter *in vivo*. The $tRNA^{Val}$-expression system enables the transcribed $tRNA^{Val}$-enzyme to be transported from the nucleus to the cytoplasm, thereby ensuring co-localization of the $tRNA^{Val}$-ribozyme with its target mRNA (Kuwabara *et al.*, 1998c; Koseki *et al.*, 1999). The co-localization of ribozymes and their target RNAs is a major determinant of high-level activity of ribozymes *in vivo* (Sullenger and Cech, 1993; Bertrand *et al.*, 1997). Indeed, this strategy yielded ribozymes that were very active in cultured cells (Kawasaki *et al.*, 1998), and I also demonstrated that the attached $tRNA^{Val}$-portion does not cause severe steric hindrance during the formation of a homodimer (Kuwabara *et al.*, 1998a).

I demonstrate in this chapter that the novel $tRNA^{Val}$-embedded heterodimeric minizymes had strong activities, regardless of the length of the common stem II. To my surprise, the $tRNA^{Val}$-embedded heterodimeric minizymes were able to reduce the level of HIV-1 tat mRNA more significantly in mammalian cells than could $tRNA^{Val}$-embedded standard hammerhead ribozymes under all sets of conditions that I tested. Therefore, despite the unfavorable dimerization process for the $tRNA^{Val}$-driven minizymes that are expected to generate a mixture (Fig. 13), the $tRNA^{Val}$-driven heterodimeric minizyme should have significantly higher activity than that of the $tRNA^{Val}$-driven standard ribozyme. Results indicate that the $tRNA^{Val}$-embedded heterodimeric minizymes are novel and more active than conventional ribozymes, and they should be powerful candidates for gene-inactivating agents in molecular biology, with potential utility in medicine as well.

Materials and methods

Construction of plasmids for expression of tRNA-embedded enzymes

Chemically synthesized oligonucleotides encoding each minizyme or the parental hammerhead ribozyme (Fig. 14) and the pol III termination sequence (Geiduschek and Tocchini-Valentini, 1988) were converted to double-stranded sequences by PCR. After digestion with *Csp* 45 I and *Sal* I, each appropriate fragment was cloned downstream of the $tRNA^{Val}$ promoter of pUC-dt (which contained the chemically synthesized promoter for a human gene for $tRNA^{Val}$ between the *Eco*RI and *Sal* I sites of pUC19). The sequences of the constructs were confirmed by direct sequencing.

Preparation of $tRNA^{Val}$-enzymes by transcription

Ribozyme-expression plasmids, p2L, p2R, p5L, p5R, pRz1 and pRz2 (Fig. 15), were used as DNA templates for PCR to construct the DNA templates for transcription. Primers were synthesized for each template, and the sense strand contained the T7 promoter. T7 transcription *in vitro* and purification were performed as described elsewhere (Kuwabara *et al.*, 1996).

Kinetic analysis

Kinetic parameters of the reactions catalyzed by the $tRNA^{Val}$-enzymes and the so-called non-embedded enzymes were measured with 2 nM 5'-^{32}P-labeled short substrate, S19 (5'-CAGAACA**GUC**AGACUCAUC-3'), which included GUC triplet-2 of HIV-1 tat mRNA (Fig. 6). In the assay of Rz1 or N-Rz1 (non-embedded Rz1), which cleaves tat mRNA at GUC triplet-1 (Fig. 5), a second short substrate [S16 (5'-

CCAGGAA**GUC**AGCCUA-3')] was used. Reaction rates were measured, in 25 mM $MgCl_2$ and 50 mM Tris-HCl (pH 8.0), under single-turnover conditions at 37°C (concentrations of enzymes: from 50 nM to 3 μM). The extent of cleavage was determined as described previously (Kuwabara *et al.*, 1996).

Luciferase assay

Luciferase activity (Fig. 16) was measured with a PicaGene kit (Toyo-inki, Tokyo, Japan) as described elsewhere (Kuwabara *et al.*, 1998a). In order to normalize the efficiency of transfection by reference to β-galactosidase activity, cells were co-transfected with pSV-β-Galactosidase Control Vector (Promega, Madison, WI) and then the chemiluminescent signal due to β-galactosidase was determined with a luminescent β-galactosidase genetic reporter system (Clontech, Palo Alto, CA) as described previously (Kuwabara *et al.*, 1998a).

Northern blotting analysis

The vectors shown in Figure 3A were used to transfect to LTR-Luc HeLa cells in combination with Lipofectin Reagent (Gibco-BRL, Rockville, MD). For the assay of expression of tat mRNA (Fig. 17), pCD-SRα tat (Fig. 16) was used (Takebe *et al.*, 1988; Koseki *et al.*, 1998). After culture for 36 hours at 37°C, total RNA was isolated with ISOGEN™ (Nippon Gene Co., Toyama). For the measurement of the steady-state level of HIV-1 tat mRNA (Fig. 17), cells were harvested 8, 20, or 36 h after transfection. Cytoplasmic RNA and nuclear RNA were separated as described previously (Huang and Carmichael, 1996). Thirty μg of total RNA per lane (50 μg for lanes in Fig. 17C) were loaded on a 3.0% NuSieve™ (3:1) agarose gel (FMC Inc., Rockland, ME), and then bands of RNA were transferred to a Hybond-N™ nylon membrane (Amersham

Co., Buckinghamshire, UK). The membrane was probed with synthetic oligonucleotides that were complementary to the sequences of respective ribozymes/minizymes (Kuwabara *et al.*, 1996). The synthetic probe complementary to the sequence of HIV-1 tat mRNA (indicated in Fig. 6)] was used for the determination of the localization and the steady-state level of HIV-1 tat mRNA. All probes were labeled with ^{32}P by T4 polynucleotide kinase (Takara Shuzo Co., Kyoto).

Results

Design of $tRNA^{Val}$-embedded minizymes

Successful inactivation by ribozymes of a specific gene *in vivo* depends not only on the selection of the target site but also on the design of the expression vector. The latter determines both the level of expression and the half-life of the expressed ribozyme (Sullenger and Cech, 1993; Bertrand *et al.*, 1997). While pol II promoters might allow tissue-specific or regulatable expression, pol III transcripts might be expressed at significantly higher levels (Perriman and de Feyter, 1997). High-level expression under control of the pol III promoter would clearly be advantageous if minizymes are to be used as therapeutic agents and it would enhance the likelihood of their dimerization. Therefore, I chose to express the minizymes under the control of the promoter of a human gene for $tRNA^{Val}$, which has previously been used successfully in the suppression of target genes by ribozymes (Kawasaki *et al.*, 1998; Ojwang *et al.*, 1992; Yu *et al.*, 1993; Yu *et al.*, 1995; Yamada *et al.*, 1994).

The specific design of the $tRNA^{Val}$-embedded enzymes was based on our previous success in attaching a ribozyme sequence to the 3' modified side of the $tRNA^{Val}$ portion of the human gene to yield very active ribozymes in cultured cells (Kawasaki *et al.*, 1998; Kuwabara *et al.*, 1998a, 1998c; Koseki *et al.*, 1999). The two different minizymes, which were targeted to HIV-1 tat mRNA at two sites simultaneously (Fig. 6), were embedded separately in the 3' modified portion of the $tRNA^{Val}$ sequence (Fig. 14). In order to compare the activities of the ribozymes in mammalian cells, I used the parental hammerhead ribozymes as controls. These ribozymes are designated Rz40 and Rz40' in my previous paper (Kuwabara *et al.*, 1996). As shown in Figure 14, in the present paper, non-embedded Rz40 and Rz40' were renamed N-Rz1 and

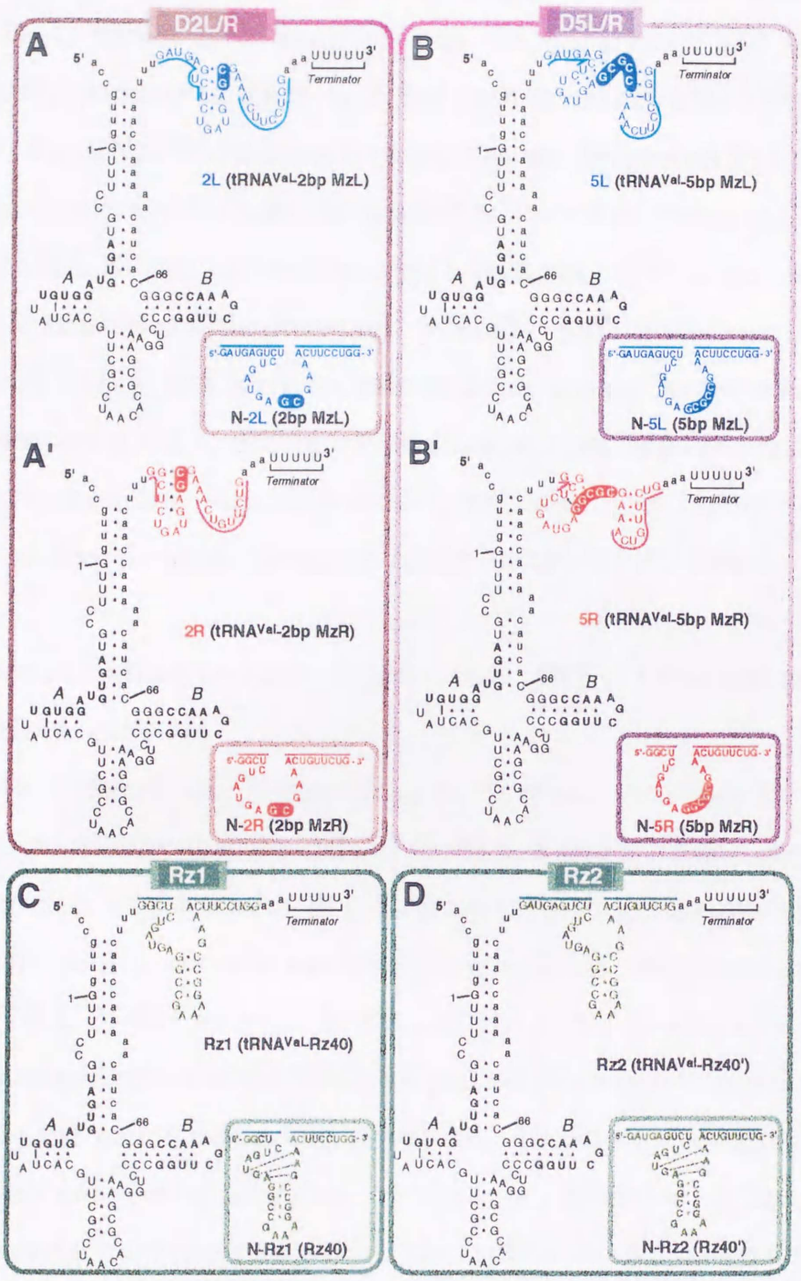

Figure 14 Predicted secondary structures, based on calculations by the MulFold program, of tRNA^{Val}-enzymes. The human tRNA^{Val} sequence, including the binding sites of transcription factor TFIIIC (labeled *A* and *B*, corresponding to the A and B box regions), is indicated in uppercase letters with numbering from 1 to 66. Extra sequences that were inserted artificially are indicated by lowercase letters. The sequences of L (minizyme left) and R (minizyme right) are shown in blue and red, respectively, and the sequences of standard ribozymes (C, D) are shown in green. Thick lines indicate the substrate-binding regions of the enzymes. The common stem II region of the dimeric minizymes (in panels A and B) are indicated by outlined letters within a solid ellipse.

N-Rz2, respectively. They targeted the same cleavage sites (GUC triplet-1 and GUC triplet-2, respectively) as the minizymes and were also embedded separately in the 3' modified portion of the $tRNA^{Val}$ sequence (Fig. 14; the $tRNA^{Val}$-embedded ribozymes are designated Rz1 and Rz2). In all cases, extra sequences, indicated by lowercase letters in Figure 14, were inserted, so that (i) the transcript would not be processed by RNase P; (ii) the structure of the transcript would be sufficiently similar to that of a tRNA so that to allow recognition by an export receptor for export to the cytoplasm and to ensure co-localization with its target; and (iii) the substrate-recognition arms, indicated by underlining in Figure 14, would be more accessible upon disruption of the intramolecular stem.

Significant steady-state levels of $tRNA^{Val}$-enzymes in mammalian cells

In the case of the $tRNA^{Val}$-embedded minizymes, I was initially worried about the possibility that the $tRNA^{Val}$ portion might cause severe steric hindrance that might inhibit dimerization, with resultant production of monomeric minizymes with extremely low activity. However, as can be seen in Table 3, the decrease in the activity of the minizyme transcript when it was embedded in the $tRNA^{Val}$ portion was smaller than that in the activity of the parental standard ribozyme. Therefore, I constructed pol III-driven enzyme-expression vectors to examine whether the corresponding transcripts might be also active in mammalian cells. I cloned the minizymes and the ribozymes downstream of a portion of the gene for $tRNA^{Val}$ (Fig. 15). Since I was also interested in the simultaneous expression of L and R (minizymes left and right) from one vector, I constructed enzyme-expression vectors that contained both pol III-driven L and R cassettes (Fig. 15 bottom; pD2L/R and pD5L/R). For comparison, I also generated the parental hammerhead ribozyme-

expression vector, pRz1/2, that contained both pol III-driven Rz1 and Rz2 cassettes.

The relative stabilities in cultured cells of transcripts from these $tRNA^{Val}$-embedded enzyme-expression vectors were estimated by Northern blotting. Transcripts of about 130 nucleotides in length (Fig. 15), which corresponded to the size of the $tRNA^{Val}$-enzymes, were detected in all samples of RNA that I isolated from cultures of LTR-Luc HeLa cells (Fig. 16) that had been transfected separately with each of the plasmids that encoded a $tRNA^{Val}$-enzyme(s) (Fig. 15). As can be seen from Figure 15, all $tRNA^{Val}$-embedded enzymes were expressed at significant levels in HeLa cells, and all transcripts were obviously stable in these mammalian cells. Steady-state levels of transcripts from the expression vectors with a pair of minizymes or ribozymes (pD2L/R, pD5L/R and pRz1/2; lower panel of Fig. 15) were slightly lower (Armentano *et al.*, 1987) than levels of similar transcripts transcribed from two independent vectors (for example, from p2L and p2R; upper panel of Fig. 15). Significant levels of expression and co-localization of a transcript with its target are prerequisites for effective ribozymes *in vivo*.

The intracellular activities of $tRNA^{Val}$-dimeric minizymes were higher than those of $tRNA^{Val}$-standard hammerhead ribozymes

In order to evaluate the intracellular activities of the $tRNA^{Val}$-embedded dimeric minizymes and $tRNA^{Val}$-embedded hammerhead ribozymes, I performed the following assay, using LTR-Luc HeLa cells that encoded a chimeric gene which consisted of the long terminal repeat (LTR) of HIV-1 and a gene for luciferase (Fig. 16). The LTR of HIV-1 contains regulatory elements that include a TAR region. The HIV-1 regulatory protein, Tat, binds to TAR and the binding of Tat stimulates transcription

Table 3 Kinetic parameters of reactions catalyzed by the $tRNA^{Val}$-embedded enzymes and the corresponding non-embedded enzymes.

		k_{cat} (min^{-1})	K_M (μM)	k_{cat}/K_M ($\mu M^{-1}min^{-1}$)
$tRNA^{Val}$-embedded enzymes	D2L/R	0.00013	0.88	0.00015
	D5L/R	0.057	0.028	2.0
	Rz1	0.083	0.15	0.55
	Rz2	0.065	0.13	0.50
Non-embedded enzymes	N-D2L/R	0.006	1.0	0.006
	N-D5L/R	0.24	0.22	1.1
	N-Rz1	0.85	0.040	21
	N-Rz2	0.55	0.020	28

Rate constants were measured, in 50 mM Tris-HCl (pH 8.0) and 25 mM $MgCl_2$, under single-turnover conditions at 37°C. In the assays of Rz1 and N-Rz1, which cleaved HIV-1 tat mRNA at GUC triplet-1 (Fig. 6), a short 16-meric substrate (S16) was used. Except in these two cases, a 19-meric short substrate (S19), which contained GUC triplet-2 of tat mRNA, was used.

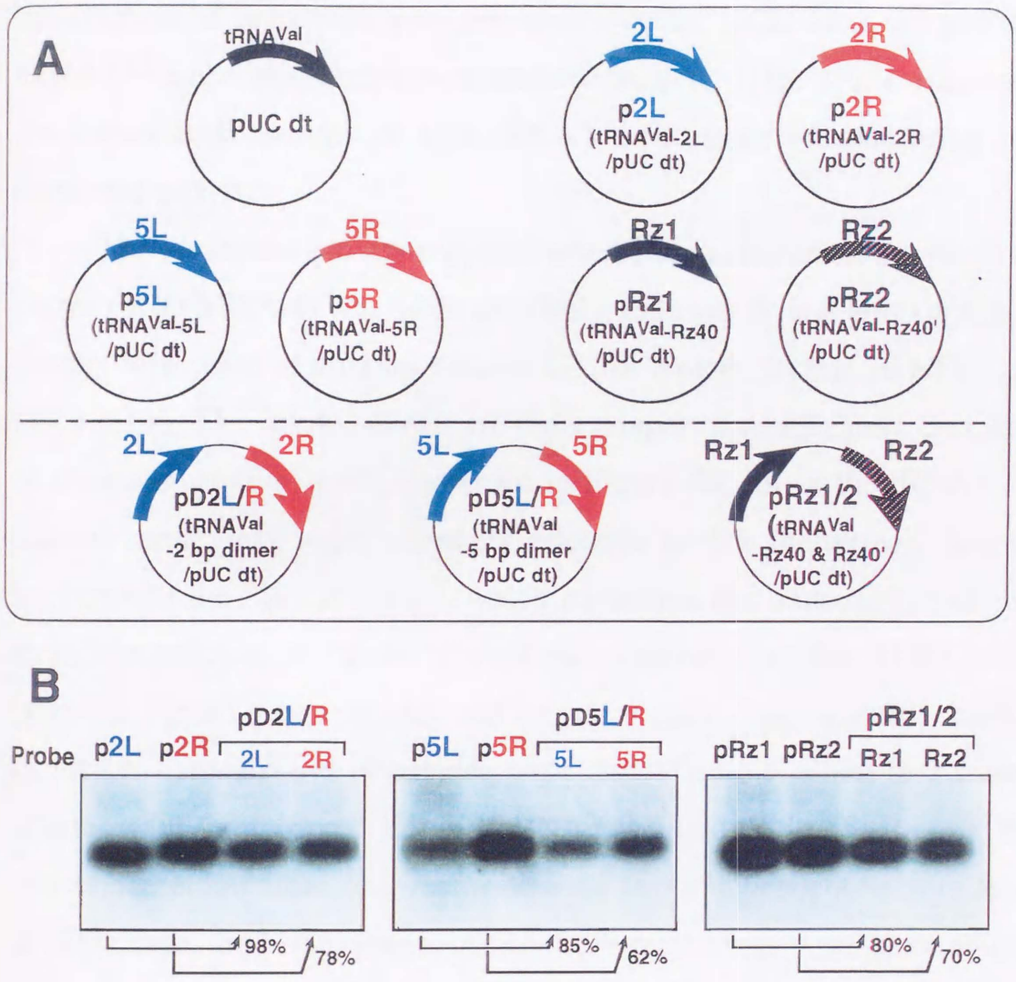

Figure 15 Schematic representation of the vectors encoding $tRNA^{Val}$-enzymes (A), and the steady-state levels of expressed $tRNA^{Val}$-enzymes (B). When vectors encoding two $tRNA^{Val}$-enzyme cassettes (lower panel in Figure 15A) had been used to transfect cells, the probe that were complementary to the sequences of respective ribozymes/minizymes was used independently. The percentage decrease in the level of expression from the vector with two cassettes (lower panel in Figure 15A), as compared to that from the corresponding vector with one cassette (upper panel in Figure 15A), is shown by an arrow in each cases.

substantially. Therefore, luciferase activity originating from the chimeric LTR-Luc gene increases in response to increases in the concentration of Tat (Koseki *et al.*, 1998). Measurements of luciferase activity allowed us to monitor the effects of $tRNA^{Val}$-embedded enzymes on the Tat-mediated transcription of the chimeric LTR-Luc gene. After transient expression of both Tat and $tRNA^{Val}$-embedded enzymes by co-transfection of cells with a tat expression-vector (pCD-SRα tat) and the $tRNA^{Val}$-embedded enzyme-expression vector(s) (Fig. 15), I estimated the intracellular activity of each $tRNA^{Val}$-ribozyme by measuring the luciferase activity.

The luciferase activity recorded when I used only the tat-expressing vector (pCD-SRα tat) was taken as 100%. Enzyme(s)- and tat-expression vectors were used at a molar ratio of 2:1 for co-transfection of LTR-Luc HeLa cells. The results shown are the averages of results from five sets of experiments (Fig. 16). As shown in Figure 4B, all of the $tRNA^{Val}$-dimeric minizymes were extremely effective (>90% inhibition), despite the fact that the SRα promoter, which controlled the transcription of the target tat mRNA, is 10- to 30-fold more active than the SV40 early promoter regardless of species and origin of cells (Takebe *et al.*, 1988). $tRNA^{Val}$-hammerhead ribozymes were also effective, albeit to a lesser extent (>60% inhibition). Clearly, $tRNA^{Val}$-L and $tRNA^{Val}$-R could be transcribed either from one vector or from two independent vectors and, in either case, the heterodimers of $tRNA^{Val}$-minizymes were more active than the standard $tRNA^{Val}$-ribozymes.

To my surprise, the $tRNA^{Val}$-embedded 2 bp dimeric minizyme (D2L/R; lanes 10 and 15), which had very weak activity *in vitro* (Table 3), turned out to have a very strong inhibitory effect in mammalian cells. This result is in accord with the separate finding that, in the presence of various facilitators of strand-displacement reactions that are known to

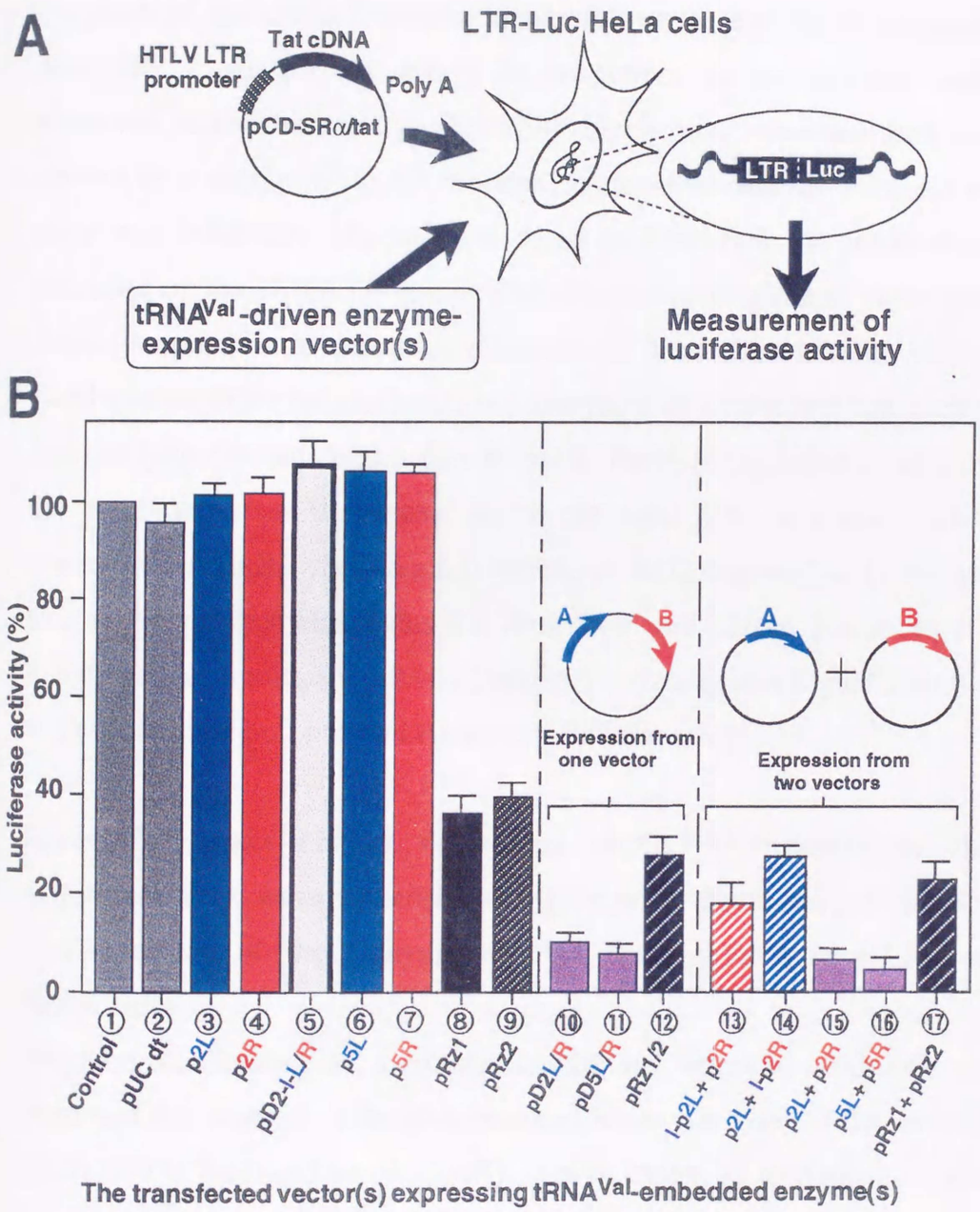

Figure 16 Assay system for measurements of activities of $tRNA^{Val}$-enzymes in LTR-Luc HeLa cells (A) and the effects of $tRNA^{Val}$-enzymes on the Tat-mediated transcription of the chimeric LTR-Luc gene (B).

exist *in vivo*, 2 bp dimeric minizymes are almost as active as 5 bp dimeric minizymes (Nakayama *et al.*, submitted for publication). It is important to note that, since each separate $tRNA^{Val}$-minizyme (2L, 2R, 5L and 5R, lanes 3, 4, 6, 7) did not, by itself, have any inhibitory effects, the activities of the $tRNA^{Val}$-embedded minizymes must have originated from the formation of active heterodimers in mammalian cells. Moreover, since the inactive $tRNA^{Val}$-driven minizymes that had been created by a single G^5 to A^5 mutation within the catalytic core did not show any inhibitory effects (lane 5), it is clear that the intracellular activities of the $tRNA^{Val}$-embedded ribozymes originated from their cleavage activities in cultured cells and not from the antisense effects. Combination of active and inactive minizymes demonstrated that each of two catalytic domains was active by itself: Note, for example in lane 13, the combination of the active minizyme right (2R) and the inactive minizyme left (I-2L) created a heterodimeric minizyme with only the half site active, nevertheless, the resulting half site active heterodimeric minizyme had significant activity [indeed, its activity was higher than that of the corresponding parental ribozyme, Rz1 (lane 8)].

Successful transport of expressed $tRNA^{Val}$-enzymes to the cytoplasm that ensured co-localization with their target mRNA and detection of the cleavage of HIV-1 tat mRNA in LTR-Luc HeLa cells

Since co-localization of a ribozyme with its target is obviously an important determinant of the ribozyme's efficiency *in vivo* (Sullenger and Cech, 1993; Bertrand *et al.*, 1997), it was essential to determine the intracellular localization of the $tRNA^{Val}$-enzymes. Total RNA from LTR-Luc HeLa cells that had been transfected with each expression vector was separated into nuclear and cytoplasmic fractions. Then levels

of each transcribed enzyme were examined by Northern blotting analysis with a probe specific for the minizyme or ribozyme. As shown in Figure 17 and as expected from the properties of the $tRNA^{Val}$-expression system (Koseki *et al.*, 1998), all $tRNA^{Val}$-embedded enzymes were found in the cytoplasmic fraction and none was detected to any significant extent in the nuclear fraction. U6 snRNA, which is known to remain in the nucleus, was included in these studies as a control (Fig. 17, lower panel). I then investigated the localization of the target tat mRNA in LTR-Luc HeLa cells by Northern blotting with a probe specific for HIV-1 tat mRNA. As shown in Figure 17 and as I had anticipated, I found tat mRNA predominantly in the cytoplasmic fraction. Thus, the $tRNA^{Val}$-driven enzymes were co-localized with the target tat mRNA (Fig. 17).

In order to confirm directly that the inhibitory effects of the novel dimeric minizymes originated from the cleavage of tat mRNA, I performed Northern blotting analysis (Fig. 17). I determined the time courses of the reduction in level of HIV-1 tat mRNA by $tRNA^{Val}$-embedded enzymes. Total RNA from LTR-Luc HeLa cells that had been transfected with the tat-expression plasmid (pCD-SRα tat) and the plasmid encoding each $tRNA^{Val}$-enzyme was extracted 8, 20, and 36 hours after transfection. Then the amount of tat mRNA was determined as shown in Figure 17. The length of the cleaved fragments was exactly as anticipated (Kuwabara *et al.*, 1996). I confirmed, by mixing cells producing only the substrate and other cells producing only the enzyme before the isolation of total RNA, that the cleavage of mRNA did not occur during my RNA isolation procedure (Kuwabara *et al.*, 1998c). No reduction in the level of expressed tat mRNA was noted in the case of the control (transfection with pUC dt) and this level of tat mRNA was taken as 100%. As can be seen in the lowest panel of Figure 17, it is clear that the decrease in the steady-state level of tat mRNA was more apparent in

cells that produced $tRNA^{Val}$-minizymes than in those that produced $tRNA^{Val}$-standard ribozymes. These results were in good agreement with the results of the assays of luciferase activity shown in Figure 16. The heterodimeric minizymes cleaved the target mRNA more efficiently, in mammalian cells, than the combination of the two independent standard ribozymes.

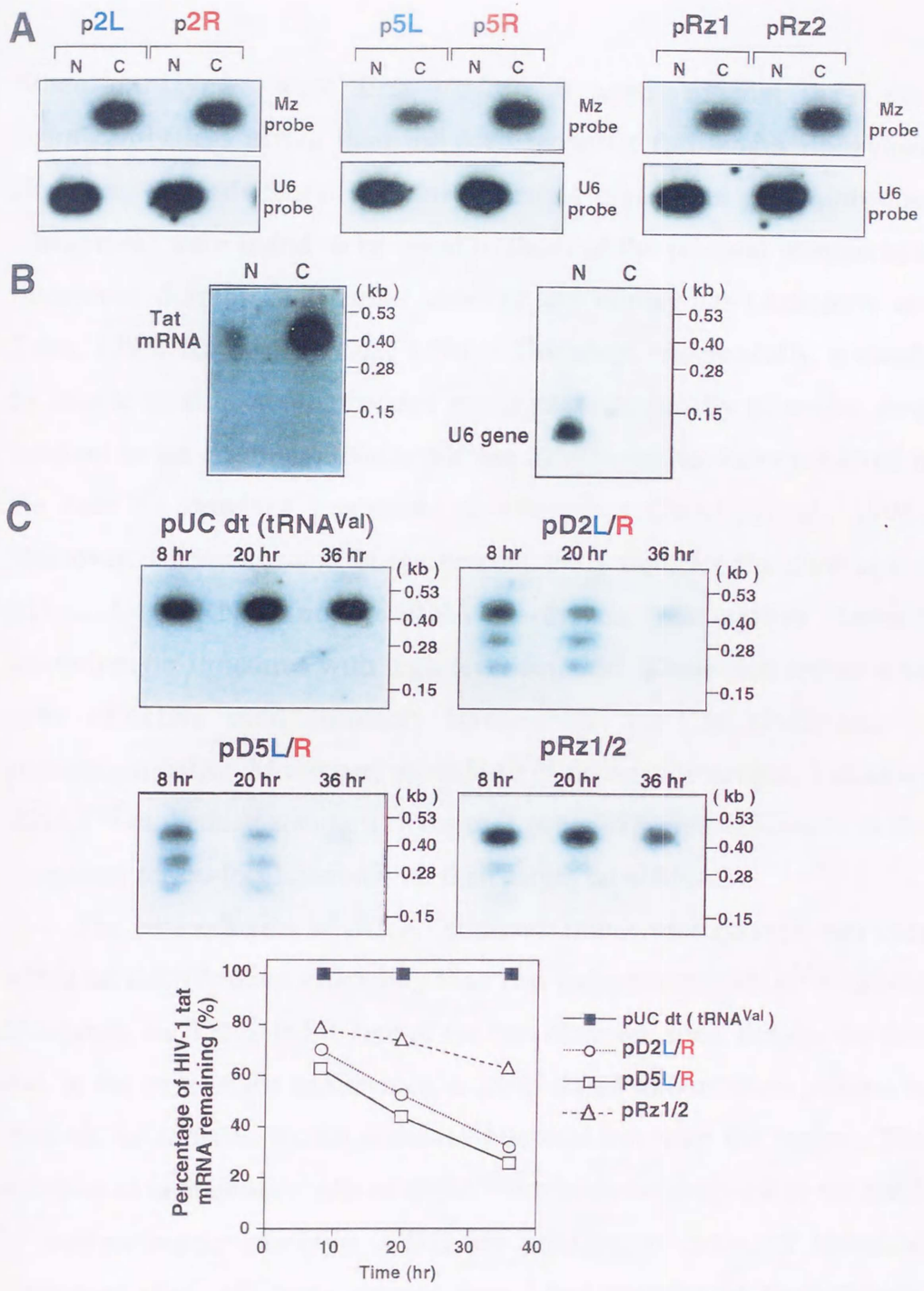

Figure 17 Intracellular localization of expressed $tRNA^{Val}$-enzymes (A) and of tat mRNA (B). U6 snRNA, which remains in the nucleus, was included as a control. Time courses of reductions in levels of HIV-1 tat mRNA by the expressed $tRNA^{Val}$-enzyme(s) are also shown in Figure 17C (calculations were based on densitometric measurements from autoradiograms).

Discussion

When minizymes were first studied, it appeared that they were significantly less active than the corresponding full-length ribozymes. However, the activities of the novel dimeric minizymes (non-embedded minizymes) were found to be equal to those of the parental hammerhead ribozymes despite the smaller sizes of the minizymes (Amontov and Taira, 1996; Kuwabara *et al.*, 1996). Therefore, theoretically, I should be able to modify non-embedded minizymes chemically to render them resistant to intracellular RNases for use *in vivo*, as has been achieved in the case of standard hammerhead ribozymes (Jarvis *et al.*, 1996). Moreover, I demonstrated in the present study that, for the cleavage of HIV-1 tat mRNA, novel $tRNA^{Val}$-driven minizymes formed heterodimeric structures with high-level activity. These minizymes were more effective than similarly transcribed standard ribozymes in mammalian cells. Moreover, all $tRNA^{Val}$-driven transcripts, including $tRNA^{Val}$-embedded standard ribozymes, were exported efficiently to the cytoplasm for co-localization with their target tat mRNA.

The heterodimers of $tRNA^{Val}$-driven minizymes cleaved two sites within tat mRNA more efficiently than two independent $tRNA^{Val}$-driven ribozymes, each targeted to one of the two cleavage sites, despite the fact that, in the case of the minizymes, a complicated dimerization process is involved in addition to the process of association with the target. The activities in mammalian cells of $tRNA^{Val}$-minizymes (especially for the 2 bp heterodimeric minizyme, D2L/R) relative to those of standard ribozymes (Fig. 16) were greater than I had anticipated from kinetic parameters determined *in vitro* (Table 3). In general, the rate-limiting step of a reaction mediated by a catalytic RNA, such as a ribozyme, *in vivo* has been considered to be the substrate-binding step (Crisell *et al.*,

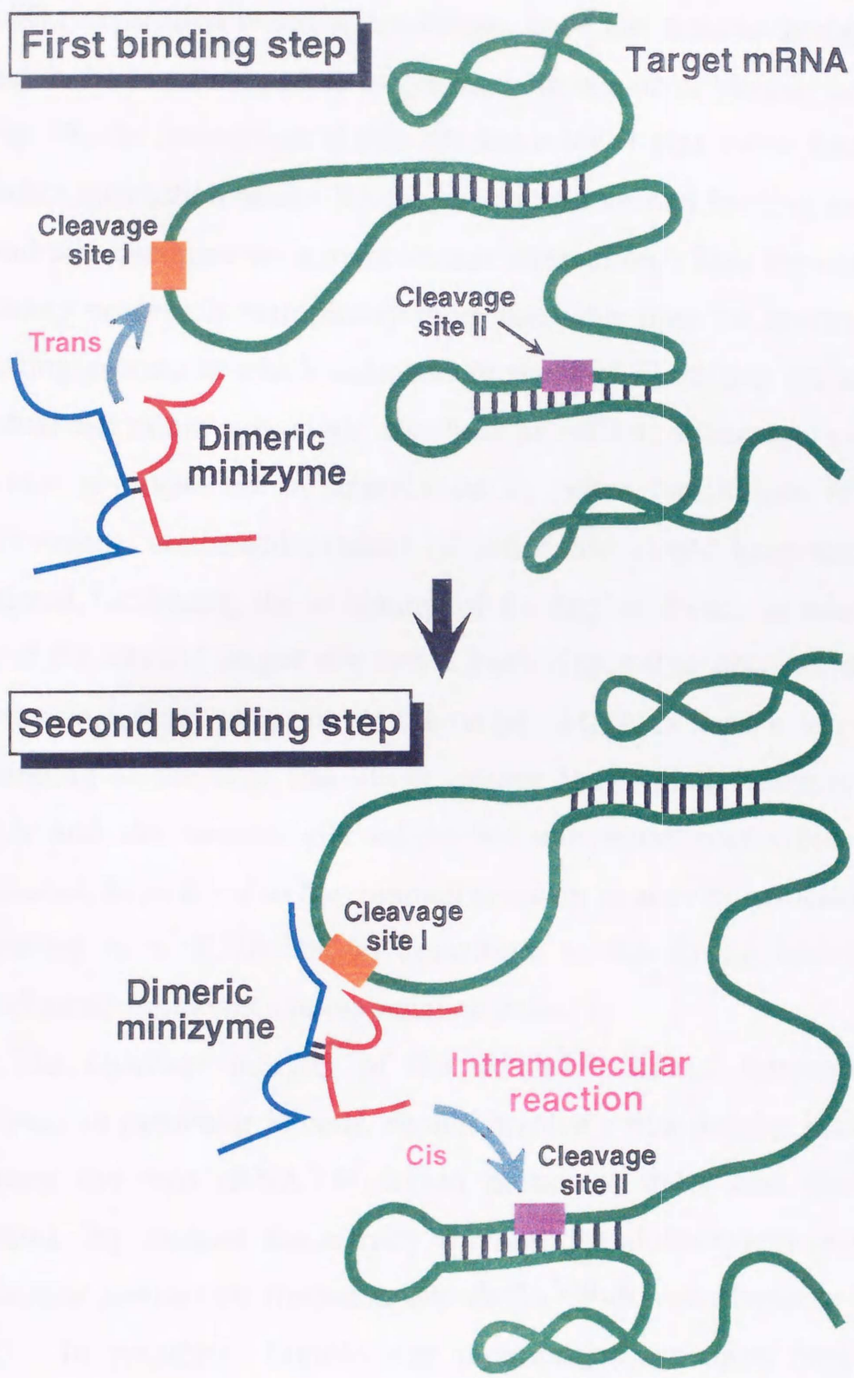

Figure 18 Schematic representation of the cleavage of an mRNA at two sites by a dimeric minizyme.

1993; Ellis and Rogers, 1993; Sullenger and Cech, 1993; Eckstein and Lilley, 1996; Kronenwett *et al.*, 1996; Bertrand *et al.*, 1997; Nedbal and Sczakiel, 1997; Sioud, 1997; Sioud and Jesperson, 1997). Under such k_{cat}/K_M controlled reaction conditions, once the dimeric minizyme has bound to the more accessible target site with one of its binding arm (site I in Fig. 18; the interaction at this site has a lower K_M value than that of the other interaction at site II), the subsequent second binding step at the second site becomes an intramolecular interaction. This intramolecular annealing process is entropically more favorable than the intermolecular annealing process in which independent standard ribozymes are involved. The dual-site minizymes might also have an off-rate advantage, i.e., while one site is displaced by translation or other facilitators of strand displacement, continued binding of other site would keep the RNAs associated, facilitating the re-binding of the displaced site. In other cases, even if the second target site has a high K_M value because of some undesirable tertiary structure of the target mRNA (a hidden target site), the binding at the first site might change the overall structure of the mRNA and the second site might become more accessible. Such phenomena, in addition to the minimal decrease in activity associated with embedding in a tRNA, might contribute to the strong activities of heterodimeric minizymes in mammalian cells.

The cleavage activity of the $tRNA^{Val}$-driven heterodimeric minizyme, in particular in cells, should involve a trimolecular interaction (between the two $tRNA^{Val}$-driven monomer units and the target substrate). By contrast, the activity of conventional ribozymes involves a bimolecular interaction (between one $tRNA^{Val}$-driven ribozyme and its target). In principle, bimolecular interactions are more rapid than trimolecular interactions. This difference would seem to indicate that conventional ribozymes might be more effective in cells than $tRNA^{Val}$-

driven heterodimeric minizymes. However, in my experiments, I found that the $tRNA^{Val}$-driven dimer was always more active than the corresponding $tRNA^{Val}$-driven ribozyme when I tested several target sequences in cultured cells (the same target site was used for each set of ribozyme and minizyme). This conclusion is further strengthened by the results of the present analysis. Therefore, as long as the $tRNA^{Val}$-expression system is used, despite the involvement of the dimerization process, the intracellular activity of the minizyme appears to be significantly higher than that of conventional hammerhead ribozymes.

In conclusion, although the $tRNA^{Val}$-expression system can produce very active ribozymes (Kawasaki *et al.*, 1998), in my hand, the corresponding dimeric minizymes are consistently more active than standard hammerhead ribozymes in mammalian cells. Therefore, I encourage molecular biologists to use $tRNA^{Val}$-driven minizymes in their attempts to suppress the expression of a specific gene of interest. The novel $tRNA^{Val}$-driven heterodimeric minizymes, which are capable of cleaving a substrate at two independent sites simultaneously, should be very useful as tools in molecular biology, with potential use *in vivo* and in a clinical setting.

Chapter V

A novel allosterically *trans*-activated ribozyme (maxizyme) with exceptional specificity *in vitro* and *in vivo*

Introduction

Hammerhead ribozymes are small and versatile nucleic acids that can cleave RNAs at specific sites (Uhlenbeck, 1987; Haseloff and Gerlach, 1988; Symons, 1989). A minizyme is a hammerhead ribozyme with a short oligonucleotide linker instead of stem/loop II (McCall *et al.*, 1992). We demonstrated previously that minizymes with low activity as monomers form very active dimeric structures with a common stem II (Amontov and Taira, 1996). An appropriately designed heterodimer cleaved a target substrate at two sites simultaneously (Kuwabara *et al.*, 1996). I explored the use of dimeric minizymes as gene-inactivating agents by placing minizymes under the control of a $tRNA^{Val}$ promoter. Although I feared initially that the $tRNA^{Val}$ portion of the transcript might hinder the dimerization, the tRNA-embedded minizyme could form an active dimeric structure (Kuwabara *et al.*, 1998). In extending the studies of dimeric minienzymes, I attempted to use one of the two substrate-binding regions of the heterodimer as sensor arms. Then, since one domain of the heterodimer was to be used solely for recognition of the target sequence of interest, I deleted its catalytic core completely to yield an even smaller monomeric unit (Fig. 19, right). The goal has been to control the activity of heterodimers allosterically by introducing sensor arms so that, only in the presence of the correct target sequence of interest, can the heterodimer create a cavity that captures catalytically indispensable Mg^{2+} ions (Fig. 20). Ribozymes are metalloenzymes (Dahm *et al.*, 1993; Steitz and Steitz, 1993; Zhou and Taira, 1998 and references therein), and an active structure of the heterodimer with a Mg^{2+}-binding pocket is formed only in the presence of the sequence of interest (Figs. 19, 20).

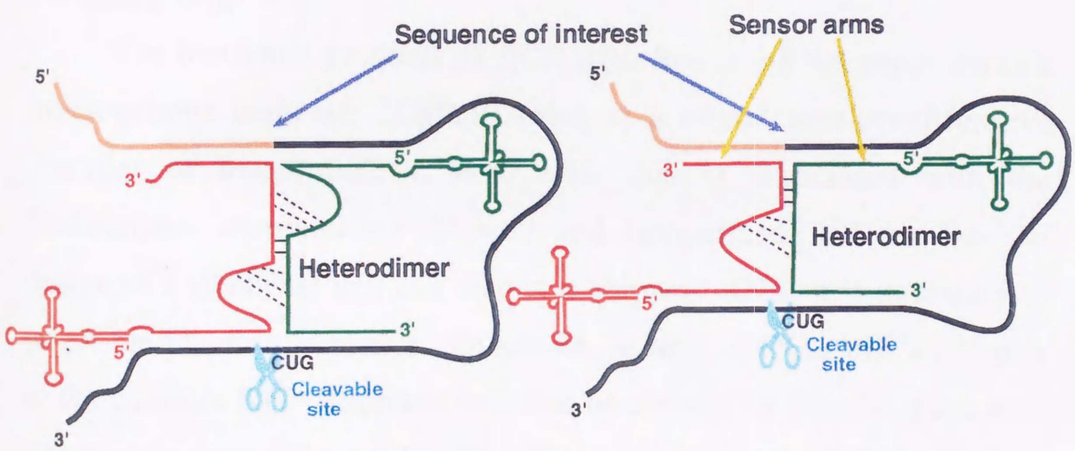

Figure 19 Design of the novel "maxizyme". Schematic representation for the specific cleavage of chimeric mRNA by the $tRNA^{Val}$-driven maxizyme. The heterodimer [MzL (maxizyme left; red) and MzR (maxizyme right; green)] can generate two different binding sites: one is complementary to the sequence of a substrate, the other is complementary to a second substrate (left structure). One of the catalytic cores of the heterodimer can be deleted completely to yield the even smaller maxizyme (right structure) in that the substrate-recognition sequences recognize the abnormal chimeric junction, acting as sensor arms.

In the present study, the sequence of interest was the junction sequence in *BCR-ABL* fusion mRNA (Fig. 21). I am now able to design ribozymes driven by a human $tRNA^{Val}$-promoter that can be transported from the nucleus to the cytoplasm, thereby ensuring the co-localization of the $tRNA^{Val}$-ribozyme with its target mRNA (Koseki *et al.*, 1999). All the monomeric forms (sequences) used in this study, unless otherwise noted, were connected to the 3' region of a human gene for $tRNA^{Val}$ with appropriate modifications. In this study, in order to distinguish monomeric forms of conventional minizymes that have extremely low activity from the novel heterodimer with high-level activity, the latter is designated "maxizyme". ***Maxizyme*** stands for ***m***inimized, ***a***ctive, ***x***-shaped (heterodimeric), and ***i***ntelligent (allosterically controllable) ribo***zyme*** (Fig. 20).

The translated products of *BCR-ABL* fusion mRNA cause chronic myelogenous leukemia (CML), which is a clonal myeloproliferative disorder of hematopoietic stem cells that is associated with the Philadelphia chromosome (Nowell and Hungerford, 1960). For the design of a ribozyme that can disrupt a chimeric RNA, it is necessary to target the junction sequence. Otherwise, normal mRNAs that share part of the chimeric RNA sequence will also be cleaved by the ribozyme, with resultant damage to host cells (Fig. 22). In the case of the b2a2 sequence (consisting of the *BCR* exon 2 and *ABL* exon 2), which results from reciprocal chromosomal translocations (Fig. 23), there are no triplet sequences that are potentially cleavable by hammerhead ribozymes within two or three nucleotides of the junction in question (Kuwabara *et al.*, 1997 and references therein). GUC triplets are generally the most susceptible to cleavage by a hammerhead ribozyme, and one such triplet is located 45 nucleotides from the junction. If this GUC triplet were cleaved by a ribozyme, normal *ABL* mRNA that shares part of the

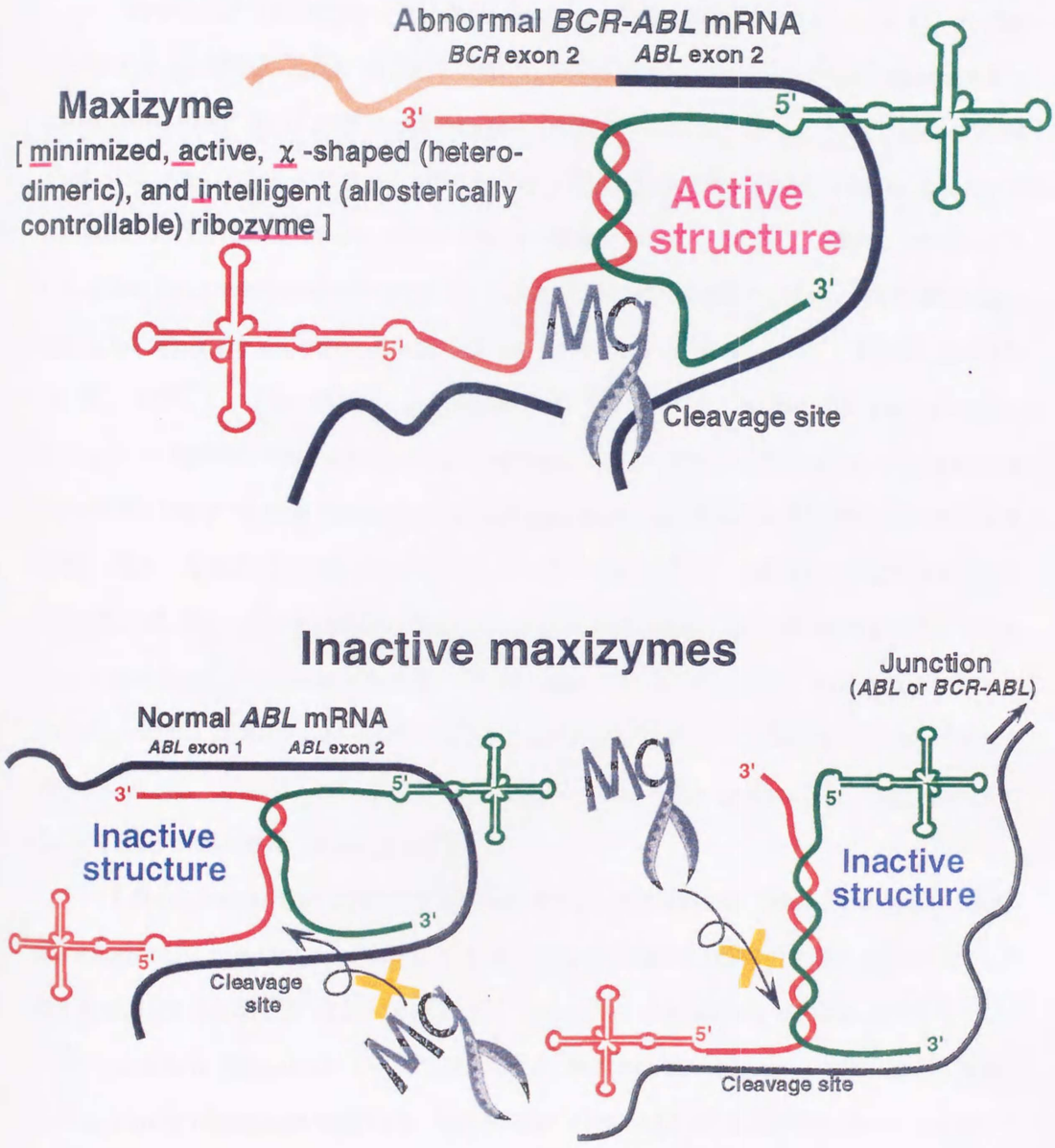

Figure 20 Formation of an active or inactive maxizyme. In order to achieve high substrate-specificity, the $tRNA^{Val}$-driven maxizyme should be in an active conformation only in the presence of the abnormal *BCR-ABL* junction (upper panel), while the conformation should remain inactive in the presence of normal *ABL* mRNA or in the absence of the *BCR-ABL* junction (lower panel).

sequence of the abnormal *BCR-ABL* mRNA would also be cleaved by the ribozyme, with resultant damage to the host cells (Fig. 22). In designing ribozymes that might cleave b2a2 mRNA, I must be sure to avoid cleavage of normal *ABL* mRNA.

Previous attempts (Pachuk *et al.*, 1994; James *et al.*, 1996) at the cleavage of *BCR-ABL* (b2a2) mRNA have involved a combination of a long antisense arm and a ribozyme sequence (Fig. 24). I demonstrated that the antisense-type of ribozyme (Fig. 24) non-specifically cleaved normal *ABL* mRNA *in vitro* (Kuwabara *et al.*, 1997), most probably because hammerhead ribozymes have cleavage ability even with binding arms of as little as three nucleotides in length (Hertel *et al.*, 1996; Birikh *et al.*, 1997). Therefore, I wondered whether it might be possible to design a novel maxizyme that would form a catalytically competent structure only in the presence of the junction in *BCR-ABL* (b2a2) mRNA (Fig. 20). Since I was interested in cleaving b2a2 mRNA specifically, I compared the specificities and catalytic activities in cultured cells of a conventional hammerhead ribozyme (wtRz), two antisense-type hammerhead ribozymes (asRz52 and asRz81, Fig. 24; Pachuk *et al.*, 1994; James *et al.*, 1996) and the novel maxizyme with respect to cleavage of *BCR-ABL* chimeric (b2a2) mRNA.

I found that the activity of the novel maxizyme could be controlled allosterically not only *in vitro* but also in cultured cells by the presence of the junction in *BCR-ABL* mRNA. Specific depletion of the p210$^{BCR-ABL}$ protein (product of *BCR-ABL* fusion gene), as a result of the maxizyme's cleavage activity, led to the cleavage of inactive procaspase-3 to yield active caspase-3, with resultant apoptosis of BaF3/p210$^{BCR-ABL}$ cells. Similarly, BV173 cells from a leukemic patient, but not normal cells, underwent apoptosis in response to the maxizyme. By contrast, conventional ribozymes caused apoptosis nonspecifically in both

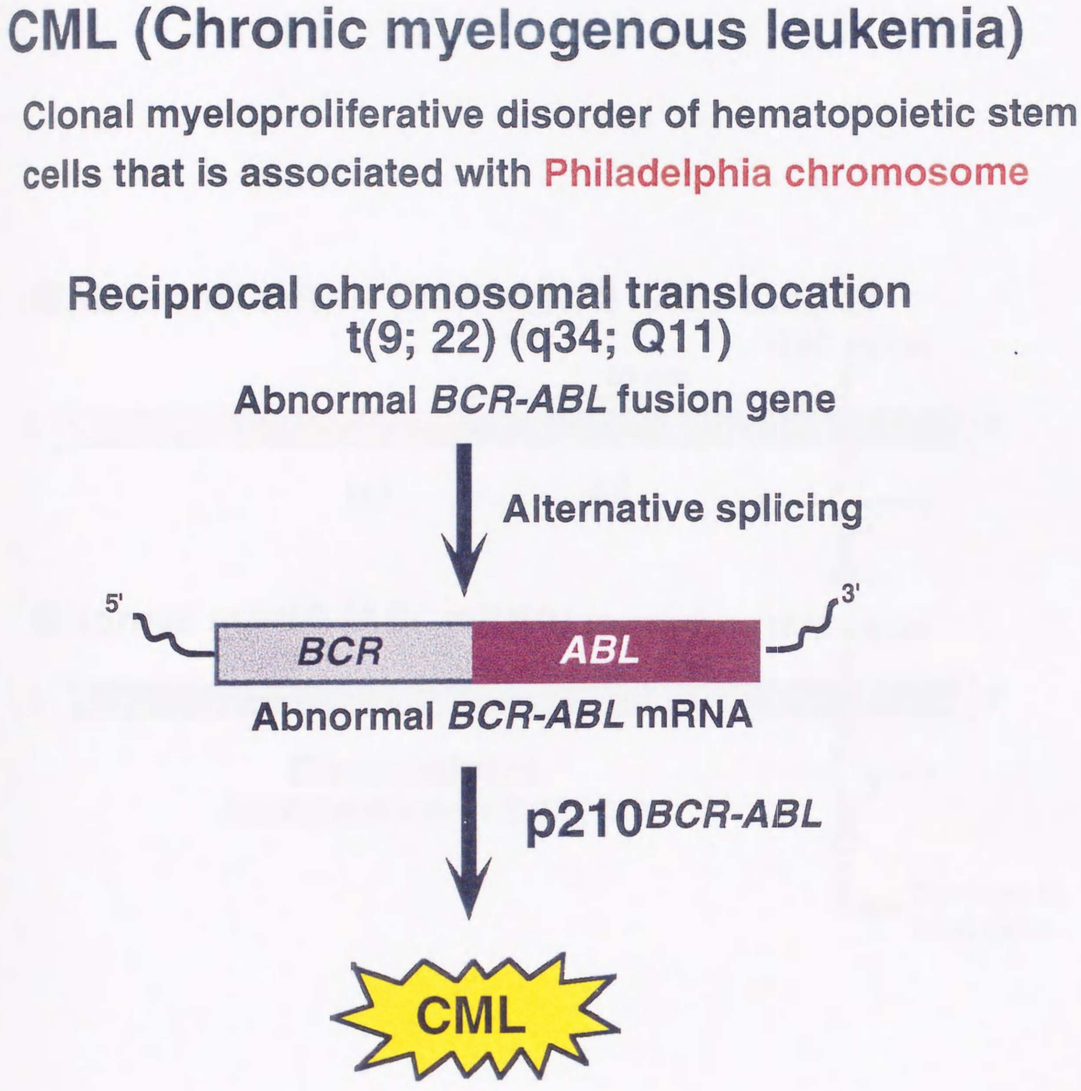

Figure 21 The *BCR-ABL* chimeric mRNA. The translated products of *BCR-ABL* fusion mRNA cause CML. The CML is a clonal myeloproliferative disorder of hematopoietic stem cells that is associated with the Philadelphia chromosome.

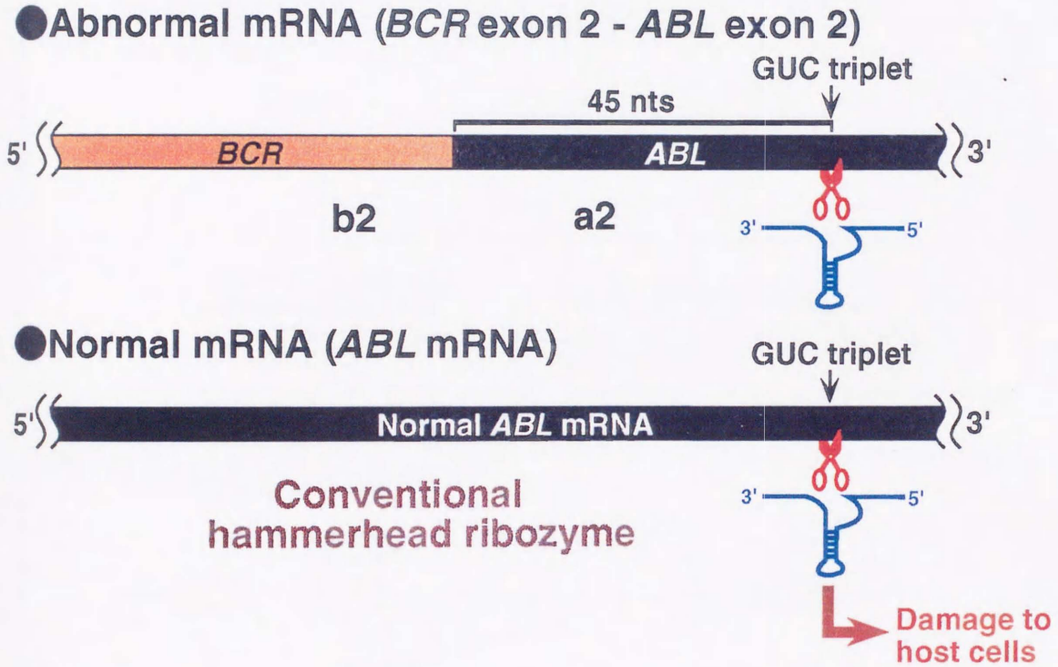

Figure 22 Non-specific cleavage of *BCR-ABL* mRNA and normal *ABL* by conventional ribozymes. A GUC triplet, which is generally the triplet that is most susceptible to cleavage by hammerhead ribozymes, is located 45 nucleotides from the junction. If such a GUC triplet were selected as the site of cleavage by ribozymes, normal *ABL* mRNA that shares part of the abnormal *BCR-ABL* RNA sequence would also be cleaved by the ribozyme, with resultant damage to the host cells.

BaF3/p210$^{BCR\text{-}ABL}$ and H9 cells. To the best of my knowledge, this is the first demonstration of an artificially created ribozyme that is under perfect allosteric control not only *in vitro* but also in cultured cells.

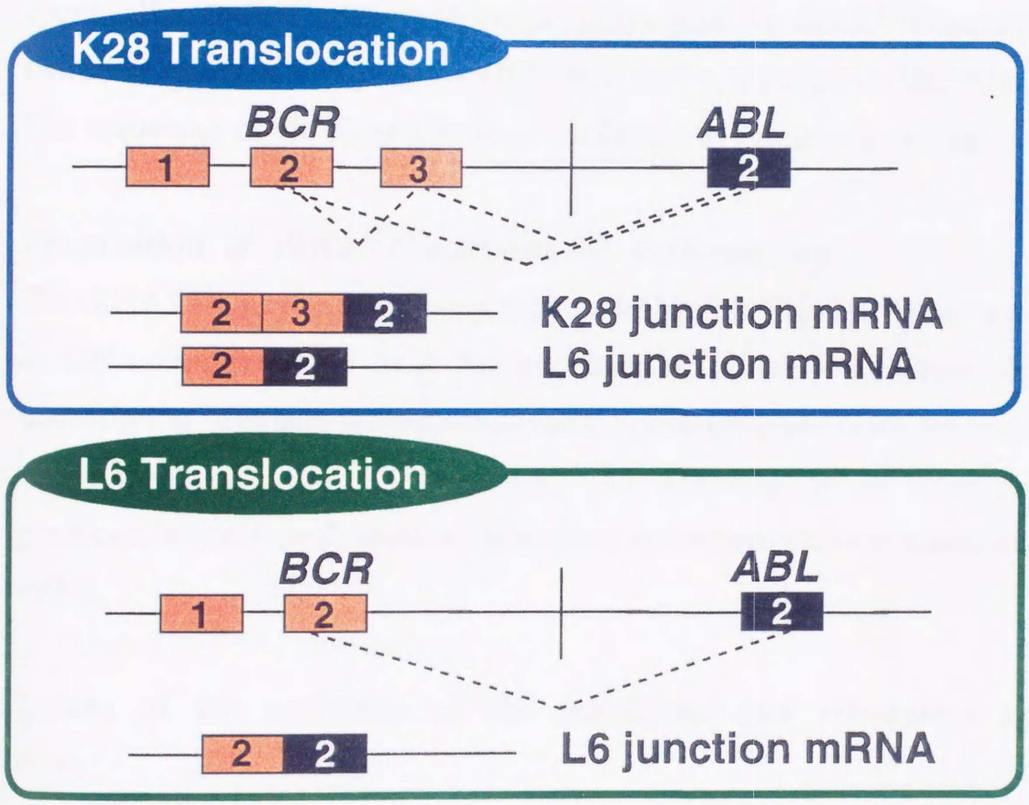

Figure 23 *BCR-ABL* translocations and fusion mRNAs. The two types of chromosomal translocation [K28-type (upper panel) and L6-type (lower panel)] that are associated with chronic myelogenous leukemia and the corresponding fusion mRNAs are depicted. Boxes shaded orange represent *BCR* exons and black boxes represent *ABL* exon 2. Dotted lines connecting *BCR* and *ABL* exons indicate alternative splicing pathways.

Materials and Methods

Construction of plasmids for expression of tRNA-embedded enzymes

Chemically synthesized oligonucleotides encoding each enzyme [MzL, MzR, wtRz, asRz52 and asRz81 (Fig. 24)] and the pol III termination sequence were converted to double-stranded sequences by PCR. After digestion with *Csp* 45 I and *Sal* I, each appropriate fragment was cloned downstream of the $tRNA^{Val}$ promoter of pV (which contained the chemically synthesized promoter of a human gene for $tRNA^{Val}$ between the *Eco*R I and *Sal* I sites of the pMX puro vector; Kitamura *et al.*, 1995). The sequences of the constructs were confirmed by direct sequencing.

Preparation of $tRNA^{Val}$-enzymes by transcription

The $tRNA^{Val}$-enzyme expression vectors depicted in Figure 27 were used as DNA templates for PCR for construction of DNA templates for transcription. Primers were synthesized for each template, with the sense strand containing the T7 promoter. T7 transcription *in vitro* and purification were performed as described elsewhere (Kuwabara *et al.*, 1996).

Assays of the activities of the maxizyme and ribozymes *in vitro*

Assays of the activities of the maxizyme were performed, in 25 mM $MgCl_2$ and 50 mM Tris-HCl (pH 8.0), under enzyme-saturating (single-turnover) conditions at 37°C, with incubation for 60 minutes (Fig. 26). The substrates were labeled with [γ-^{32}P]-ATP by T4 polynucleotide kinase (Takara Shuzo, Kyoto, Japan). Each enzyme was incubated at 0.1 μM with 2 nM 5'-[^{32}P]-labeled S16. Reactions were initiated by the

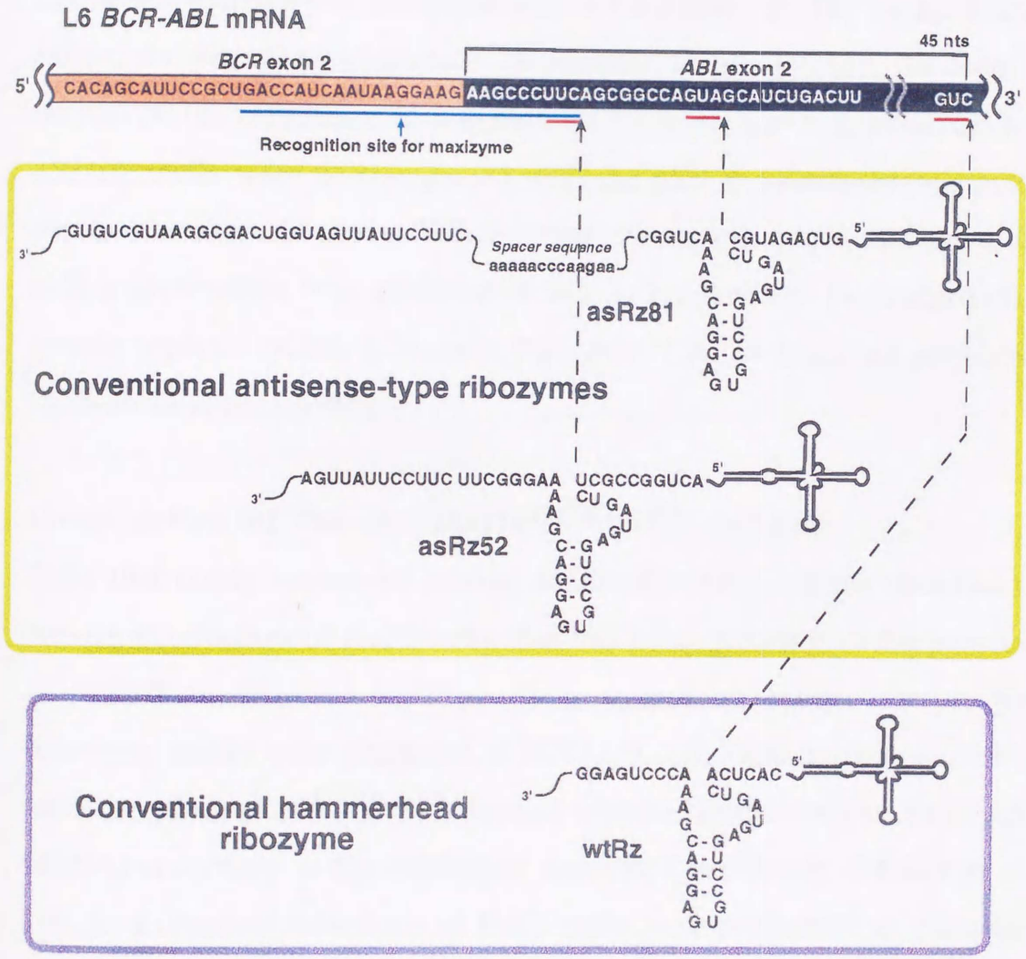

Figure 24 Nucleotide sequences of conventional hammerhead and antisense-type ribozymes. The sequence of L6 *BCR-ABL* mRNA near the junction is expanded. The sites of cleavage by antisense-type ribozymes (asRz81 and asRz52) and by the control ribozyme (wtRz) are shown. The site of cleavage by the maxizyme is identical to that by wtRz and the recognition site for the maxizyme is indicated by a blue line.

addition of $MgCl_2$ to a buffered solution that contained each enzyme with the substrate, and each resultant mixture was then incubated at 37°C. Finally, reaction mixtures were subjected to electrophoresis on an 8% polyacrylamide/7 M urea gel.

Assays of reporter activity after transient transfection

Luciferase activity was measured with a PicaGene kit (Toyo-inki, Tokyo, Japan) as described elsewhere (Kuwabara *et al.*, 1998a). In order to normalize the efficiency of transfection by reference to β-galactosidase activity, cells were co-transfected with the pSV-β-galactosidase control vector (Promega, Madison, WI) and then the chemiluminescent signal due to β-galactosidase was quantitated with a luminescent β-galactosidase genetic reporter system (Clontech, Palo Alto, CA) as described previously (Kuwabara *et al.*, 1998a).

Construction of the BaF3/p210*BCR-ABL* cell line

Cells that stably expressed human *BCR-ABL* mRNA were obtained by retroviral infection of BaF3 cells that had been growing in the presence of WEHI-conditioned medium as a source of IL-3. Helper-free retrovirus stocks were produced in BOSC23 cells (Kitamura *et al.*, 1995) with the pMX-p210*BCR-ABL* vector, which encoded human *BCR-ABL* mRNA, according to the procedure described previously (Muller *et al.*, 1991). Retroviral infections of BaF3 cells were performed as described previously (Pendergast *et al.*, 1993). IL-3 was removed 72 hours after infection to allow selection for populations that expressed the fusion gene. BaF3/p210*BCR-ABL* cells were maintained in RPMI-1640 medium supplemented with 10% fetal calf serum (FCS; Gibco-BRL, Rockville, MD) and 3 μg/mL puromycin (Gibco-BRL).

Northern blotting analysis

For the assay of expression of target mRNA and $tRNA^{Val}$-enzymes in BaF3/p210*BCR-ABL* cells, total RNA was isolated with ISOGEN™ (Nippon Gene Co., Toyama). Cytoplasmic RNA and nuclear RNA were separated as described previously (Huang and Carmichael, 1996). Thirty μg of total RNA per lane were loaded on an agarose gel (FMC Inc., Rockland, ME), and then bands of RNA were transferred to a Hybond-N™ nylon membrane (Amersham Co., Buckinghamshire, UK). The membrane was probed with synthetic oligonucleotides, which were complementary to the sequence of MzL, MzR, wtRz and *BCR-ABL* junction sequence that had been labeled with ^{32}P by T4 polynucleotide kinase (Takara).

Cell viability and apoptosis

Cell viability was determined by trypan blue exclusion. Dead cells were removed by the Ficol separation procedure with Histopaque-1077 (SIGMA). Apoptosis was determined as described previously (Reuther *et al.*, 1998), and the cells were stained with 10 μg/mL Hoechst 33342 (Nippon Gene) for nuclear morphology for 15 min. After washing and mounting in 90% glycerol/20 mM Tris (pH 8.0)/0.1% N-propyl gallate, samples were examined using a fluorescent microscope (Nikon, Tokyo).

Western blot analysis

Cell lysates were subjected to SDS-PAGE on a 15% polyacrylamide gel. A rabbit polyclonal αCPP32 antibody that recognizes both procaspase-3 and the processed p17 (caspase-3) was used to detect procaspase-3 activation in apoptotic BaF3/p210*BCR-ABL* and H9 cells. The blocking and detection were performed as described previously (Dubrez *et al.*, 1998).

Results

Specific design of a novel maxizyme under the control of a human $tRNA^{Val}$-promoter and demonstration *in vitro* of the allosteric control of its activity by the junction sequence in *BCR-ABL* mRNA

For potential application of a maxizyme to gene therapy for the treatment of CML (Fig. 21), it is important that the maxizyme be expressed constitutively and under the control of a strong promoter *in vivo*. I embedded each monomeric unit downstream of the sequence of a human $tRNA^{Val}$-promoter (Yu *et al.*, 1995; Kawasaki *et al.*, 1996, 1998; Bertrand *et al.*, 1997) that is recognized by RNA polymerase III (Perriman and de Feyter, 1997), to generate MzL (maxizyme left) and MzR (maxizyme right; Fig. 25). High-level expression under the control of the pol III promoter would clearly be advantageous if maxizymes are to be used as therapeutic agents and such expression would also increase the likelihood of dimerization. The specific design of the $tRNA^{Val}$-constructs was based on the previous success in attaching a ribozyme sequence to the 3'-modified side of the $tRNA^{Val}$-portion of the human gene (Koseki *et al.*, 1999). This strategy yielded ribozymes that were very active in cultured cells (Kawasaki *et al.*, 1996, 1998).

In order to achieve high substrate-specificity, the maxizyme should adopt an active conformation only in the presence of the abnormal *BCR-ABL* junction (Fig. 25), while the conformation should remain inactive in the presence of the normal *ABL* mRNA and in the absence of the abnormal *BCR-ABL* junction (Fig. 25). The specifically designed sequences, which are shown in Figure 25 (note that the lengths and sequences of sensor arms and those of common stem II are the variables), should permit such conformational changes depending on the presence or

absence of the abnormal b2a2 mRNA. This phenomenon would resemble the changes in conformation of allosteric proteinaceous enzymes in response to their effector molecules. In order to compare the activity and specificity of the maxizyme with that of a conventional wild-type ribozyme (wtRz) targeted to the same cleavage site, and with those conventional antisense-type ribozymes (asRz52 and asRz81; Pachuk *et al.*, 1994; James *et al.*, 1996), I embedded the latter two types of ribozyme similarly in the 3' portion of the gene for $tRNA^{Val}$ (Fig. 24).

In order to prove *in vitro* that conformational changes depended on the presence or absence of the abnormal b2a2 mRNA, I prepared a short 16-nucleotide (nt) *BCR-ABL* substrate (S16) that corresponded to the target (cleavage) site indicated by capital letters in the upper panel of Figure 25 (within *ABL* exon 2). The specificity was tested by incubating the *in vitro* transcribed maxizyme with the 5'-[^{32}P]-labeled short 16-mer substrate (S16) in the presence and in the absence of either a 20-mer normal *ABL* effector molecule or a 28-mer *BCR-ABL* effector molecule. These latter molecules corresponded, respectively, to the sequences indicated by capital letters in the normal *ABL* mRNA of the left structure in the lower panel of Figure 25 (junction sequence of *ABL* exon 1 - *ABL* exon 2) and in the abnormal b2a2 mRNA in the upper panel of Figure 25 (junction sequence of *BCR* exon 2 - *ABL* exon 2). In this case, the 28-mer *BCR-ABL* effector molecule corresponding to the junction sequence in b2a2 mRNA acts *in trans* and it should be recognized for annealing by the sensor arms of MzL and MzR and should serve to direct formation of the active dimer. The other recognition arms of the maxizyme should recognize the cleavage triplet in the short 16-mer *BCR-ABL* substrate RNA and specific cleavage should occur (Fig. 26, on the right). Indeed, no products of cleavage of the substrate (S16) were detected in the absence of the *BCR-ABL* junction or in the presence of the normal *ABL*

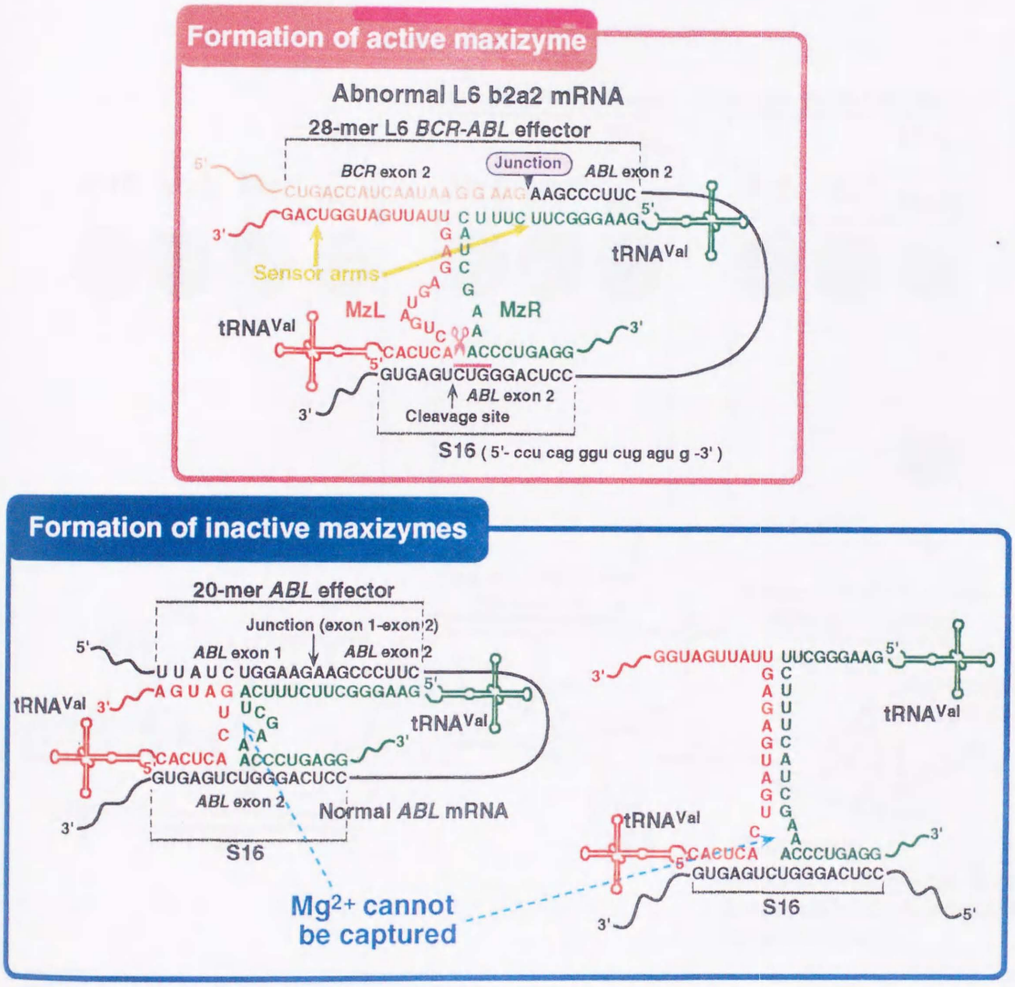

Figure 25 Nucleotide sequences and secondary structures of the active and inactive maxizyme. In order to achieve high substrate-specificity, the maxizyme should be in an active conformation only in the presence of the abnormal *BCR-ABL* junction, while the conformation should remain inactive in the presence of normal *ABL* mRNA or in the absence of the *BCR-ABL* junction. MzL and MzR should allow such conformational changes to occur, depending on the presence or absence of the abnormal b2a2 mRNA.

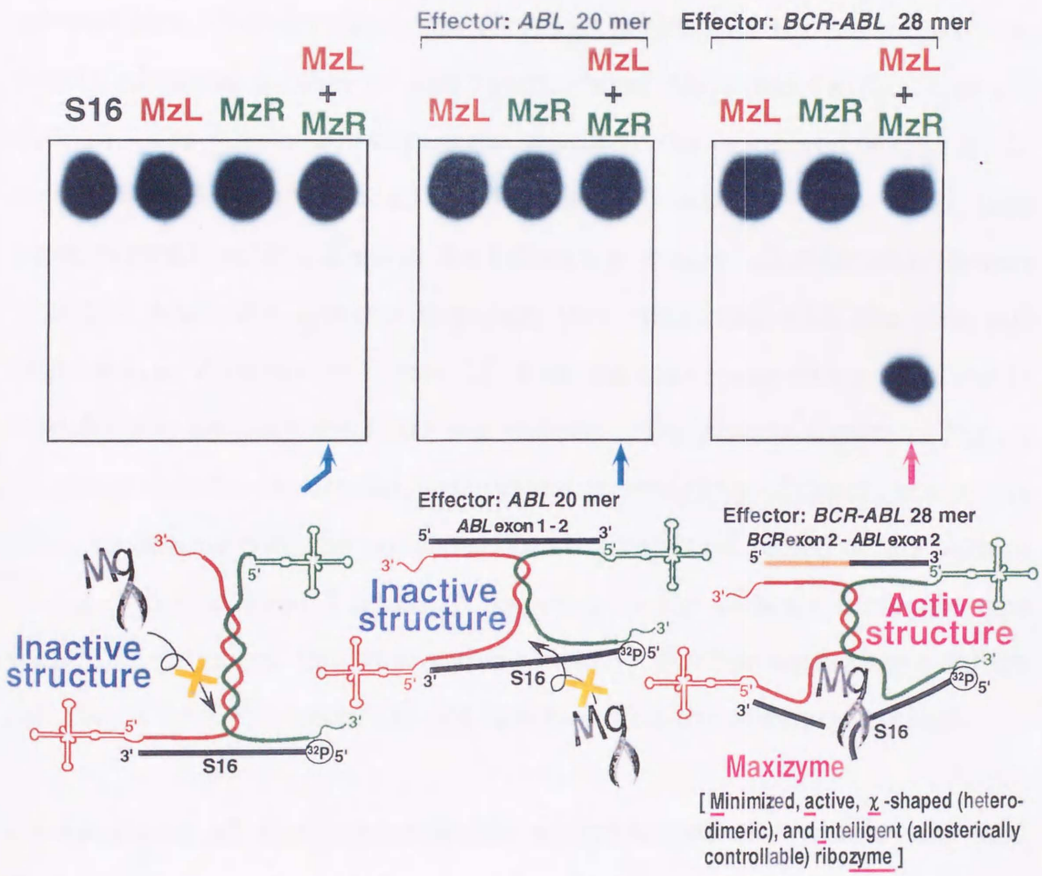

Figure 26 Allosteric control of the activity of the maxizyme *in vitro*. The specificity of maxizyme-mediated cleavage was examined by incubating $tRNA^{Val}$-driven component(s) with the 5'-^{32}P-labeled short 16-mer substrate (S16) in the presence and in the absence of an allosteric effector molecule, namely, either a short 20-mer normal *ABL* sequence (*ABL* 20 mer) or a short 28-mer *BCR-ABL* sequence (*BCR-ABL* 28 mer). Sequences of these effector molecules are shown in Figure 3B. MzL and/or MzR were incubated at 0.1 μM with 2 nM 5'-^{32}P-labeled substrate (S16). When applicable, the concentration of the effector, 20-mer *ABL* or 28-mer *BCR-ABL*, was 1 μM.

sequence (effector molecule), demonstrating the expected high substrate-specificity of the maxizyme (Fig. 26).

Since MzL or MzR by itself, in the presence and in the absence of effector molecules, did not have any cleavage activity, the active species was clearly the heterodimeric form of the maxizyme, as depicted at the bottom right in Figure 26, which was involved in a tetramolecular interaction. In principle, the bimolecular interactions of the conventional ribozyme should be more strongly favored than tetramolecular interactions. Nevertheless, the cleavage activity of the maxizyme was nearly identical to that of the hammerhead ribozyme (wtRz; data not shown). The greater activity of the maxizyme as compared to that of the conventional hammerhead ribozyme in cultured cells was also demonstrated, as described in the following section. Similar results were obtained when the effector sequence was connected with the cleavage sequence, as depicted in Figure 25, with the maxizyme being involved in trimolecular interactions (data not shown). The results shown in Figure 26 prove that the maxizyme was subject to complete allosteric control *in vitro*, in accord with the conformational changes (depicted at the bottom in Fig. 26) that should occur in response to the effector molecule (the *BCR-ABL* junction) that was added *in trans*. Furthermore, they confirm that the $tRNA^{Val}$-portion did not interfere with the allosteric control.

Comparison of the intracellular activities of the maxizyme and those of conventional hammerhead ribozymes in mammalian cells

I next examined the action of the maxizyme in mammalian cells using a reporter construct. To evaluate the intracellular activity of the maxizyme (Fig. 27), I co-transfected HeLa cells with expression plasmids that encoded an appropriate enzyme unit(s) under the control of the human

$tRNA^{Val}$-promoter, together with a target gene-expressing plasmid that encoded a chimeric target *BCR-ABL* (or *ABL* alone) sequence and a gene for luciferase, pB2A2-luc (or p*ABL*-luc). The junction-expressing plasmid pB2A2-luc contained a sequence of 300 nt that encompassed the *BCR-ABL* junction and the target cleavage site in the b2a2 mRNA. The plasmid, p*ABL*-luc contained a sequence of 300 nt that encompassed the same target cleavage site and the junction between exon 1 and exon 2 of the normal *ABL* mRNA. After transient expression of both genes, in individual cell lysate, I estimated the intracellular activity of each enzyme by measuring the luciferase activity.

The luciferase activity recorded when I used the target gene-expressing plasmid (pB2A2-luc or p*ABL*-luc) was taken as 100% (Fig. 27). Expression of the $tRNA^{Val}$-portion (pV) by itself had no inhibitory effect. By contrast, the novel maxizyme (pV-MzL/R) was extremely effective in cell culture (>95% inhibition) in suppressing the *BCR-ABL*-luciferase gene (Fig. 27, right panel; indicated by a star), and it had no inhibitory effect on expression of the *ABL*-luciferase gene (Fig. 27, left panel; indicated by a star), demonstrating the extremely high specificity of the maxizyme. As expected, the conventional hammerhead ribozyme (pVwtRz), targeted to the same site as the maxizyme, suppressed the expression of both the *BCR-ABL*-luciferase gene and the *ABL*-luciferase gene. It is important to note that, despite the original expectations of high specificity, the conventional antisense-type ribozymes (pVasRz81 and pVasRz52) also suppressed the expression of both the *BCR-ABL*-luciferase and the *ABL*-luciferase gene, acting non-specifically, in agreement with my previous findings *in vitro* (Kuwabara *et al.*, 1997). Moreover, the extent of suppression by the conventional (antisense-type) ribozymes was not as great as that by the maxizyme.

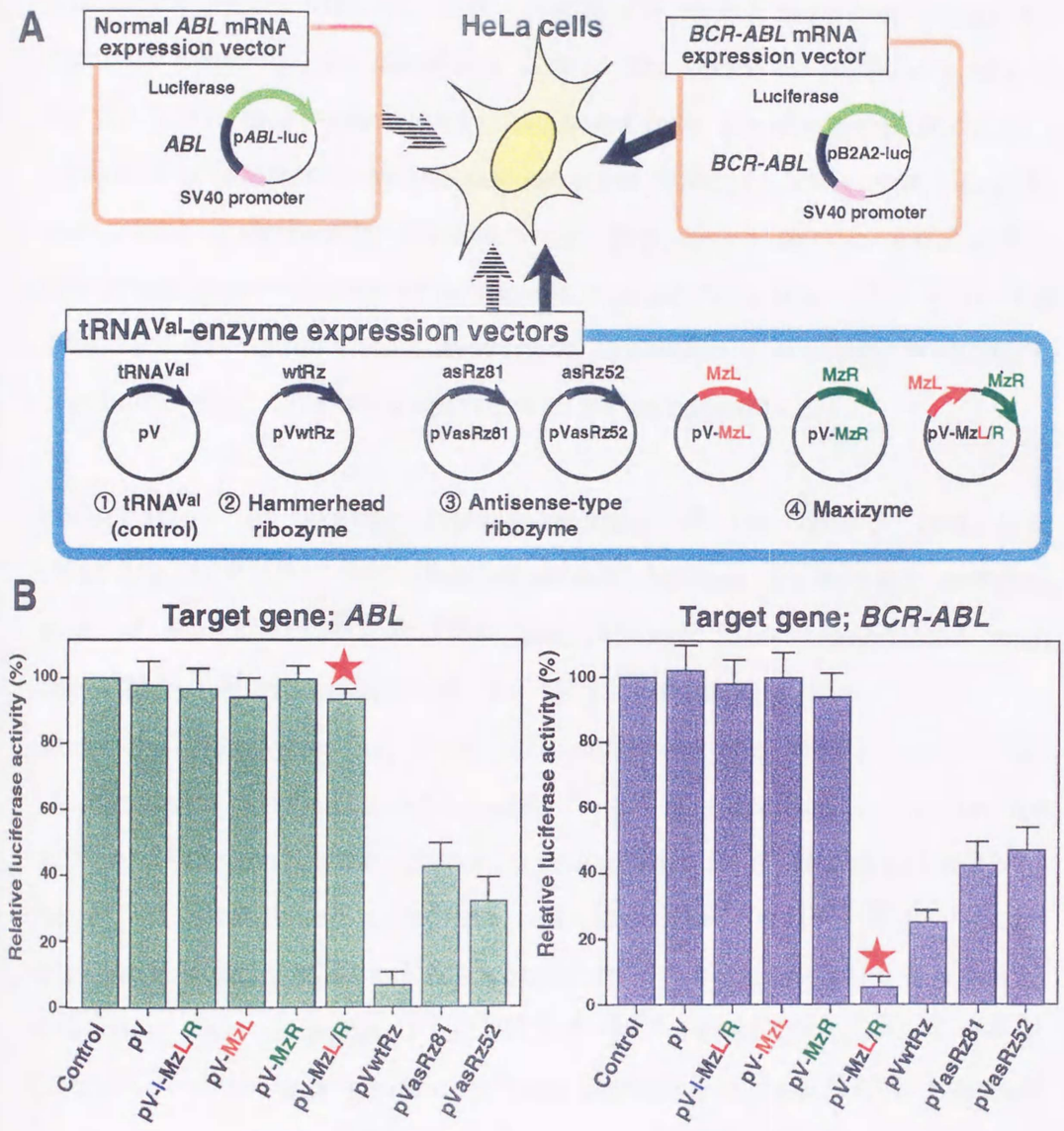

Figure 27 Intracellular activities and specificities of $tRNA^{Val}$-enzymes in HeLa cells. (A) Assay system for measurements of activities of $tRNA^{Val}$-enzymes in HeLa cells and (B) the effects of $tRNA^{Val}$-enzymes on the chimeric *BCR-ABL*-luciferase and *ABL*-luciferase genes. Luciferase activity was normalized by reference to the efficiency of transfection which was determined by monitoring activity of a co-transfected gene for β-galactosidase.

The individual subunits of the maxizyme (MzL and MzR) had no inhibitory effects. Thus, the activity of the maxizyme must have originated from the formation of active heterodimers in the mammalian cells. It should also be emphasized that, since a mutant, crippled maxizyme (pV-I-MzL/R), by a single G^5 to A^5 mutation within the catalytic core, had no inhibitory effects, the observed inhibitory effects for the active maxizyme clearly originated from the ribozyme mechanism of action (chemical cleavage; not antisense effects). Moreover, since the maxizyme specifically inhibited the expression of the *BCR-ABL*-luciferase gene without affecting the related *ABL*-luciferase gene that contained a potential site of cleavage by the maxizyme, complete allosteric regulation must have been operative in the mammalian cells.

Generation of stable transformants of the BaF3 cell line (BaF3/p210*BCR-ABL*) that expressed human *BCR-ABL* mRNA, and of BaF3/p210*BCR-ABL* and H9 cell lines transduced with the $tRNA^{Val}$-ribozymes or the $tRNA^{Val}$-maxizyme

Since the maxizyme had acted efficiently and specifically against the reporter gene construct in HeLa cells (Fig. 27), I decided to examine the activity of the maxizyme against an endogenous *BCR-ABL* (b2a2 mRNA) target. I established a murine cell line, BaF3/p210*BCR-ABL*, that expressed human b2a2 mRNA constitutively, by integrating a plasmid construct that expressed p210*BCR-ABL* (pMX/p210*BCR-ABL*; p210*BCR-ABL* was generated from human b2a2 mRNA). I should emphasize that this cell line (which expressed b2a2 mRNA) was different from the one (BaF3+p210 cells that expressed K28 b3a2 mRNA) used previously by Daley and Baltimore (1988) and Choo *et al.* (1994). Although the parental BaF3 cell line is an interleukin-3-dependent (IL-3-dependent) hematopoietic cell line (Daley and Baltimore, 1988; left panel

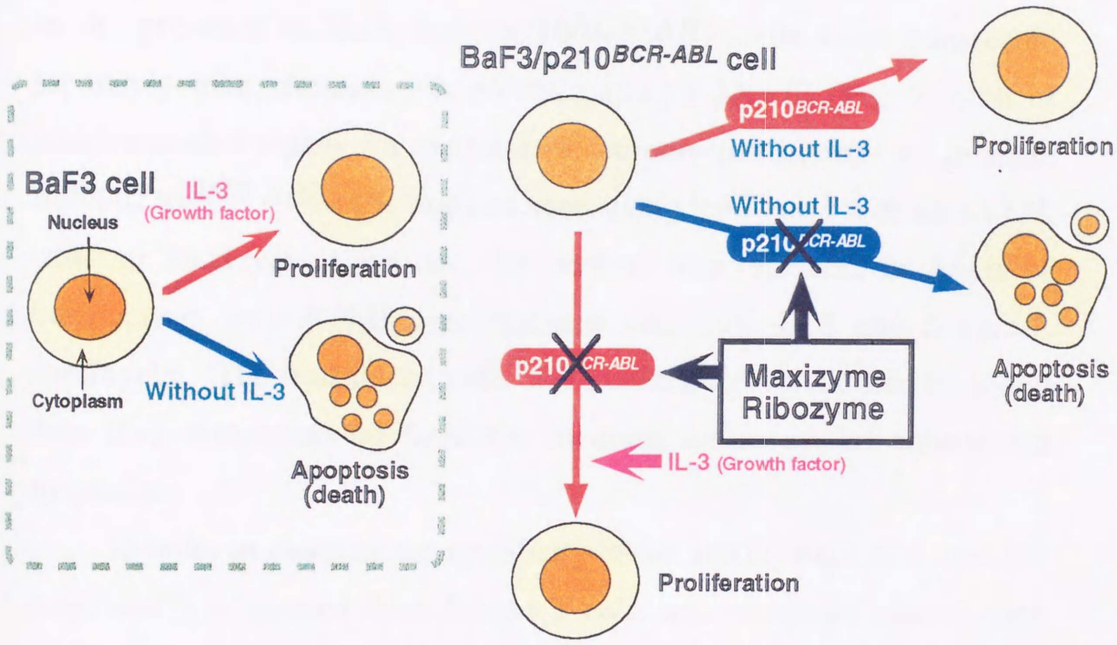

Figure 28 Schematic representation of the dependence on IL-3 of BaF3 cells and transduced BaF3 cells that expressed human *BCR-ABL* mRNA.

of Fig. 28), the transformed BaF3/p210$^{BCR\text{-}ABL}$ cells were IL-3-independent because of the tyrosine kinase activity of p210$^{BCR\text{-}ABL}$ and, thus, the latter transformed cells were able to grow in the absence of IL-3 (Fig. 28, right). However, if the expression of p210$^{BCR\text{-}ABL}$ were to be inhibited, BaF3/p210$^{BCR\text{-}ABL}$ cells should become IL-3-dependent and, in the absence of IL-3, they should undergo apoptosis. Therefore, during the selection of maxizyme- or ribozyme-transduced BaF3/p210$^{BCR\text{-}ABL}$ cells, I used 10% WEHI-conditioned RPMI medium as a source of IL-3. In the presence of IL-3, BaF3/p210$^{BCR\text{-}ABL}$ cells were transfected separately with plasmids pV, pVwtRz and pV-MzL/R (Fig. 27), all of which encoded a gene for resistance to puromycin. In order to generate BaF3/p210$^{BCR\text{-}ABL}$ cells that had been stably transduced with tRNA^{Val}, wtRz or maxizyme construct, the medium was replaced, 24 hours of transfection, with RPMI supplemented with 10% FCS and 3 μg/mL puromycin. The transduced cells were cultured for a further 60 h and then IL-3 was removed from the medium for assays of subsequent apoptosis.

In order to examine the specificity of the maxizyme, I also used H9 cells, which originated from human T cells and expressed normal *ABL* mRNA, as control cells. Stably transduced H9 cells that harbored a maxizyme or ribozyme construct were generated using the respective plasmids (described above). The efficiency of transfection was very low, so I generated transduced cells using a line of retroviral producer cells (BOSC23 cells). Filtered supernatants of BOSC23 cells, which had been transfected with plasmids pV, pVwtRz or pV-MzL/R, were added to H9 cells. The H9 cells were cultured for 72 hours and then puromycin was added for selection of resistant cells. The various lines of transduced cells allowed us to examine the activity and specificity of the maxizyme and of

ribozymes against an endogenous target gene (instead of a reporter construct).

Efficient expression and transport to the cytoplasm of the maxizyme

In addition to the level of expression and the half-life of an expressed ribozyme, the co-localization of the ribozyme with its target is obviously an important determinant of the ribozyme's efficiency *in vivo* (Sullenger and Cech, 1993; Eckstein and Lilley, 1996; Bertrand *et al.*, 1997). Therefore, it was essential to determine the intracellular localization of each of the $tRNA^{Val}$-enzymes. To confirm the expression and relative stability of the maxizyme in BaF3/p210$^{BCR\text{-}ABL}$ cells, I performed Northern blotting analysis (Fig. 29). Total RNA from BaF3/p210$^{BCR\text{-}ABL}$ cells that had been transfected with the various plasmids was extracted 2, 4, 6, 12, 18, 24, 30 and 36 hours after transfection. Samples of total RNA were also separated into nuclear and cytoplasmic fractions. Transcripts of about 130 nucleotides in length, which corresponded in size to MzL were detected (Fig. 29). Even initially, MzL transcripts were found in the cytoplasmic fraction and none was detected in the nuclear fraction (Fig. 29). The time course of changes in the level of the maxizyme in the cytoplasm is shown in the right panel of Figure 30. MzL was detected within 4 h and its level of expression reached a plateau 24 h after transfection.

I next estimated the steady-state levels and localization of MzL, MzR and wtRz in BaF3/p210$^{BCR\text{-}ABL}$ cells that had been stably transduced with the respective maxizyme-encoding and ribozyme-encoding plasmids. Total RNA that had been isolated 3 days after removal of IL-3 (Fig. 29), as described in the previous section, was used in this analysis. The results in Figure 30 clearly demonstrate that each

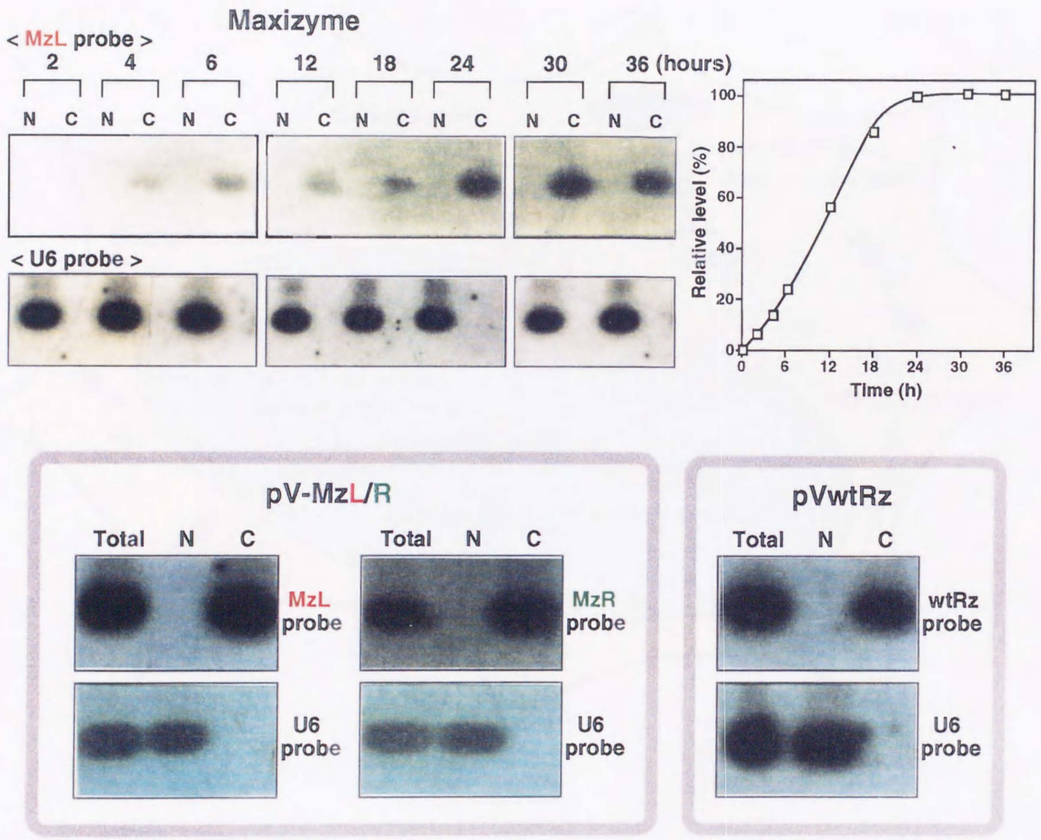

Figure 29 Steady-state levels of expression and intracellular localization of the $tRNA^{Val}$-enzyme in BaF3/p210$^{BCR\text{-}ABL}$ cells. Time course of transport to the cytoplasm of the MzL transcript (upper panel). The steady-state levels of expressed $tRNA^{Val}$-enzymes and their localization (lower panel). N, Nuclear fraction; C, cytoplasmic fraction.

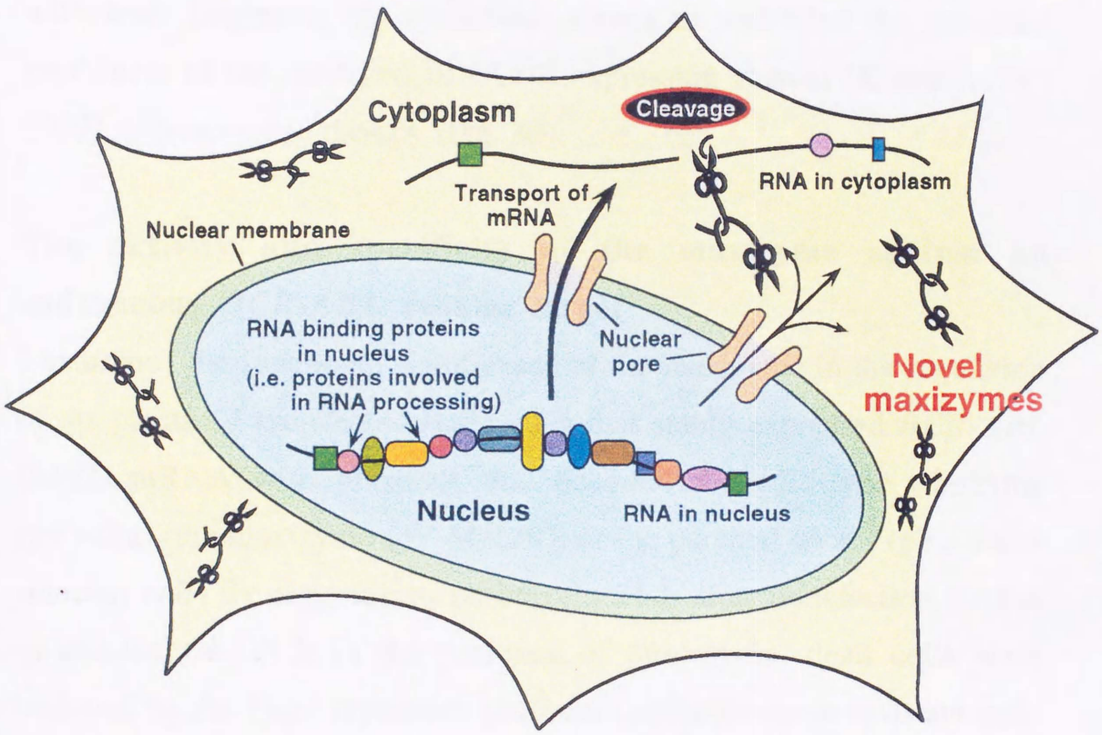

Figure 30 The potential usefulness of the modified $tRNA^{Val}$-expression system in future gene therapy.

$tRNA^{Val}$-enzyme was expressed at significant levels and the transcripts were obviously stable. Furthermore, all $tRNA^{Val}$-enzymes were found in cytoplasmic fractions and none was detected to any significant extent in nuclear fractions. Analysis of the localization of U6 snRNA, which is known to remain in the nucleus, was included in these studies as a control (Fig. 29).

The finding that both the transiently expressed transcripts and transcripts in stable transformants (Fig. 29) were stable and co-localized with their targets in the cytoplasm serves to underline the potential usefulness of the modified $tRNA^{Val}$-expression system (Koseki *et al.*, 1999) in future gene therapy (Fig. 30).

The activity and specificity of the maxizyme against an endogenous *BCR-ABL* cellular target

I examined the functional significance of the maxizyme in the regulation of apoptosis. I transfected BaF3 cells that stably expressed *BCR-ABL* (b2a2) mRNA with plasmids that encoded the wild-type ribozyme (pVwtRz), the maxizyme (pV-MzL/R), or the parental vector (pV), and I selected cells by exposure to puromycin 24 h after transfection. After incubation for 60 h in the presence of puromycin, dead cells were removed by the Ficol separation procedure and puromycin-resistant cells were cultured for various times in medium without IL-3. Cell viability was assessed in terms of the ability to exclude trypan blue dye. In addition to BaF3/p210*BCR-ABL* cells, I used H9 cells that expressed normal *ABL* mRNA at high levels as controls. As shown in the left panel of Figure 31, BaF3/p210*BCR-ABL* cells that expressed the maxizyme died rapidly whereas the control-transfected BaF3/p210*BCR-ABL* (pV) cells remained alive 10 days after withdrawal of IL-3. Moreover, the maxizyme did not kill any H9 cells that expressed

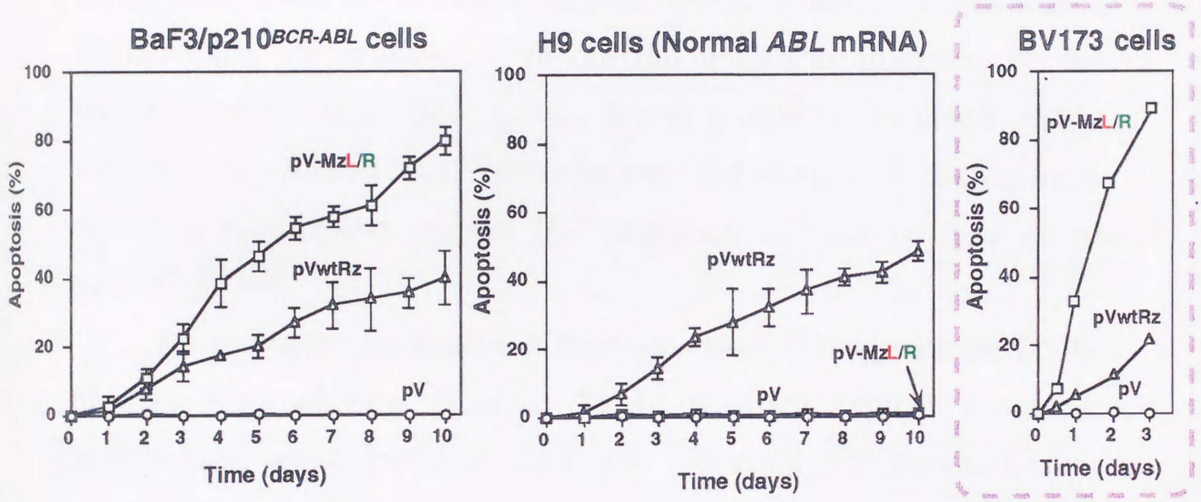

Figure 31 Efficiency of cleavage by the maxizyme of the endogenous *BCR-ABL* mRNA target. Measurements of viability of $tRNA^{Val}$-enzyme-transduced BaF3/p210$^{BCR-ABL}$ cells and H9 cells. The viability of BV173 cells, that were derived from a patient with a Philadelphia chromosome and that were transiently expressing $tRNA^{Val}$-enzymes, was also shown.

normal *ABL* mRNA (Fig. 31, middle), a result that demonstrates the high specificity for targeting the chimeric *BCR-ABL* gene. By contrast, the conventional hammerhead ribozyme, wtRz, induced apoptosis in both BaF3/p210$^{BCR\text{-}ABL}$ and H9 cells (Fig. 31, left and middle), consistent with the observation that wtRz can target the transcripts of both the *BCR-ABL* gene and the normal *ABL* gene *in vitro* and in cultured cells (Fig. 27: Since none of the conventional ribozymes demonstrated any specificity, I chose wtRz, that had the highest level of activity among the conventional ribozymes, as a control). Furthermore, the maxizyme also killed many more BV173 cells, derived from a leukemic patient with a Philadelphia chromosome, than did the wild-type ribozyme or the parental vector (Fig. 31, right). I was unable to establish stably maxizyme-transduced BV173 cells because of the extremely high activity of the maxizyme and because IL-3 could not replace the function of p210$^{BCR\text{-}ABL}$.

Microscopic examination of dead cells after staining with the DNA-binding fluorochrome Hoechst 33342 revealed typical apoptotic morphology, which included condensed chromatin, fragmented nuclei, and shrunken profiles (Fig. 32). It was clear that the maxizyme (pV-MzL/R) had caused apoptotic cell death specifically in BaF3/p210$^{BCR\text{-}ABL}$ cells without affecting normal H9 cells, whereas the ribozyme (pVwtRz) had induced apoptosis in both BaF3/p210$^{BCR\text{-}ABL}$ and H9 cells. As expected, the expression of the control tRNA^{Val} RNA itself (pV) did not change the morphology of either type of cell. The frequency of apoptosis induced by the maxizyme was higher than that induced by wtRz in BaF3/p210$^{BCR\text{-}ABL}$ cells, demonstrating the higher cleavage activity of the maxizyme than that of the conventional ribozyme against the endogenous target.

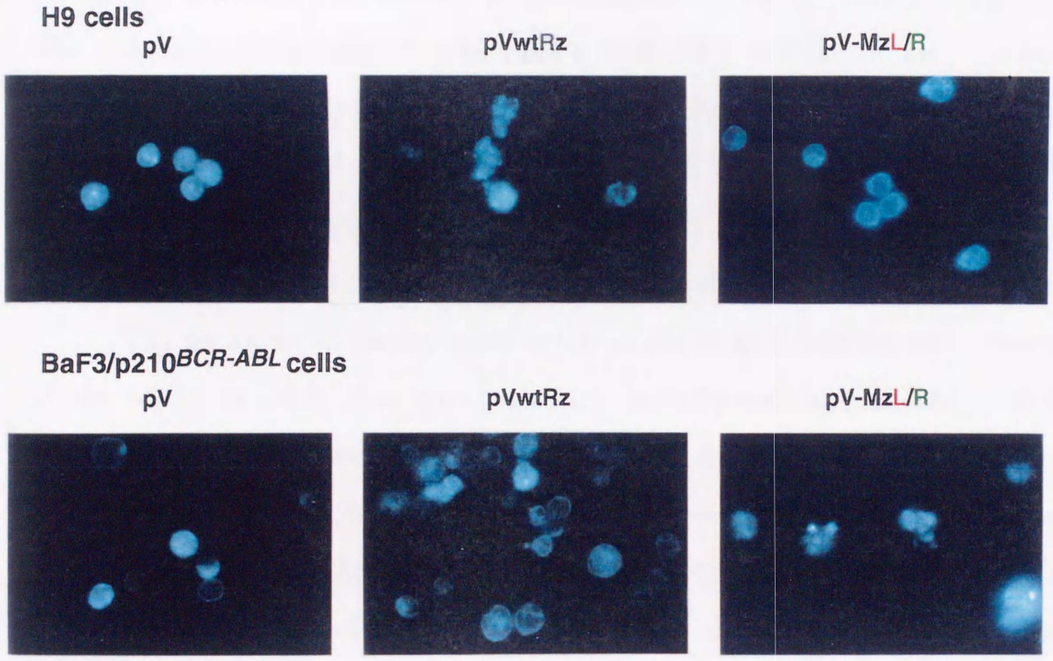

Figure 32 Morphology of $tRNA^{Val}$-enzyme-transduced BaF3/p210$^{BCR-ABL}$ cells and H9 cells.

Direct evidence for the cleavage of *BCR-ABL* mRNA and enhanced activation of caspase-3 by the maxizyme and ribozyme

Since the maxizyme and the ribozyme overcame the *BCR-ABL*-mediated inhibition of apoptosis, I tried to detect the anticipated cleavage products directly by Northern blotting analysis (Fig. 33). Total RNA from $tRNA^{Val}$-enzyme-transduced BaF3/p210$^{BCR-ABL}$ cells was extracted 0.5, 1, 3 and 5 days after the removal of IL-3. The levels of *BCR-ABL* mRNA were determined from the autoradiogram. The length of the cleavage products was exactly as anticipated (3.5 kb). Time courses of the reductions in steady-state levels of *BCR-ABL* mRNA in the presence of the $tRNA^{Val}$-enzymes are shown in the lower panel in Figure 33, in which the basal level of *BCR-ABL* mRNA in the BaF3/p210$^{BCR-ABL}$ cells was taken as 100%. No reduction in the level of expressed *BCR-ABL* mRNA was observed in the case of the control $tRNA^{Val}$ RNA (pV).

The decrease in steady-state levels of *BCR-ABL* mRNA was clearly more rapid in cells that produced the maxizyme than in those that produced wtRz. Detection of the cleavage fragment proved that the maxizyme and the conventional ribozyme were catalytically active and cleaved specifically the target mRNA in cultured cells. In one set of a control experiment, cells (BaF3/p210$^{BCR-ABL}$ cells) expressing only the target RNA (substrate) were mixed, just before the RNA isolation procedure, with cells (transformed BaF3 cells) that had been expressing the maxizyme but not the substrate, and the mixed total RNAs were isolated. In this case, no cleavage products were detectable by Northern blotting, a clear demonstration that, in the experiments shown in Figure 33, the cleavage had occurred in cells but not during the RNA isolation procedure *in vitro*. Thus, I confirmed that the apoptosis of cells, as

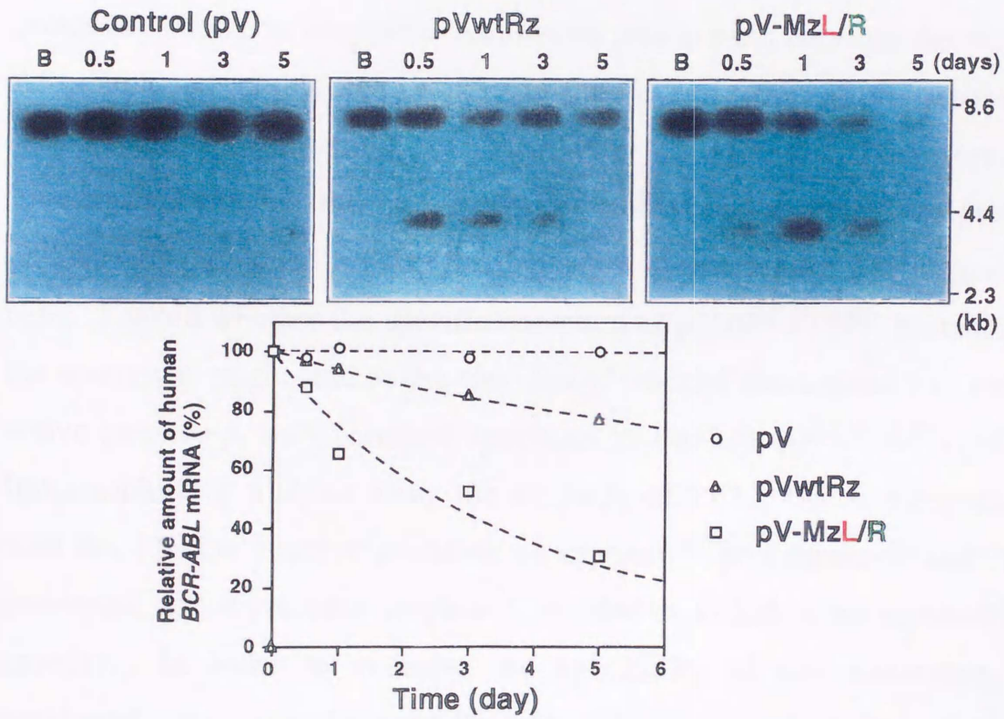

Figure 33 Depletion of p210$^{BCR\text{-}ABL}$ upon cleavage of *BCR-ABL* mRNA by the maxizyme. Direct detection of the products of cleavage of *BCR-ABL* mRNA in BaF3/p210$^{BCR\text{-}ABL}$ cells by Northern blotting analysis.

shown in Figures 31 and 32, originated from the cleavage of *BCR-ABL* mRNA by the maxizyme or of *BCR-ABL* and *ABL* mRNAs by the ribozyme, with resultant depletion of p210$^{BCR\text{-}ABL}$ and/or p145 c-*ABL* proteins in the respective hematopoietic cells (The p145 c-*ABL* protein is a nuclear protein with low intrinsic tyrosine kinase activity, whereas the p210$^{BCR\text{-}ABL}$ protein is a cytoplasmic, membrane-associated protein with a constitutively high level of tyrosine kinase activity that prolongs the survival of hematopoietic cells by inhibiting apoptosis).

Transduction of the apoptotic signal and execution of apoptosis require the coordinated actions of several aspartate-specific cysteine proteases, known as caspases. An inverse relationship between the *BCR-ABL*-mediated inhibition of apoptosis and the activation of procaspase-3 was recently established by Dubrez, *et al.* (1998). Therefore, I investigated whether the maxizyme- (or ribozyme-) mediated apoptotic pathway might indeed involve the activation of procaspase-3 in leukemic cells. I asked whether the specific depletion of p210$^{BCR\text{-}ABL}$ protein by the maxizyme might lead to the cleavage of inactive procaspase-3 to yield active caspase-3, with resultant apoptosis in BaF3/p210$^{BCR\text{-}ABL}$ cells. Immunoblotting analysis using the antibody αCPP32, which recognizes both the 32-kDa inactive precursor of caspase-3 (procaspase-3) and the processed, active protease, caspase-3, enabled us to follow the maturation process. In order to examine the specificity of the maxizyme, I performed a similar study using H9 cells. The basal level of procaspase-3 was almost the same in both BaF3/p210$^{BCR\text{-}ABL}$ and H9 cells (Fig. 34). In maxizyme-transduced BaF3/p210$^{BCR\text{-}ABL}$ cells, the level of procaspase-3 decreased and the level of the p17 active subunit of caspase-3 increased. In stably maxizyme-transduced H9 cells, the level of procaspase-3 remained unchanged. By contrast, expression of the wild-type ribozyme was associated with the processing of procaspase-3 in both

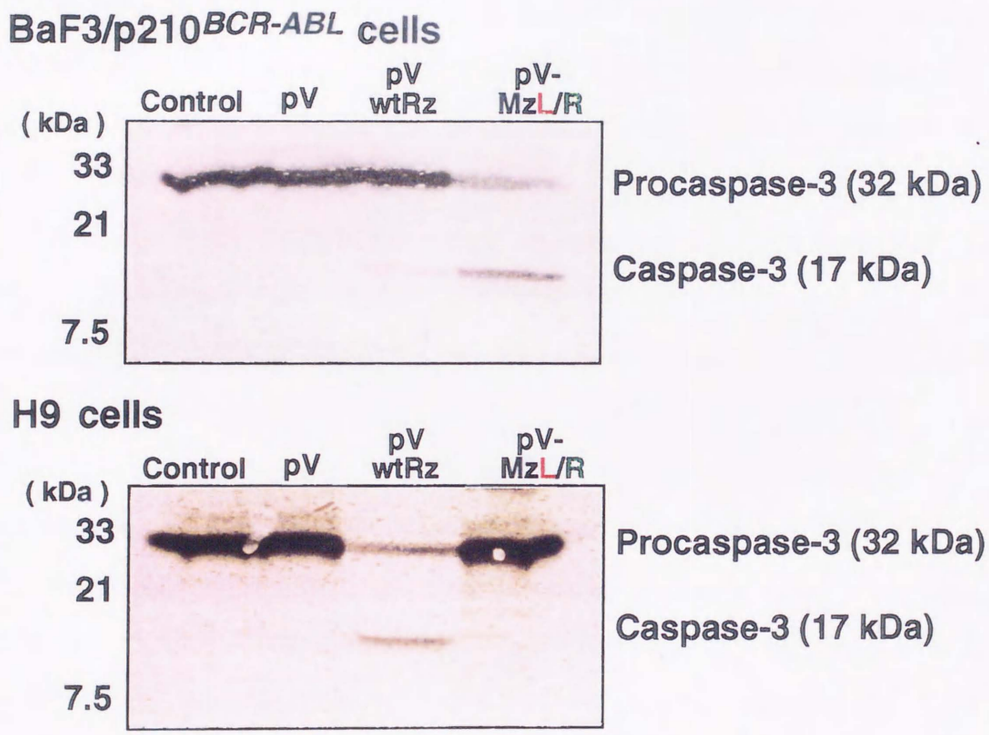

Figure 34 Cleavage of inactive procaspase-3 yielded active caspase-3 upon specific depletion of p210$^{BCR-ABL}$ protein by the maxizyme. Immunoblotting analysis was performed using the antibody αCPP32, which recognizes the 32-kDa precursor to caspase-3 (procaspase-3) and caspase-3 itself.

BaF3/p210$^{BCR\text{-}ABL}$ and H9 cells. The level of conversion of procaspase-3 to caspase-3 in stably maxizyme-transduced BaF3/p210$^{BCR\text{-}ABL}$ cells was higher than that in wtRz-transduced BaF3/p210$^{BCR\text{-}ABL}$ cells. These data strengthen my conclusions that the maxizyme is more active than conventional ribozymes in mammalian cells and that the maxizyme induced apoptosis as a result of specific depletion of p210$^{BCR\text{-}ABL}$ protein, thereby promoting activation of caspase-3 in leukemic cells.

Discussion

The specific association of nucleic acid-based drugs, such as the novel maxizymes, with their targets *via* base pairing and subsequent cleavage of the RNA substrate suggests that these catalytic molecules might be useful for gene therapy. There are basically two ways to introduce ribozymes into cells. One such technique is an exogenous delivery (drug-delivery) system (DDS) in which chemically pre-synthesized ribozymes are encapsulated in liposomes or other related compounds and delivered to target cells. For this exogenous delivery, chemical modifications to make nuclease-resistant maxizymes and/or DNA enzymes (Kuwabara *et al.*, 1997, 1998b) should be useful. Another way to introduce ribozymes into cells is by transcription from the corresponding DNA template (gene therapy). Current gene-therapy technology is limited primarily by the necessity for *ex vivo* manipulations of target tissues and, practically, the technology is suited for endogenous delivery system. Ribozymes with natural components but not chemically modified counterparts can be transcribed *in vivo*. In this context, the novel maxizymes driven by a pol III promoter are superior over the other nucleic acid-based drugs, because of their extremely high substrate-specificity and high cleavage activity, for the treatment of chronic myelogenous leukemia (CML), especially in the case of L6 translocations.

Chapter VI
General discussion

I have described herein the first successful *de novo* design, to my knowledge, of an allosterically modulated RNA catalyst (maxizyme) that selectively cleaves a specific phosphodiester bond. The design was based on a heterodimeric RNA motif that is catalytically activated by interaction with a specified short sequence (sequence of interest; Fig. 25) that is recognized by the sensor arms that are at some distance from the active site. The design of the $tRNA^{Val}$-embedded maxizyme monomer unit is based on the previous successful attachment of a ribozyme sequence to the 3'-modified side of the $tRNA^{Val}$-portion of a human gene for this tRNA (Koseki *et al.*, 1999), which yielded very active ribozymes with high specificity in cultured cells (Kawasaki *et al.*, 1996, 1998). Although I feared initially that the $tRNA^{Val}$-portion of the transcript might hinder the dimerization of the $tRNA^{Val}$-driven RNAs, the analysis indicated that the $tRNA^{Val}$-portions were located at some distance from each other during dimerization and, thus, they did not interfere with the dimerization process (Kuwabara *et al.*, 1998a). The present analysis confirmed the dimerization of the $tRNA^{Val}$-driven monomer units of the maxizyme. More importantly, the resultant maxizyme underwent a conformational change in response to allosteric effectors (Fig. 25) not only *in vitro* (Fig. 26) but also in various kinds of cultured cell that included cells from a patient with leukemia (Figs. 27-34).

Although creation of artificial allosteric enzymes is of great current interest (Porta and Lizardi, 1995; Tang and Breaker, 1997), to my knowledge, no such enzyme has yet been tested in animals or in cultured cells. The novel maxizyme cleaved *BCR-ABL* mRNA specifically without damaging the normal *ABL* mRNA in cultured cells, providing the first example of successful allosteric control of the activity of an artificially created allosteric enzyme. In past efforts to destroy *BCR-ABL* mRNA by antisense molecules, it was difficult to demonstrate

specificity. Since both the p210$^{BCR\text{-}ABL}$ chimeric protein and the p145 c-*ABL* protein are negative regulators of apoptosis (McGahon, *et al.*, 1994; Bedi *et al.*, 1995; Dubrez *et al.*, 1998), antisense molecules with low specificity can induce apoptosis in leukemic cells by inhibiting expression of normal *ABL* mRNA in addition to blocking the *BCR-ABL* pathway. Indeed, it was reported in recent publications that no reduction in the level of p210$^{BCR\text{-}ABL}$ protein was observed in apoptotic cells that had been treated with antisense molecules, and nonspecific inhibition by such antisense oligonucleotides resulted from non-antisense effects of these oligonucleotides (Maekawa *et al.*, 1995; Vaerman *et al.*, 1995; Smetsers *et al.*, 1997). Therefore, in this kind of investigation, it is very important to confirm that cell death does indeed originate from specific suppression by the antisense molecule --- this point is at least as important as estimations of the efficacy of inhibition. Since the specificity of the maxizyme was considerable and since the lengths and sequences of the sensor arms and of common stem II are variables that can very easily be adjusted, maxizymes in general should be considered to be a novel class of potentially powerful gene-inactivating agents that should be able to cleave other chimeric mRNAs.

The cleavage activity of the maxizyme, in particular in cells, should involve a trimolecular interaction (between the two tRNA^{Val}-driven monomer units of the maxizyme and the target substrate). By contrast, the activity of conventional ribozymes involves a bimolecular interaction (between one tRNA^{Val}-driven ribozyme and its target). In principle, bimolecular interactions are more rapid than trimolecular interactions. This difference would seem to indicate that conventional ribozymes might be more effective in cells than a maxizyme. However, in my experiments, I found that the tRNA^{Val}-driven dimer was always more active than the corresponding tRNA^{Val}-driven ribozyme when I tested

several target sequences in cultured cells (the same target site was used for each set of ribozyme and maxizyme; Kuwabara *et al*, submitted for publication). This conclusion is further strengthened by the results of the present analysis. The maxizyme cleaved the junction in *BCR-ABL* mRNA more effectively than the ribozyme, not only in reporter constructs (Fig. 27) but also when the target was endogenous molecule (Figs. 28-34). Therefore, as long as the $tRNA^{Val}$-expression system is used, despite the involvement of the dimerization process, the intracellular activity of the maxizyme appears to be significantly higher than that of conventional hammerhead ribozymes.

Klug's group demonstrated, in an elegant experiment, that a carefully *de novo* designed DNA-binding peptide, which consisted of three zinc-finger motifs, bound specifically to a unique nine-base-pair region of a *BCR-ABL* fusion oncogene in preference to the parent genomic sequences (Choo *et al.*, 1994). Moreover, murine cells that had been rendered independent of growth factors (IL-3) by the action of the oncogene reverted to dependence on IL-3 upon transient transfection with a vector that expressed the DNA-binding peptide. Note that the $p210^{BCR-ABL}$ protein does not trigger the endogenous expression of IL-3 or of other growth factors that are capable of stimulating proliferation of BaF3 cells in an autocrine manner. Rather, $p210^{BCR-ABL}$ provides the stimulus for proliferation of BaF3 cells that is normally provided through the IL-3 signal transduction pathway (Daley and Baltimore, 1988). Klug's group further demonstrated that levels of *BCR-ABL* mRNA in the transiently transfected cells fell by 15-18% within 24 hours as compared to those in untransfected cells. I found that a similar reduction in the level of *BCR-ABL* mRNA (35% reduction within 24 hours in the case of the maxizyme; Fig. 33) restored dependence on IL-3 (Fig. 28).

The mechanism by which deregulated *BCR-ABL* tyrosine kinases delay apoptotic cell death remains poorly understood. Transduction of the apoptotic signal and execution of apoptosis require the coordinated actions of several caspases. Recent evidence indicates that activation of procaspases in apoptosis occurs via a proteolytic cascade (Nagata, 1997). For example, caspase-4 activates procaspase-1 which, in turn, cleaves procaspase-3 to yield active caspase-3 that recognizes the Asp-Glu-Val-Asp (DEVD) motif and cleaves poly (ADP-ribose) polymerase (Enari *et al.*, 1996). The very recent finding that, in the *BCR-ABL*-mediated inhibition of apoptosis, the apoptotic pathway is interrupted upstream of activation of procaspase-3 in *BCR-ABL*$^+$ cell lines (Dubrez *et al.*, 1998) was confirmed in the present study. Depletion of p210$^{BCR-ABL}$ as a result of expression of the maxizyme clearly enhanced the processing of inactive procaspase-3 to yield active caspase-3 (Fig. 34). The specific cleavage of *BCR-ABL* mRNA by the maxizyme and the eventual activation of caspase-3, which led to apoptosis in leukemic cells but not in normal cells, demonstrated that the designed novel maxizyme was fully functional in cells.

In conclusion, I demonstrated that, for cleavage of *BCR-ABL* mRNA, the novel maxizyme formed a heterodimeric structure with high-level activity in cells, and cleavage activity was successfully controlled allosterically within cells such that only in the presence of the junction of *BCR-ABL* mRNA did the maxizyme form an active catalytic core. The maxizyme was more effective than similarly transcribed standard ribozymes in cells. To the best of my knowledge, the novel maxizyme is superior to other nucleic acid-based drugs reported to date because of its extremely high substrate-specificity and high cleavage activity. Novel maxizymes, whose activity can be controlled allosterically by sensor arms that recognize abnormal mRNAs specifically should be powerful tools for

disruption of abnormal chimeric targets and might provide the basis for future gene therapy for the treatment of CML.

Acknowledgements

First of all, the author wishes to heartily express my gratitude to Professor Kazunari Taira. Without his advises and supports, I should been unable to complete this study.

The author thanks Professor Hong-Gang Wang at the College of Medicine, University of South Florida, for providing the antibody αCPP32 and for helpful suggestions. The author also thank Dr. Tsuyoshi Tanabe, Professor Kenzaburo Tani and Professor Shigetaka Asano at the Institute of Medical Science, the University of Tokyo for useful discussions.

The author is specially thank to the present and former members of Taira's laboratory.

This research was supported by various grants from the Ministry of International Trade and Industry (MITI) of Japan and also by a Grant-in-Aid for Scientific Research from the Ministry of Education, Science, Sports and Culture, Japan. The author is recipient of JSPS research fellowships for young scientists.

Finally, thanks are also due to my parents and my sister for their constant support, forbearance, understanding and patience.

References

Altman, S. (1993) RNA enzyme-directed gene therapy. Proc. Natl. Acad. Sci. USA 90, 10898-10900.

Amontov, S. and K. Taira. (1996) Hammerhead minizymes with high cleavage activity: a dimeric structure as the active conformation of minizymes. J. Am. Chem. Soc. 118, 1624-1628.

Amontov, S., S. Nishikawa and K. Taira. (1996) Dependence on Mg^{2+} ions of the activities of dimeric hammerhead minizymes. FEBS Lett. 386, 99-102.

Armentano, D., D.-F. Yu, T. von Rude, W. F. Anderson and E. Gilboa. (1987) Effect of internal viral sequences on the utility of retroviral vectors. J. Virol. 61, 1647-1650.

Baier, G., K. M. Coggeshall, G. Baier-Bitterlich, L. Giampa, D. Telford, E. Herbert, W. Shih and A. Altman. (1994) Construction and characterization of *lck*- and *fyn*-specific tRNA: ribozyme chimeras. Mol. Immunol. 31, 923-932.

Bedi, A., J. P. Barber, G. C. Bedi, W. S. el-Deiry, D. Sidransky, M. S. Vala, A. J. Akhtar, J. Hilton and R. J. Jones. (1995) *BCR-ABL*-mediated inhibition of apoptosis with delay of G2/M transition after DNA damage: a mechanism of resistance to multiple anticancer agents. Blood 86, 1148-1153.

Bertrand, E., D. Castanotto, C. Zhou, C. Carbonnelle, G. P. Lee, S. Chatterjee, T. Grange, R. Pictet, D. Kohn, D. Engelke and J. J. Rossi. (1997) The expression cassette determines the functional activity of ribozymes in mammalian cells by controlling their intracellular localization. RNA 3, 75-88.

Birikh, K. R., P. A. Heaton and F. Eckstein. (1997) The hammerhead ribozyme-structure, function and application. Eur. J. Biochem. 245, 1-16.

Choo, Y., I. Sánchez-García and A. Klug. (1994) *In vivo* repression by a site-specific DNA-binding protein designed against an oncogenic sequence. Nature 372, 642-645.

Crisell, P., S. Thompson and W. James. (1993) Inhibition of HIV-1 replication by ribozymes that show poor activity *in vitro*. Nucleic Acids Res. 21, 5251-5255.

Dahm, S. C., W. B. Derrick and O. C. Uhlenbeck. (1993) Role of divalent metal ions in the hammerhead RNA cleavage reaction. Biochemistry 30, 9464-9469.

Daley, G. Q. and D. Baltimore. (1988) Transformation of an interleukin 3-dependent hematopoietic cell line by the chronic myelogenous leukemia-specific $P210^{bcr/abl}$ protein. Proc. Natl. Acad. Sci. USA 85, 9312-9316.

Dubrez, L., B. Eymin, O. Sordet, N. Droin, A. G. Turhan and E. Solary. (1998) BCR-ABL delays apoptosis upstream of procaspase-3 activation. Blood 7, 2415-2422.

Eckstein, F. and D. M. J. Lilley. (eds.) Catalytic RNA, Nucleic Acids and Molecular Biology, vol. 10. Springer-Verlag, Berlin, (1996).

Ellis, J. and J. Rogers. (1993) Design and specificity of hammerhead ribozymes against calretinin mRNA. Nucleic Acids Res. 21, 5171-5178.

Enari, M., R. V. Talanian, W. W. Wong and S. Nagata. (1996) Sequential activation of ICE-like and CPP32-like proteases during Fas-mediated apoptosis. Nature 380, 723-726.

Forster, A. C. and R. H. Symons. (1987) Self-cleavage of plus and minus RNAs of a virusoid and a structural model for the active sites. Cell 49, 211-220.

Fu, D. and L. W. Mclaughlin. (1992) Importance of specific purine amino and hydroxyl groups for efficient cleavage by a hammerhead ribozyme. Proc. Natl. Acad. Sci. USA 89, 3985-3989.

Geiduschek, E. P. and G. P. Tocchini-Valentini. (1988) Transcription by RNA polymerase III. Annu. Rev. Biochem. 57, 873-914.

Good, P. J., A. J. Krikos, S. X. Li, E. Bertrand, N. S. Lee, L. Giver, A. Ellington, J. A. Zaia, J. J. Rossi and D. R. Engelke. (1997) Expression of small, therapeutic RNAs in human cell nuclei. Gene Ther. 4, 45-54.

Haseloff, J. and W. L. Gerlach. (1988) Simple RNA enzymes with new and highly specific endonuclease activities. Nature 334, 585-591.

Hendry, P., M. J. Moghaddam, M. J. McCall, P. A. Jennings, S. Ebel and T. Brown. (1994) Using linkers to investigate the spatial separation of the conserved nucleotides A9 and G12 in the hammerhead ribozyme. Biochim. Biophys. Acta 1219, 405-412.

Hendry, P., M. J. MaCall, F. S. Santiago and P. A. Jennings. (1995) *In vitro* activity of minimized hammerhead ribozymes. Nucleic Acids Res. 23, 3922-3927.

Hertel, K. J., D. Herschlag and O. C. Uhlenbeck. (1996) Specificity of hammerhead ribozyme cleavage. EMBO J. 15, 3751-3757.

Huang, Y. and G. G. Carmichael. (1996) Role of polyadenylation in nucleocytoplasmic transport of mRNA. Mol. Cell. Biol. 16, 1534-1542.

James, H., K. Mills and I. Gibson. (1996) Investigating and improving the specificity of ribozymes directed against the *bcr-abl* translocation. Leukemia 10, 1054-1064.

Jarvis, T. C., F. E. Wincott, L. J. Alby, J. A. McSwiggen, L. Beigelman, J. Gustofson, A. DiRenzo, K. Levy, M. Arthur, J. Matulic-Adamic, A. Karpeisky, C. Gonzalez, T. M. Woolf, N. Usman and D. T. Stinchcomb. (1996) Optimizing the cell efficacy of synthetic ribozymes. Site selection and chemical modifications of ribozymes targeting the proto-oncogene *c-myb*. J. Biol. Chem. 271, 29107-29112.

Kawasaki, H., J. Ohkawa, N. Tanishige, K. Yoshinari, T. Murata, K. K. Yokoyama and K. Taira. (1996) Selection of the best target site for ribozyme-mediated cleavage within a fusion gene for adenovirus E1A-associated 300 kDa protein (p300) and luciferase. Nucleic Acids Res. 24, 3010-3016.

Kawasaki, H., R. Eckner, T.-P. Yao, K. Taira, R. Chiu, D. M. Livingston and K. K. Yokoyama (1998) Distinct roles of the co-activators p300 and CBP in retinoic-acid-induced F9-cell differentiation. Nature 393, 284-289.

Kazakov, S. and S. Altman. (1991) Site-specific cleavage by metal ion cofactors and inhibitors of M1 RNA, the catalytic subunit of RNase P from *Escherichia coli*. Proc Natl. Acad. Sci. USA 88, 9193-9197.

Kitamura, T., M. Onishi, S. Kinoshita, A. Shibuya, A. Miyajima, and G. P. Nolan. (1995) Efficient screening of retroviral cDNA expression libraries. Proc. Natl. Acad. Sci. USA 92, 9146-9150.

Koizumi, M., S. Iwai and E. Ohtsuka. (1988) Cleavage of specific sites of RNA by designed ribozymes. FEBS Lett. 239, 285-288.

Koseki, S., J. Ohkawa, R. Yamamoto, Y. Takebe and K. Taira. (1998) A simple assay system for examination of the inhibitory potential *in vivo* of decoy RNAs, ribozymes and other drugs by measuring the Tat-mediated transcription of a fusion gene composed of the long terminal repeat of HIV-1 and a gene for luciferase. J. Control. Release 53, 159-173.

Koseki, S., T. Tanabe, K. Tani, S. Asano, T. Shiota, T. Shimada, Y. Nagai, J. Ohkawa and K. Taira. (1999) Stability *in vivo* of RNA polymerase III-driven ribozymes depends on transcribed structure and is the determinant of ribozyme's efficiency *in vivo* J. Virol. in press.

Kronenwett, R., R. Haas and G. Sczakiel. (1996) Kinetic selectivity of complementary nucleic acids: *bcr-abl*-directed antisense RNA and ribozymes. J. Mol. Biol. 259, 632-644.

Kuwabara, T., S. Amontov, M. Warashina, J. Ohkawa and K. Taira. (1996) Characterization of several kinds of dimer minizyme: simultaneous cleavage at two sites in HIV-1 tat mRNA by dimer minizymes. Nucleic Acids Res. 24, 2302-2310.

Kuwabara, T., M. Warashina, T. Tanabe, K. Tani, S. Asano and K. Taira. (1997) Comparison of the specificities and catalytic activities of hammerhead ribozymes and DNA enzymes with respect to the cleavage of *BCR-ABL* chimeric L6 (b2a2) mRNA. Nucleic Acids Res. 25, 3074-3082.

Kuwabara, T., M. Warashina, M. Orita, S. Koseki, J. Ohkawa and K. Taira. (1998a) Formation of a catalytically active dimer by $tRNA^{Val}$-driven short ribozymes. Nature Biotechnology 16, 961-965.

Kuwabara, T., M. Warashina, A. Nakayama, M. Hamada, S. Amontov, Y. Takasuka, Y. Komeiji and K. Taira. (1998b) Comparison of

the specificities and catalytic activities of conventional hammerhead ribozymes, Joyce's DNA enzymes, and novel dimeric minizymes with respect to the cleavage of *BCR-ABL* chimeric L6 (b2a2) mRNA. Gene Ther. Mol. Biol. 1, 435-449.

Kuwabara, T., M. Warashina, T. Tanabe, K. Tani, S. Asano and K. Taira. (1998c) A novel allosterically *trans*-activated ribozyme, the maxizyme, with exceptional specificity in vitro and in vivo. Mol. Cell 2, 617-627.

Leavitt, M. C., M. Yu, F. Wong-Staal and D. J. Looney. (1996) *Ex vivo* transduction and expansion of $CD4^+$ lymphocytes from HIV^+ donors: Prelude to a ribozyme gene therapy trial. Gene Ther. 3, 599-606.

Leontis, N. B., M. E. Piotto, M. T. Hills, A. Malhotra, I. V. Ouporov, J. N. Nussbaum and D. G. Gorenstein. (1995) Structural studies of DNA three-way junctions. Methods in Enzymol. 261, 183-207.

Long, D. M. and O. C. Uhlenbeck. (1994) Kinetic characterization of intramolecular and intermolecular hammerhead RNAs with stem II deletions. Proc. Natl. Acad. Sci. USA 91, 6977-6981.

Lott, W. B., B. W. Pontius and P. H. von Hippel. (1998) A two-metal ion mechanism operates in the hammerhead ribozyme-mediated cleavage of an RNA substrate. Proc. Natl. Acad. Sci. USA 95, 542-547.

Maekawa, T., S. Kimura, K. Hirakawa, A. Murakami, G. Zon and T. Abe. (1995) Sequence specificity on the growth suppression and induction of apoptosis of chronic myeloid leukemia cells by BCR-ABL anti-sense oligonucleoside phosphorothioates. Int. J. Cancer 62, 63-69.

Marschall, P., J. B. Thomson and F. Eckstein. (1994) Inhibition of gene expression with ribozymes. Cell Mol. Neurobiol. 14, 523-538.

McCall, M. J., P. Hendry and P. A. Jennings. (1992) Minimal sequence requirements for ribozyme activity. Proc. Natl. Acad. Sci. USA 89, 5710-5714.

McGahon, A., R. Bissonnette, M. Schmitt, K. M. Cotter, D. R. Green and T. G. Cotter. (1994) BCR-ABL maintains resistance of chronic myelogenous leukemia cells to apoptotic cell death. Blood 83, 1179-1187.

Muller, A. J., J. C. Young, A. M. Pendergast, M. Pondel, N. R. Landau, D. R. Littman and O. N. Witte. (1991) BCR first exon sequences specifically activate the BCR/ABL tyrosine kinase oncogene of Philadelphia chromosome-positive human leukemias. Mol. Cell. Biol. 11, 1785-1792.

Nagata, S. (1997) Apoptosis by death factor. Cell 88, 355-365.

Nakayama, A. T. Kuwabara, M. Warashina and K. Taira. (1998) CTAB-mediated enrichment for active forms of novel dimeric minizymes. FEBS Lett., submitted for publication.

Nedbal, W. and G. Sczakiel. (1997) Hammerhead ribozyme activity in the presence of low molecular weight cellular extract. Antisense Nucleic Acids Drug Dev. 7, 585-589.

Nowell, P. C. and D. A. Hungerford. (1960) A minute chromosome in human chronic granulocytic leukemia. Science 132, 1497-1499.

Ojwang, J. O., A. Hampel, D. J. Looney, F. Wong-Staal and J. Rappaport. (1992) Inhibition of human immunodeficiency virus type 1 expression by a hairpin ribozyme. Proc. Natl. Acad. Sci. USA 89, 10802-10806.

Ohkawa, J., N. Yuyama, Y. Takebe, S. Nishikawa and K. Taira. (1993) Importance of independence in ribozyme reactions: kinetic behavior of trimmed and of simply connected multiple ribozymes with potential activity against human immunodeficiency virus. Proc. Natl. Acad. Sci. USA 90, 11302-11306.

Orita, M., R. Vinayak, A. Andrus, M. Warashina, A. Chiba, H. Kaniwa, F. Nishikawa, S. Nishikawa and K. Taira. (1996) Magnesium-mediated conversion of an inactive form of a hammerhead ribozyme to an active complex with its substrate. J. Biol. Chem. 271, 9447-9454.

Pachuk, C. J., K. Yoon, K. Moelling and L. R. Coney. (1994) Selective cleavage of bcr-abl chimeric RNAs by a ribozyme targeted to non-contiguous sequence. Nucleic Acids Res. 22, 301-307.

Pendergast, A. M., M. L. Gishizky, M. H. Havlik and O. N. Witte. (1993) SH1 domain autophosphorylation of p210 BCR/ABL is required for transformation but not growth factor independence. Mol. Cell. Biol. 13, 1728-1736.

Perriman, R., A. Delves and W. L. Gerlach. (1992) Extended target-site specificity for a hammerhead ribozyme. Gene 113, 157-163.

Perriman, R. and R. de Feyter. tRNA-delivery systems for ribozymes. In Turner, P.C. (ed.) Methods in Molecular Biology, Ribozyme Protocols. Humana Press, Totowa, NJ, pp. 393-40, (1997).

Piccirilli, J. A., J. S. Vyle, M. H. Caruthers and T. R. Cech. (1993) Metal ion catalysis in the *Tetrahymena* ribozyme reaction. Nature 361, 85-88.

Pley, H. W., K. M. Flaherty and D. B. Mackay. (1994) Three-dimensional structure of a hammerhead ribozyme. Nature, 372, 68-74.

Pontius, B. W., W. B. Lott and P. H. von Hippel. (1997) Observations on the catalysis by hammerhead ribozymes are consistent with a two-divalent-metal-ion mechanism. Proc. Natl. Acad. Sci. USA 94, 2290-2294.

Porta, H. and P. M. Lizardi. (1995) An allosteric hammerhead ribozyme. Biotechnology 13, 161-164.

Pyle, A. M. (1993) Ribozymes: a distinct class of metalloenzymes. Science 261, 709-714.

Reuther, J. Y., G. W. Reuther, D. Cortez, A. M. Pendergast and A. S. Baldwin, Jr. (1998) A requirement for NF-κB activation in Bcr-Abl-mediated transformation. Genes & Dev. 12, 968-981.

Ruffer, D. E., G. D. Stormo and O. C. Uhlenbeck. (1990) Sequence requirements of the hammerhead RNA self-cleavage reaction. Biochemistry 29, 10695-10702.

Sarver, N., E. M. Cantin, P. S. Chang, J. A. Zaida, P. A. Ladne, D. A. Stepenes and J. J. Rossi. (1990) Ribozymes as potential anti-HIV-1 therapeutic agents. Science 247, 1222-1225.

Sawata, S., M. Komiyama and K. Taira. (1995) Kinetic evidence based on solvent isotope effects for the nonexistence of a proton-transfer process in reactions catalyzed by a hammerhead ribozyme: implication to the double-metal-ion mechanism of catalysis. J. Am. Chem. Soc. 117, 2357-2358.

Scott, W. G., J. T. Finch and A. Klug. (1995) The crystal structure of an all-RNA hammerhead ribozyme: a proposed mechanism for RNA catalytic cleavage. Cell 81, 991-1002.

Scott, W. G. and A. Klug. (1996) Ribozymes: structure and mechanism in RNA catalysis. Trends Biochem. Sci. 21, 220-224.

Scott, W. G., J. G. Murray, J. R. P. Arnold, B. L. Stoddard and A. Klug. (1996) Capturing the structure of a catalytic RNA

intermediate: the hammerhead ribozyme. Science 274, 2065-2069.

Shimayama, T., S. Nishikawa and K. Taira. (1995) Generality of the NUX rule: kinetic analysis of the results of systematic mutations in the trinucleotide at the cleavage site of hammerhead ribozymes. Biochemistry 34, 3649-3654.

Sioud, M. (1997) Effects of variations in length of hammerhead ribozyme antisense arms upon the cleavage of longer RNA substrate. Nucleic Acids Res. 25, 333-338.

Sioud, M. and L. Jesperson. (1997) Enhancement of hammerhead ribozyme catalysis by glyceraldehyde-3-phosphate dehydrogenase. J. Mol. Biol. 257, 775-789.

Smetsers, T. F., E. H. Linders, L. T. van de Locht, T. M. de Witte and E. J. Mensink. (1997) An antisense Bcr-Abl phosphodiester-tailed methylphosphonate oligonucleotide reduces the growth of chronic myeloid leukemia patient cells by a non-antisense mechanism. Br. J. Hematol. 96, 377-381.

Steitz, T. A. and J. A. Steitz. (1993) A general two-metal-ion mechanism for catalytic RNA. Proc. Natl. Acad. Sci. USA 90, 6498-6502.

Sugiyama, H., K. Hatano, I. Saito, S. Amontov and K. Taira. (1996) Catalytic activities of hammerhead ribozymes with a triterpenoid linker instead of stem/loop II. FEBS Lett. 392, 215-219.

Sullenger, B. A. and T. R. Cech. (1993) Tethering ribozymes to a retroviral packaging signal for destruction of viral RNA. Science 262, 1566-1569.

Sun, L-Q., W. L. Gerlach and G. Symonds. In Catalytic RNA, The Use of Ribozymes to Inhibit HIV Replication, Nucleic Acids and

Molecular Biology. Vol. 10, Springer-Verlag Press, Berlin, Germany, pp. 329-342, (1996).

Sussman, J. L., S. R. Holbrook, R. W. Warrant, G. M. Church and S. H. Kim (1978) Crystal structure of yeast phenylalanine transfer RNA. I. Crystallographic refinement. J. Mol. Biol. 123, 607-630.

Symons, R. H. (1989) Self-cleavage of RNA in the replication of small pathogens of plants and animals. Trends Biochem. Sci. 14, 445-450.

Takagi, Y. and K. Taira. (1995) Temperature-dependent change in the rate-determining step in a reaction catalyzed by a hammerhead ribozyme. FEBS Lett. 361, 273-276.

Takebe, Y., M. Seiki, J. Fujisawa, P. Hoy, K. Yokota, K. Arai, M. Yoshida and N. Arai. (1988) SRα promoter: an efficient and versatile mammalian cDNA expression system composed of the simian virus 40 early promoter and the R-U5 segment of human T-cell leukemia virus type 1 long terminal repeat. Mol. Cell. Biol. 8, 466-472.

Tang, J. and R. R. Breaker. (1997a) Rational design of allosteric ribozymes. Chem. Biol. 4, 453-459.

Tang, J. and R. R. Breaker. (1997b) Examination of the catalytic fitness of the hammerhead ribozyme by *in vitro* selection. RNA 3, 914-925.

Thomson, J. B., T. Thschl and F. Eckstein. (1993) Activity of hammerhead ribozymes containing non-nucleotidic linkers. Nucleic Acids Res. 21, 5600-5603.

Tuschl, T. and F. Eckstein. (1993) Hammerhead ribozymes: importance of stem-loop II activity. Proc. Natl. Acad. Sci. USA 90, 6991-6994.

Uchimaru, T., M. Uebayasi, K. Tanabe and K. Taira. (1993) Theoretical analyses on the role of Mg^{2+} ions in ribozyme reactions. FASEB J. 7, 137-142.

Uebayasi, M., T. Uchimaru, T. Koguma, S. Sawata, T. Shimayama and K. Taira. (1994) Theoretical and experimental considerations on the hammerhead ribozyme reactions: divalent magnesium ion-mediated cleavage of phosphorus-oxygen bonds. J. Org. Chem. 59, 7414-7420.

Uhlenbeck, O. C. (1987) A small catalytic oligonucleotide. Nature 328, 596-600.

Warashina, M., T. Takagi, S. Sawata, D.-M. Zhou, T. Kuwabara and K. Taira. (1997) Entropically driven enhancement of cleavage activity of a DNA-armed hammerhead ribozyme: Mechanism of action of hammerhead ribozymes. J. Org. Chem. 62, 9137-9147.

Weinstein, L. B., B. C. Jones, R. Cosstick and T. R. Cech. (1997) A second catalytic metal ion on group I ribozyme. Nature 388, 805-808.

Yamada, O., M. Yu, J.-K. Yee, G. Kraus, D. Looney and F. Wong-Staal. (1994) Intracellular immunization of human T cells with a hairpin ribozyme against human immunodeficiency virus type 1. Gene Ther. 1, 38-45.

Yarus, M. (1993) How many catalytic RNAs? Ions and the Cheshire cat conjecture. FASEB J. 7, 31-39.

Yu, M., J. Ojwang, O. Yamada, A. Hampel, J. Rapapport, D. Looney and F. Wong-Staal. (1993) A hairpin ribozyme inhibits expression of diverse strains of human immunodeficiency virus type 1. Proc. Natl. Acad. Sci. USA 90, 6340-6344.

Yu, M., M. C. Leavitt, M. Maruyama, O. Yamada, D. Young, A. D. Ho and F. Wong-Staal. (1995) Intracellular immunization of human fetal cord blood stem/progenitor cells with a ribozyme against human immunodeficiency virus type 1. Proc. Natl. Acad. Sci. USA 92, 699-703.

Vaerman, J. L., C. Lammineur, P. Moureau, P. Lewalle, F. Deldime, M. Blumenfeld and P. Martiat. (1995) BCR-ABL antisense oligodeoxyribonucleotides suppress the growth of leukemic and normal hematopoietic cells by a sequence-specific but nonantisense mechanism. Blood 86, 3891-3896.

Zhou, D.-M., P. K. R. Kumar, L.-H. Zhang and K. Taira. (1996) Ribozyme mechanism revisited: Evidence against direct coordination of a Mg^{2+} ion with the pro-R oxygen of the scissile phosphate in the transition state of a hammerhead ribozyme-catalyzed reaction. J. Am. Chem. Soc. 118, 8969-8970.

Zhou, D.-M., L.-H. Zhang and K. Taira. (1997) Explanation by the double-metal-ion mechanism of catalysis for the differential metal ion-effects on the cleavage rates of 5'-oxy and 5'-thio substrates by a hammerhead ribozyme. Proc. Natl. Acad. Sci. USA 94, 14343-14348.

Zhou, D.-M. and K. Taira. (1998) The hydrolysis of RNA: from theoretical calculations to the hammerhead ribozyme-mediated cleavage of RNA. Chem. Rev. 98, 991-1026.

Zoumadakis, M. and M. Tabler. (1995) Comparative analysis of cleavage rates after systematic permutation of the NUX consensus tartget motif for hammerhead ribozymes. Nucleic Acids Res. 23, 1192-1196.

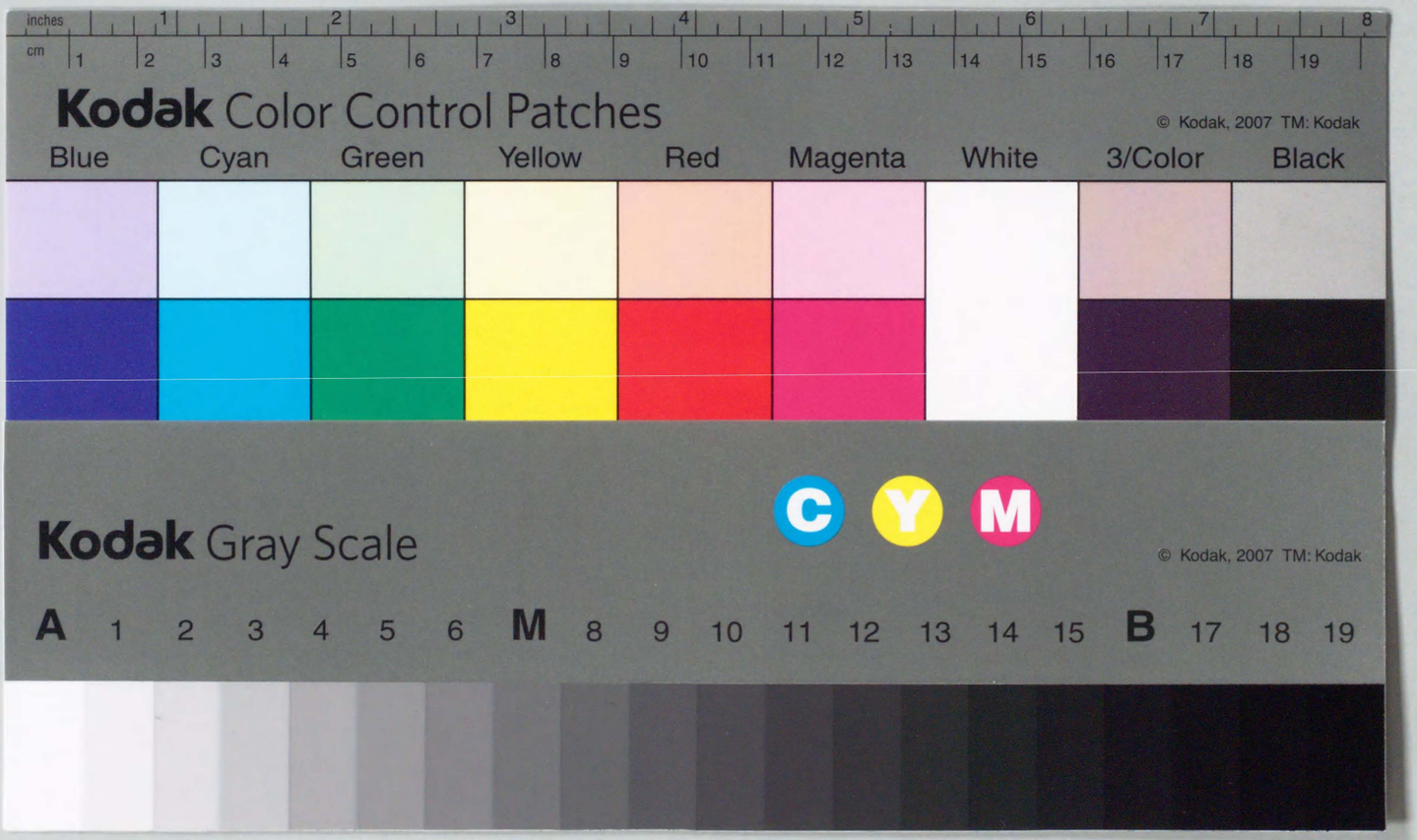
inches
cm
Kodak Color Control Patches
© Kodak, 2007 TM: Kodak
Blue
Cyan
Green
Yellow
Red
Magenta
White
3/Color
Black
Kodak Gray Scale
C
Y
M
© Kodak, 2007 TM: Kodak
A 1 2 3 4 5 6 M 8 9 10 11 12 13 14 15 B 17 18 19